Studies on the oxidative protein folding pathway in yeast

Alexander Blayney Dove

Genetics MSc

School of Biosciences

University of Kent

Date of Submission: July 2017

Supervisor:- Prof. Mick Tuite

Declaration

No part of this thesis has been submitted in support of an application for any degree or qualification of the University of Kent or any other university or institute of learning.

Alexander Dove

Acknowledgements

I would like to say a special thank you to Professor. Mick Tuite for all of his support and guidance over the duration of this project.

I am also grateful to Dr. Campbell Gourlay for his very helpful suggestions and to Dr. Tobias von der Haar for the assembly of certain gene constructs used in this study.

I would also like to thank the members of the Kent Fungal Group for their continued support, with a special thank you to both Gemma Staniforth and Dave Beal who have helped immeasurably over the course of this project.

Abbreviations

Oxidative protein folding – OPF

Endoplasmic Reticulum – ER

Protein disulphide isomerase –PDI

Suppressor of Δ*pdi1* lethality – *supX*

Endoplasmic reticulum oxidoreductin – Ero1p

Glutathione peroxidase 7 – GPx7

Glutathione peroxidase 8 – GPx8

Peroxiredoxin IV – PRxIV

Polymerase chain reaction – PCR

Saccharomyces cerevisiae – *S. cerevisiae* / yeast

Escherichia coli – *E.coli*

Hydrogen peroxide – H_2O_2

Reactive oxygen species – ROS

2', 7'–dichlorofluorescein – H_2DCFDA

1, 4 dithiothreitol – DTT

Distilled water – dH_2O

Sterile distilled water – sdH_2O

Reduced glutathione – GSH

Oxidised glutathione –GSSG

Flavin adenine dinucleotide – FAD

Orotidine-5'-monophosphate decarboxylase – ODCase

Orotidine-5'-monophosphate – OMP

Uridine-5'-monophosphate – UMP

Orotate phosphoribosyltransferase - OPRTase

Table of Contents

Declaration 2

Acknowledgements 3

Abbreviations 4

Abstract 11

Chapter 1 - Introduction 12

1.1 The oxidative protein folding pathway 12

1.1.1 Components of the yeast endoplasmic reticulum oxidative protein folding pathway 12

1.1.1.1 Protein disulphide isomerase 12

1.1.1.2 Endoplasmic reticulum oxidoreductin 1 14

1.1.2 The mechanism of oxidative protein folding in yeast 16

1.1.3 Homologues of protein disulphide isomerase in yeast 20

1.2 Mechanisms of hydrogen peroxide detoxification within the endoplasmic reticulum 21

1.2.1 Glutathione peroxidases in humans and yeast 21

1.2.2 Regulation of hydrogen peroxide production in yeast 21

1.2.3 Glutathione peroxidase 7 22

1.2.4 Glutathione peroxidase 8 24

1.2.5. Mechanism of hydrogen peroxide detoxification by glutathione peroxidases 7 and 8 25

1.3 Localisation of proteins to the endoplasmic reticulum in yeast 28

1.3.1 Endoplasmic reticulum signal sequences 28

1.3.2 Endoplasmic reticulum retention sequences 29

1.4 Aims of the project 30

Chapter 2 – Materials and Methods 31

2.1 Materials 31

2.1.1 Yeast and bacterial strains 31

2.1.1.1 *Saccharomyces cerevisiae* strains 31

2.1.1.2 *Escherichia coli* strains **32**

2.1.2 Media Recipes **33**

2.1.2.1 Making killer toxin assay solid medium **34**

2.1.2.1.1 Base Agar **34**

2.1.2.1.2 Top Agar **34**

2.1.3 Chemicals used **34**

2.1.4 Oligonucleotide sequences **35**

2.1.5 Antibodies used **36**

2.1.6 Plasmids used **37**

2.1.6.1 Cloning vector maps **39**

2.2 DNA techniques **42**

2.2.1 DNA extraction from *E.coli* **42**

2.2.2 Extraction of genomic DNA from yeast **42**

2.2.3 Methods of quantification of DNA concentrations **42**

2.2.3.1 NanoDrop **42**

2.2.3.2 Spectrophotometry **42**

2.2.3 *E.coli* transformation with plasmid DNA **43**

2.2.3.1 Z-Competent™ *E.coli* Cells **43**

2.2.3.2 Top10 *E.coli* cells **43**

2.2.4 Yeast transformation **43**

2.2.5 Standard polymerase chain reaction **43**

2.2.6.1 NEB Taq polymerase **44**

2.2.6.2 Invitrogen Taq polymerase **44**

2.2.7 Gradient polymerase chain reaction **45**

2.2.8 Agarose gel electrophoresis **45**

2.2.9 Restriction enzyme digests **45**

2.2.10 Oligonucleotide primer design **45**

2.2.11 Plasmid construction **46**

2.3 Protein techniques **46**

2.3.1 Cell lysates **46**

2.3.2 Protein gel electrophoresis **47**

2.3.3 Western blot **47**

2.3.3.1 Transfer **47**
2.3.3.2 Imaging **47**
2.4 In vitro oxygen consumption assay **48**
2.5 Yeast techniques **49**
2.5.1 Spontaneous generation of ∆*pdi1* mutants **49**
2.5.2 Generation of ∆*pdi1* mutants through mutagenesis **49**
2.5.3 Producing -80˚C glycerol stocks **50**
2.5.4 Measuring growth in liquid culture **50**
2.5.5 Spectrophotometry **50**
2.5.6 Replica plating **50**
2.5.7.1 Cell counts using a haemocytometer **51**
2.5.8 Fluorescence analysis of cells by flow cytometry **51**
2.5.9 Killer toxin assay **51**
Chapter 3 – Results **53**
3.1 Screen for viable ∆*pdi1* mutants **53**
3.1.1 Duration of ultraviolet radiation exposure for a 50% kill rate **54**
3.1.2 Growth of potential viable ∆*pdi1* mutants on YNB–Ura solid medium **55**
3.1.3 Assaying for absence of protein disulphide isomerase in the potential ∆*pdi1* mutants **56**
3.1.4 Growth of putative mutants in YPD liquid medium **58**
3.1.5 Polymerase chain reaction of genomic DNA to amplify *PDI1* gene and check for a recombination event **60**
3.2 The phenotypic impact upon expressing glutathione peroxidases 7 and 8 in yeast **61**
3.2.1 Construction of plasmids carrying *GPX7* and *GPX8* genes **61**
3.2.1.1 pBEVY-L vector carrying native *GPX7* and *GPX8* **61**
3.2.1.2 Native *GPX7* and *GPX8* with a *GFP* fusion **64**
3.2.1.3 pTH644 vector carrying *GPX7* and *GPX8* chimeric constructs **66**

3.2.1.3.1 *GPX7* and *GPX8* with native ER signal sequence but yeast ER retention sequence **67**
3.2.2 Expression and cellular retention of GPx7 and GPx8 proteins **68**
3.2.2.1 Native *GPX7* and *GPX8* **68**
3.2.2.1.1 Confirming expression of glutathione peroxidases 7 and 8 **68**
3.2.2.1.2 Cellular retention of native glutathione peroxidases 7 and 8 **71**
3.2.2.2 BY4741 expressing glutathione peroxidases 7 and 8 constructs **71**
3.2.2.2.1 Confirming expression of glutathione peroxidases 7 and 8 constructs **71**
3.2.2.2.2 Cellular retention of glutathione peroxidases 7 and 8 constructs **72**
3.2.2.3 A ∆*pdi1* strain expressing glutathione peroxidases 7 and 8 constructs **73**
3.2.2.3.1 Confirming expression of glutathione peroxidases 7 and 8 constructs **73**
3.2.2.3.2 Western Blot to assay for cellular retention of protein **73**
3.2.3 Changes to sensitivity to hydrogen peroxide as a result of expressing glutathione peroxidases 7 and 8 **73**
3.2.3.1 Growth in YNB-Leu liquid medium in presence of hydrogen peroxide **73**
3.2.3.1.1 BY4741 and 2736 expressing native glutathione peroxidases 7 and 8 **74**
3.2.3.1.2 BY4741 expressing glutathione peroxidases 7 and 8 constructs **80**
3.2.3.1.3 A ∆*pdi1* strain expressing glutathione peroxidases 7 and 8 constructs **84**
3.2.3.2 Growth on solid YNB-Leu medium with a range of **89**

hydrogen peroxide concentrations
3.2.3.2.1 2736 expressing native glutathione peroxidases 7 and 8 **89**
3.2.3.2.2 BY4741 expressing glutathione peroxidases 7 and 8 constructs **90**
3.2.4 Changes in levels of intracellular hydrogen peroxide as a result of expressing glutathione peroxidases 7 and 8 **92**
3.2.4.1 Intracellular hydrogen peroxide in BY4741, 2736 and DN5 expressing native glutathione peroxidases 7 and 8 **92**
3.2.4.2 Intracellular hydrogen peroxide in BY4741 expressing glutathione peroxidases 7 and 8 constructs **98**
3.2.4.3 Intracellular hydrogen peroxide in a ∆*pdi1* strain expressing glutathione peroxidases 7 and 8 constructs **99**
3.2.5 Effects of glutathione peroxidases 7 and 8 on the rate of oxidative folding *in vivo* **100**
3.2.5.1 Sensitivity of BY4741 expressing glutathione peroxidases 7 and 8 constructs to 1,4 -Dithiothreitol **100**
3.2.5.2 Secretion of an over expressed extracellular disulphide bonded protein **102**
3.2.5.2.1 Levels of killer toxin secretion in BY4741 expressing native glutathione peroxidases 7 and 8 **102**
3.2.5.2.2 Levels of killer toxin secretion in BY4741 expressing glutathione peroxidases 7 and 8 constructs **103**
3.2.5.2.3 Levels of killer toxin secretion in a ∆*pdi1* strain expressing native, and chimeric construct versions of glutathione peroxidases 7 and 8 **104**
3.2.5.3 Effect of glutathione peroxidases 7 and 8 on rate of expression of an intracellular disulphide bonded protein **105**
3.2.6 The effect of glutathione peroxidases 7 and 8 on oxidative folding with yeast PDI *in vitro* **105**

Chapter 4 – Discussion **108**

4.1 Can viable ∆*pdi1* mutants be generated? **108**

4.2 What are the impacts of expression of native human glutathione peroxidase 7 and 8 in yeast? **111**

4.2.1. Engineering expression of GPx7 and GPx8 in yeast **111**

4.2.2 Identifying Native GPx7 and GPx8 localisation **112**

4.3 Does addition of a yeast ER signal sequence and ER retention sequence to glutathione peroxidases 7 and 8 result in any favourable phenotypic characteristics? **113**

4.4 Does expression of glutathione peroxidases 7 and 8 result in any changes to the phenotype of a ∆*pdi1* strain? **116**

Abstract

The oxidative protein folding (OPF) pathway is conserved across prokaryotic and eukaryotic organisms. In yeast, the OPF is catalysed by the essential proteins protein disulphide isomerase (PDI) and endoplasmic reticulum oxidoreductin (Ero1p) within the endoplasmic reticulum (ER). It is unclear why *PDI1* is an essential gene, as upregulation of some yPDI homologues can restore viability to a Δ*pdi1* strain. The essentiality of PDI was therefore investigated to identify a potential suppressor of Δ*pdi1* lethality (*supX*), with the hypothesis that *supX* would be upregulation of yPDI homologues. As the purpose of the non-essential yPDI homologues is unknown this would help characterise the yeast OPF pathway as well as providing a potential mechanism to increase OPF *in vivo*. A genetic screen was carried out to search for potential extragenic suppressors of the lethality seen in a Δ*pdi1* mutant using a plasmid shuffling strategy. A number of viable mutants were obtained but these arose either via genomic recombination with the plasmid-borne *PDI1* or through direct resistance to 5-FOA used in the screen. Two other PDI-less mutants obtained showed a loss of viability upon storage. Glutathione peroxidase 7 (GPx7) and glutathione peroxidase 8 (GPx8) are ER localised mammalian proteins that couple the detoxification of hydrogen peroxide (H_2O_2) to reoxidation of PDI, simultaneously alleviating H_2O_2 stress in the ER and increasing the rate of OPF. There are no known ER-localised peroxiredoxin proteins in *S. cerevisiae* and so GPx7 and GPx8 were expressed in yeast to remove accumulated H_2O_2 as this may be a limiting factor in OPF. Neither GPx7 nor GPx8 had any effect on levels of intracellular H_2O_2 *in vivo* or cellular sensitivity to H_2O_2. Furthermore there was no effect on the rate of OPF *in vivo* and *in vitro*. It is possible that there is no functional interaction between yeast PDI and the mammalian proteins GPx7 and GPx8.

Chapter 1 – Introduction

1.1 The oxidative protein folding pathway

The oxidative protein folding (OPF) pathway is a highly conserved system in both eukaryotes and prokaryotes as disulphide bonds are essential for the proper activity of many proteins[1]. In eukaryotic cells the OPF in proteins synthesised in the secreted protein pathway are catalysed in the endoplasmic reticulum (ER) by protein disulphide isomerase (PDI) and endoplasmic reticulum oxidoreductin 1 (Ero1).

1.1.1 Components of the yeast endoplasmic reticulum oxidative protein folding pathway

1.1.1.1 Protein disulphide isomerase

PDI is an endoplasmic reticulum (ER) localised protein which primarily has roles in OPF and isomerisation[2]. In humans there are 21 known members of the PDI family[3], whereas yeast expresses only a single known essential PDI[4] protein encoded for by the *PDI1* gene, with four non-essential homologues[4]. PDI is within the top 4% of most abundant proteins at ~66000 molecules per cell[5] and it accounts for 2% of protein in the ER[6].

PDI has 5 domains: a, a', b', b and c, with an x linker domain connecting the a' and b' domains forming a 'twisted U' formation[7] (Fig 1.1.). The 522 amino acid long yeast PDI (yPDI) molecule is approximately 80Å wide, 60Å tall[7] and has a molecular weight of ~58.2 kDa. The a, a', b' and b domain each contain a variant on

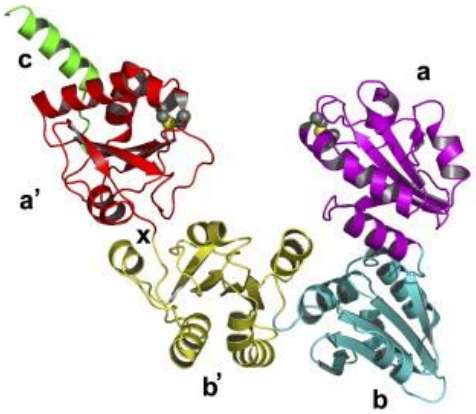

Fig 1.1. Structure of yeast PDI
Ribbon diagram of the structure of yeast PDI, the a (purple), b (cyan), b' (yellow), a' (red) and c (green) domains of PDI are shown as well as the X linker. The side chains of the CXXC active sites of the a and a' domains are shown in yellow. Figure from Tian, G., et al[7].

a thiorexodin fold[7], a common fold found in enzymes for catalysis of reduced thiol domains to disulphide bonds[8].

The active sites of PDI are located in the a and a' domains of yPDI (Fig 1.1.) and consist of a CGHC domain[9] in the N-terminal region of the second α helix, this is a conserved characteristic across the thioredoxin family[10]. From C61 of the first catalytic domain to C406 of the second measures 28Å, this opening and the hydrophobic cleft results in PDI being able to contain a peptide of approximately 100 residues[7].

There are several key resides involved in substrate binding other than the pair of cysteines directly involved in catalysis, one of which is a conserved tyrosine residue located immediately prior to the active sites, this hydrophobic residue is likely to be important for substrate binding as point mutations of these amino acids to non-hydrophobic residues cuts the oxidative activity of PDI by ~50%[7]. Another important residue is the glycine domain located between the two cysteines in the CGHC catalytic site, the absence of a side chain on this residue may increase flexibility of the active site[7].

The orientation of the domains of PDI established from the crystal structure suggests that the a domain is in contact with both the b and b' domains while the a' domain is only able to contact the b' domain[7]. The a' and b' domains are connected via the x-linker (Fig 1.1.), a 17 amino acid peptide. The x linker gives a large degree of flexibility to the a' relative to the b' domain allowing it to tilt and twist[11], this flexibility provides PDI with specificity for a greater range of substrates. All of the domain linking regions display flexibility, but none to the same degree as the x linker domain. The interdomain junction between the a and b domains are restricted to a twist while between the b and b' domains there is no ability for twisting[11]. The lesser flexibility of the b and b' domains form a stable base for the 'U' shape of the protein while the a and a' domains have increased flexibility for allowing a wide range of substrates into the cleft.

The a and a' domains of yPDI bare striking resemblance to each other but possess a few distinct differences that give them different characteristics[7]. One of these distinct differences are the native redox states of the active sites, predominantly the active site a' domain exists in a partially oxidised state where as the a domain exists predominantly in the fully oxidised state[7][12][13].

The individual a' and a domains possess high oxidative activity having approximately 50% of the activity as WT yPDI, but only 5% of the isomerase activity[13][14]. Additionally a sole yPDI a' domain expressed in yeast in approximately double concentrations is able to rescue cells viability, this indicates that the oxidative activity of yPDI is essential for cell viability and that the isomeration activity is less essential[14]. Expressing just 60% of the WT levels of PDI maintain growth rates similar to those of WT[14], this suggests that yPDI is expressed in greater quantities than is required for the cell and that high isomerase activity is not required for viability.

The C terminal tail of PDI is an acidic C terminal extension from residues 486 to 522 which forms an alpha helix[7]. This domain helps maintain the native state of PDI enabling chaperone activity[15]. This stability is likely induced by a relatively high composition of negatively charged residues[7][16].

There are external hydrophilic regions that gives PDI its solubility but there are also a number of external hydrophobic regions, two of which are present around the active sites of domains a[17] and a' and there is an exposed hydrophobic region present on the b and b' domains which results in a continuous hydrophobic surface[7]. The continuation of the hydrophobic regions from the b' domain into the b domain increases the binding area for potential substrates[7]. This hydrophobic surface likely has a role in generating the high affinity, wide specificity of PDI[18] that enables binding and catalysis of a wide range of protein substrates and also facilitates PDI's chaperone activity. *In vitro* studies have demonstrated that it is possible that absence of the b domain results in lowered efficiency of folding of scrambled protein but not of reduced protein, while loss of b' domain resulted in lowered efficiency of OPF of both scrambled and reduced proteins[7].

1.1.1.2 Endoplasmic reticulum oxidoreductin 1

ERO1 is an essential gene[19] in yeast for disulphide formation and encodes Endoplasmic Reticulum Oxidoreductin 1(Ero1p), an ER protein that facilitates reoxidation of PDI. Ero1p is a flavoprotein as it has a non-convelantly bound flavine adenine dinucleotide (FAD) co-factor, which is essential for its ability to oxidise PDI[20].

Ero1p has two pairs of cysteines that are involved in reoxidation of PDI: C100/C105 and C352/C355, named the shuttle cysteines and active-site cysteines respectively[21]. These residues are essential for efficient OPF in the ER[21]. The shuttle cysteines are located in approximately the first 100 residues forming a flexible loop which can assume at least two conformations. A conformation that brings the shuttle cysteines in close proximity to the active site cysteines[22] and a distant conformation that may enable interaction of the shuttle cysteines with PDI[23] (Fig 1.2.).

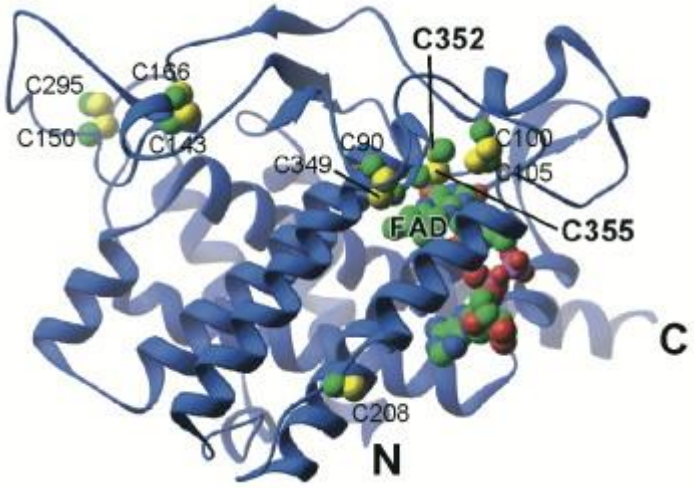

Fig 1.2. Structure of Ero1p
A ribbon diagram of the structure of Ero1p that shows the shuffle cysteine pair (C100-C105) on the flexible peptide, the active site cysteine pair (C352-C355) which is in close proximity to FAD and the pairs of regulatory cysteines (C90/C349, C150/C295, C143/C166). Figure from Gross, E., et al[22]

As well as these catalytically active disulphide bonds there are also six cysteines that partake in the formation of three regulatory disulphide bonds: C90/C349, C150/C295 and C143:C166[24] (Fig 1.2.). While these cysteine pairs are reduced Ero1p is active, however, should either of these regulatory cysteine pairs become oxidised Ero1p inactivates[24]. This therefore forms a negative feedback loop where, should the ER conditions become more oxidising, the regulatory cysteine pairs will form disulphide bonds and hence inactive Ero1p. The inactivation of Ero1p will prevent the ER environment from becoming even more oxidising. Additionally there is evidence that regulation upon Ero1p can mediate the flow of oxidising molecules to the ER and therefore provides homeostatic control over the redox environment of the ER[24].

The structural mechanism by which Ero1p regulation is achieved through the redox states of the regulatory cysteines C90/C349 and C150/C295 is likely due to the dependence on the motility of the flexible polypeptide for protein function[24]. Both of these pairs of these cysteines capable of forming disulphide link the flexible polypeptide to the helically structured domain of the protein[24]. Therefore oxidation of either regulatory cysteine pairs would result in decreased motility of the flexible polypeptide and by extension, the shuffle cysteines[24]. This would prevent transfer of the electrons from the shuffle cysteines to the active-site cysteines as a conformational shift is a key step in the electron transfer in Ero1p[24], or, if locked in an alternate conformation, could prevent interactions of shuffle cysteines with PDI. There is cooperation between these two disulphide bonds relating to Ero1p regulation, on its own the C90/C349 bond isn't stable, but is given stability through the concurrent formation of the C150/C295 disulphide bond[24].

Ero1p, in the absence of substrate, is able to self-oxidise its regulatory disulphides this allows Ero1p to inactive itself preventing uncontrolled oxidative activity in the lack of substrate[24].

1.1.2 The mechanism of oxidative protein folding in yeast

The OPF of target proteins initiates with the binding of unfolded protein to PDI. The b' domain is essential and acts as the principle binding site for ligands. Acting solely the b' domain is able to bind small peptides but for larger or misfolded proteins additional domains are necessary to facilitate binding[18]. The b domain is responsible for ligand alignment. Removal of the a', a and c terminal domains from PDI do not result in a decrease affinity of substrate binding *in vitro*[25].

Following substrate binding the redox active a and a' domains of PDI catalyse OPF within substrate proteins (Fig 1.3.). The highly conserved CGHC site of either the a or a' domains of yPDI in its oxidised form oxidises a pair of cysteines in a target peptide forming a disulphide bond[26]. In hPDI, however, the a' domain oxidises target proteins while the a domain reoxidises the a' domain through disulphide transfer[27].

For PDI to catalyse formation and isomerisation of disulphide bonds in a wide range of proteins it must be able to distinguish stable, correctly folded proteins from unfolded proteins or proteins with non-native disulphide bonds. In human PDI this

is achieved through altered affinities for the different types of substrates, unfolded proteins bound with the highest affinity, partly folded proteins had a K_D approximately 3x higher than the unfolded proteins and native proteins had a K_D approximately 9 times higher than the unfolded proteins[25]. As PDI is able to bind not only unfolded protein but also native protein, albeit weakly, suggests that substrate binding to PDI is mediated by exposure of unfolded regions to the catalytic site[25]. As native proteins undergo regular, short-lived, conformation alternations resulting in exposure of domains associated with being unfolded hence allowing binding to PDI[25]. Unfolded substrates therefore bind to PDI with higher affinity than partially folded or native proteins and undergo OPF. The OPF of unfolded protein results in a decrease in affinity of the protein which allows Ero1p, which has a K_D of approximately 1.7µM with reduced PDI[27] in human cells. This is significantly lower than the K_D of partially folded protein: ~4.9[25], to bind. It is likely that in yeast the change in affinity for substrate following OPF mediates substitution of protein substrate for Ero1p in a similar manor.

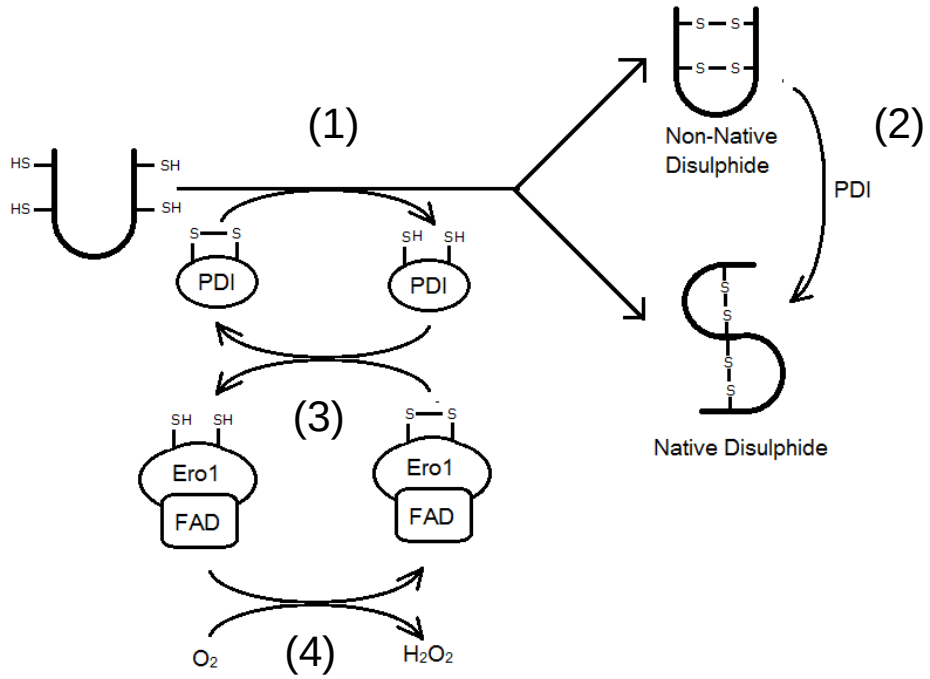

Fig 1.3. The pathway of OPF in yeast
The OPF of unfolded target proteins is catalysed by oxidised PDI through disulphide exchange, which therefore becomes reduced as a result (1). PDI can also isomerase non-native disulphide bonded proteins to the correct native folding (2). Reduced PDI is reoxidised by oxidised Ero1 which in turn becomes reduced (3). Ero1 is reoxidsed by passing the donated protons to FAD which passes them to molecular oxygen generating H_2O_2 (4).

Oxidative of protein folding of substrate by PDI leaves the enzyme in the reduced state (Fig 1.3.). Therefore for continued OPF reactions to occur PDI must be reoxidised, this is performed by Ero1p. Estimates for numbers of molecules of Ero1p suggest that they're at 1/10th that of PDI[27]. Although typically Ero1p is responsible for reoxidation of the active site of PDI, evidence shows that some alternate electron acceptors, such as reduced glutathione (GSH), are capable of reoxidisng the a' domain of hPDI[27].

Human Ero1α interacts with PDI through contact of a β-hairpin of Ero1α and the b' domain of hPDI[28], however, yeast does not have this β hairpin and hence the mechanism of interaction of Ero1p with PDI likely differs between human and yeast systems[28].

Reoxidation of PDI initiates through reduction of the shuttle cysteines in the flexible polypeptide loop of Ero1p by one of the reduced thiols of PDI[23], in yPDI the a domain more readily donates electrons than the a' domain[12]. The electrons of the thiol of PDI are passed to C105 and a temporary disulphide bond is formed between the now oxidised thiol of PDI and C100 of Ero1p resulting in the partially oxidised state of PDI[23] (Fig 1.4.). The electrons from the second thiol of PDI is then passed to C100 of Ero1p resolving the bond between Ero1p and PDI and leaving oxidised PDI and reduced Ero1p[23] (Fig 1.4.).

There are shifts in conformation of the flexible polypeptide domain resulting in a decreased distance between the shuffle cysteines and the active-site cysteines enabling disulphide transfer to occur[23] (Fig 1.4.). The reduced shuffle cysteines then attack the disulphide bond of the active-site cysteines, the electrons from C105 are passed to C355 and a temporary disulphide bond forms between C100 and C352[23] (Fig 1.4.). Electrons from C105 resolves this disulphide bond leaving the active-site cysteines reduced and the shuffle cysteines oxidised, the flexible polypeptide then returns to the original conformation and the Ero1p molecule is ready to oxidise another molecule of PDI[23] (Fig 1.4.).

The active-site cysteines, C352/C355 are surrounded by 4 alpha helices and is in close proximity to the isoalloxazine of FAD[22]. The active-site cysteines then donate 2 protons to the FAD cofactor which becomes reduced[22]. The FAD cofactor then donates the 2 protons to the final electron acceptor: molecular oxygen[22], resulting in the formation of one hydrogen peroxide (H_2O_2) molecule for each disulphide bond

oxidised. In anoxic conditions Ero1p is able to utilise an alternative to molecular oxygen for the final electron acceptor, such as free oxidised FAD[29].

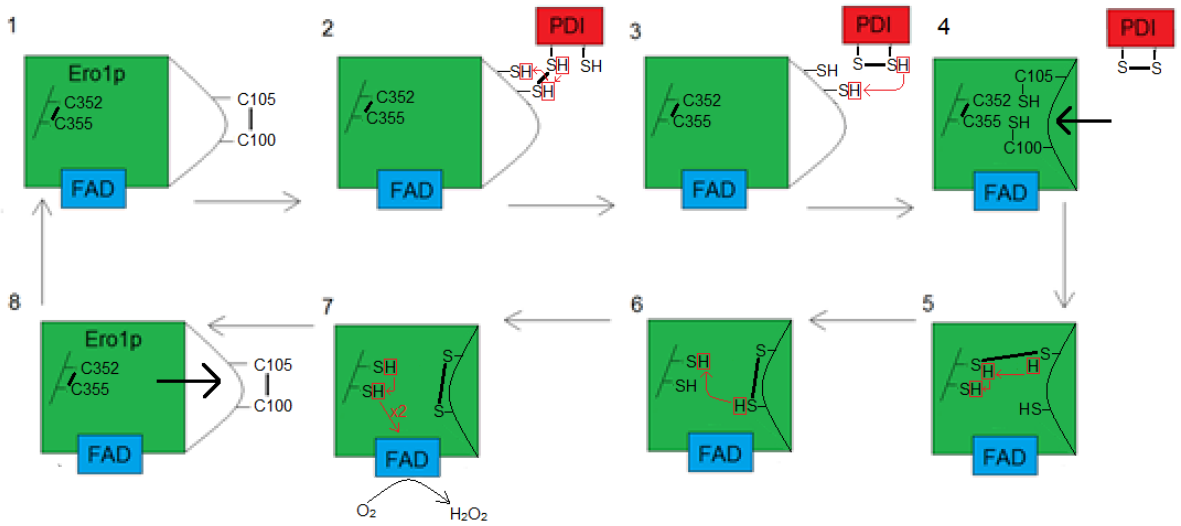

Fig 1.4. The pathway of reoxidation of PDI by Ero1p
The pathway for reoxidation of reduced PDI by Ero1p initiates with a two-step disulphide transfer from the shuttle cysteines of Ero1p (C100/C105) to reduced PDI (Steps 1-3). This results in the reoxidation of PDI and reduction of the shuttle cysteines. This induces a conformational change in the flexible peptide on which C100 and C105 are situated bringing the shuttle cysteines in close proximity with the active site cysteines (C352/C255) (Step 4). Through another two-step disulphide exchange the active site cysteines are reduced leaving the shuttle cysteines oxidised (Steps 5 and 6). The active site cysteines become reoxidised through reduction of FAD, through which the protons are passed to molecular oxygen (Step 7). The flexible peptide then returns to the original conformation to enable another reoxidation reaction (Step 8). Figure adapted from Sevier, C., et al[23]

The flexible peptide of Ero1p does not just facilitate disulphide exchange between the shuffle and active-site cysteines. It also likely obstructs the active-site cysteines from direct binding of substrates requiring oxidation which would result in non-specific formation of disulphide bonds[23].

The components of the OPF pathway are under careful regulation governed by the oxidising conditions of the ER. Excessive oxidising conditions in the ER leads to inactivation of Ero1p which would also result in accumulation of reduced PDI, which may have enhanced isomerase activity[30], enabling it to refold non-native disulphide bonds that would form in an oxidising environment, as well PDIs chaperone activity being dependent upon the protein being in the reduced state[31]. Regulation of Ero1p is primarily governed through PDI and assisted by reduced substrate as PDI is able to directly reduce the regulatory bonds of Ero1p[32]. The oxidation of PDI can be catalysed by inactive Ero1p which, in turn, becomes active[32] through disulphide

transfer from one of the pairs of regulatory cysteines to the active site of the PDI molecule hence reducing the regulatory cysteine and enabling activation of Ero1p[32].

Ero1p possesses multiple regulatory disulphide bonds, the first of which to become reduced by PDI is the C143-C166 non catalytic cysteine pair, followed by C150-C295[33] and finally the longest disulphide bond C90-C349[24]. This results in a range of activation states of Ero1p dependent upon the oxidising conditions and abundance of substrate within the ER[33].

PDI activity is therefore regulated by its requirement, in an excess of substrate PDI is required to continually catalyse OPF and therefore Ero1p must remain active to catalyse PDI reoxidation. In conditions of scarce substrate PDI is more often in the oxidised state and so Ero1p will inactivate through oxidation of the regulator disulphide bonds from the active-site cysteines of Ero1p[32]. Evidence for this is that in mutants containing point substitutions of the shuffle cysteines auto-oxidation of a regulatory cysteine from the active-site cysteines can occur[32].

Ero1p can also be efficiently inactivated by oxidised PDI[32]. The a' domain of PDI in its partially oxidised state is more able to oxidise the regulatory bonds of Ero1p than the a domain in its fully oxidised state[32]. Oxidised PDI inactivates Ero1p quickly but Ero1p is activated slowly by reduced PDI[32]. Such rapid inactivation is to be expected as Ero1p needs to respond quickly to an oxidising environment.

A by-product of Ero1p oxidative activity is the formation of H_2O_2, a member of the reactive oxygen species (ROS) family, which is produced in equimolar amounts for each oxidation event Ero1p catalyses[29]. H_2O_2 has both oxidative and reductive effects *in vivo* and can cause damage to a number of vital cellular components such as lipids, nucleic acids and proteins[34]. A build-up of ROS can therefore have detrimental effects upon the cells survival and hence careful control on Ero1p may act to regulate ROS build up[24].

1.1.3 Homologues of protein disulphide isomerase in yeast

As well as PDI in yeast there are four non-essential ER-located PDI homologues whose upregulation in Δ*pdi1* mutants can restore viability[4]. These are Mpd1p, Mpd2p, Eug1p and Eps1p, which share some functional homology with PDI, but are expressed in low levels[4]. Mpd1p and Mpd2p are the only two homologues that have

significant OPF activity, although dramatically decreased compared with PDI[35] and hence can restore viability from upregulation, albeit with significant cell defects[4]. Eug1p and Eps1p instead have roles in isomerisation[4] and ER chaperoning[36], respectively. These homologues appear to fill niche roles[37] and therefore a knock-out of *pdi1* may lead to upregulation of one or more of these PDI homologues to restore viability[38].

1.2 Mechanisms of hydrogen peroxide detoxification within the endoplasmic reticulum

1.2.1 Glutathione peroxidases in humans and yeast

Within the mammalian ER there are 3 known peroxidases that act to detoxify H_2O_2: Peroxiredoxin IV (PRxIV), glutathione peroxidase 7 (GPx7) and glutathione peroxidase 8 (GPx8)[39], although at high concentrations of H_2O_2 PRxIV is inactivated[40]. In *S. cerevisiae*, however, there are no obvious ER-localised homologues of these proteins[32][41] suggesting that disulphide bond formation may be capped to prevent accumulation of ROS. Yeast contains multiple proteins involved in detoxification of H_2O_2 including 5 peroxiredoxins, a cytosolic catalase, a peroxisomal catalase, a mitochondrial resident cytochrome C peroxidase[42], as well as evidence for GPx1, GPx2 and GPx3 also being expressed within yeast[43]. GPx2 and GPx3 are localised to the cytosol[44] while GPx1 is localised to the cytosol and mitochondria[45]. GPx1, GPx2 and GPx3 are in fact phospholipid hydroperoxide glutathione peroxidases and are therefore responsible for the repair of the peroxidation of membrane lipids[43], the damage of which is a result of the oxidising activity of ROS. Presence of these proteins prevent accumulation of ROS as a result of other cellular functions in particular the leakage of electrons from the electron transport chain within the mitochondria but also as a result of environmental stresses[46]. None of these proteins, however, are localised to the ER, and therefore a regulatory system is in place to control levels of H_2O_2 production.

1.2.2 Regulation of hydrogen peroxide production in yeast

As there are no proteins in yeast that have been identified to directly detoxify H_2O_2 in the ER therefore H_2O_2 accumulation must be prevented through another means. Sevier, C. S., et al. have suggested that levels of H_2O_2 are controlled through inactivation of Ero1p[24]. As ROS are oxidising agents they oxidise of the regulatory

cysteine pairs of Ero1p[24] therefore inhibiting OPF and with it H_2O_2 production, thereby forming a negative feedback loop. Overexpression of a disulphide bonded protein in a yeast is therefore limited by this H_2O_2 regulation mechanism as unlike the mammalian ER there are no proteins such as GPx7 and GPx8 that can directly detoxify H_2O_2.

1.2.3 Glutathione peroxidase 7

GPx7, also known as NPGPx, is 187 amino acids in length and has a 19 residue N terminal cleavable signal sequence that mediates its localisation to the ER and retention in the ER lumen[47].

GPx7 is structurally similar other members of the GPx family, in particularly GPx4[48] and is able to catalyse the degradation of H_2O_2. Despite this similarity the function of GPx7 is considerably different to that of other members of the GPx family. One distinct difference is that, unlike the other members of the GPx family, with the exception of GPx5[49], a catalytically active cysteine is utilised over a selenocysteine in GPx7[47]. As GPx4 and GPx7 share a common ancestor, there has been a substitution of this selenocysteine for the non-selenium containing form[50] during divergence of GPx7 from the other members of the GPx family[51]. Another key difference is that GPx7 is lacking in the loop for GSH specificity[47]. This results in GPx7 having decreased affinity for GSH but allows for interaction with PDI[47]. Therefore GPx7 is able to couple detoxification of H_2O_2 in the ER to the reoxidation of PDI.

GPx7 is expressed in a range of tissue types in mammalian systems[48], allowing for ubiquitous detoxification of H_2O_2 produced in the ER as a result of OPF[29]. A conserved characteristic of all known members of the human GPx family is the catalytic tetrad, this consists of four residues that forms an active site for the catalysis of decomposition of H_2O_2. These conserved residues are the catalytic cysteine or selenocysteine, a glutamine and a tryptophan and an asparagine directly adjacent to each other in the primary structure of the peptide (Fig 1.5., Fig 1.6.)[52]. It is suggested that this tetrad enables the hydroxylation of the thiol of the catalytically active Cys[52][53] hence enabling the detoxification of H_2O_2 and thereby making GPx7 an oxidising agent for PDI. In GPx7 these residues are C57, Q92, W142 and N143[52] (Fig 1.6.).

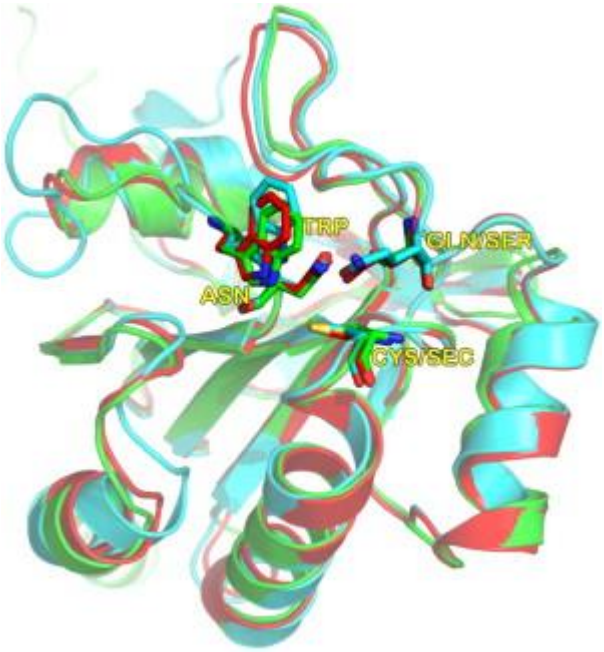

Fig 1.5. Overlay of the structures of the monomeric subunits of GPx4, GPx7 and GPx8.
The structures of overlayed monomeric GPx4(cyan), GPx7(red) and GPx8(green) indicating structural similarities between the three proteins. The residues of the catalytic tetrad is indicated by yellow text showing the conserved Trp and Asn residue of all three peptides as well as Gln(present in GPx7 and GPx8)/Ser(present in GPx8) and Cys(present in GPx7 and GPx8)/Sec(selenocysteine present in GPx4). Figure from Maiorino, M., et al.[52].

```
Relative Position
     1         10         20         30         40         50         60
     |         |          |          |          |          |          |
GPx7 ----------------------MVAATVAAAWLLLWAAACAQQEQDFYDFKAVNIRGKLVSLEKYRG
GPx8 MEPLAAYPLKCSGPRAKVFAVLLSIVLCTVTLFLLQLKFLKPKINSFYAFEVKDAKGRTVSLEKYKG
       70         80         90         100        110        120        130
       |          |          |          |          |          |          |
GPx7 SVSLVVNVASECGFTDQHYRALQQLQRDLGPHHFNVLAFPCNQFGQQEPDSNKEIESFARRTYSVSF
GPx8 KVSLVVNVASDCQLTDRNYLGLKELHKEFGPSHFSVLAFPCNQFGESEPRPSKEVESFARKNYGVTF
          140        150        160        170        180        190        200
          |          |          |          |          |          |          |
GPx7 PMFSKIAVTGTGAHPAFKYLAQTSGKEPTWNFWKYLVAPDGKVVGAWDPTVSVEEVRPQITALVRKL
GPx8 PIFHKIKILGSEGEPAFRFLVDSSKKEPRWNFWKYLVNPEGQVVKFWKPEEPIEVIRPDIAALVRQV


GPx7 ILLKREDL
GPx8 IIKKKEDL
```

Fig 1.6. Protein sequence alignment of human GPx7 and GPx8
A comparison of the protein sequence of human GPx7 and GPx8 and the following conserved regions of interest identified: the cleavable signal peptide of GPx7$^{(CP)}$(red), the transmembrane domain of GPx8$^{(CP)}$(blue), the catalytic cysteine of the catalytic tetrad(dark green), the remaining three residues of the catalytic tetrad(light green), the auto-oxidative cysteine(grey) and the ER retention sequence(pink).

As well as having roles in the detoxification of H_2O_2 GPx7 also has a general role in the indirect involvement in reducing intracellular oxidative stress through regulation of certain target proteins. One of these proteins is GRP78[54], a 78kDA essential ER chaperone which is considered a master regulator of the unfolded protein response[55]. The formation of a disulphide bond between C86 of oxidised GPx7 and either C420 or C41 and induces the formation of the intramolecular C41 to C420 disulphide bond in GRP78, which increases its affinity for denatured or misfolded proteins[54]. Therefore in the absence of a reducing substrate for GPx7, as would occur under ER oxidative stress, the chaperone effects of GRP78 on misfolded proteins are increased.

1.2.4 Glutathione peroxidase 8

Less is known about GPx8 than GPx7, but it is a type 1 a transmembrane ER protein[47][56] that is 209 amino acids in length. Unlike the other members of the GPx family both GPx7 and GPx8 are ER localised, although resident to the ER lumen and transmembrane respectively for GPx7 and GPx8 respectively. It also appears to serve a similar function as GPx7 and likely operates by a similar mechanism[47]. GPx8, similar to GPx7, also is lacking both a loop for GSH specificity and has a cysteine rather than a selenocysteine and therefore also has a substrate preference of PDI over GSH[47]. The catalytic tetrad of GPx8 is similar to that of GPx7, possessing a cysteine rather than a selenocysteine but there is a substitution of glutamine for serine (Fig1.6.), it is suspected that this substitution does not result in any significant changes to the functionality of the protein as serine would still be able to accept a proton from the catalytically active cysteine[52]. The residues of the catalytic tetrad in GPx8 are therefore C79, S114, W164 and N165[52](Fig 1.6.).

One key difference between Gpx7 and GPx8 is that GPx8 is an ER transmembrane protein. This allows GPx8 to serve a role in preventing passing of Ero1p derived H_2O_2 across the ER membrane and into the cytosol[57]. Importantly as both GPx8 and Ero1p are upregulated in response to ER stress[57], the positive feedback loop of increased OPF leading to more ROS generation and therefore further increases to ER stress is interrupted by the H_2O_2 detoxifying effects of GPx8[57].

The crystal structure of GPx8 is shown below(Fig 1.7).

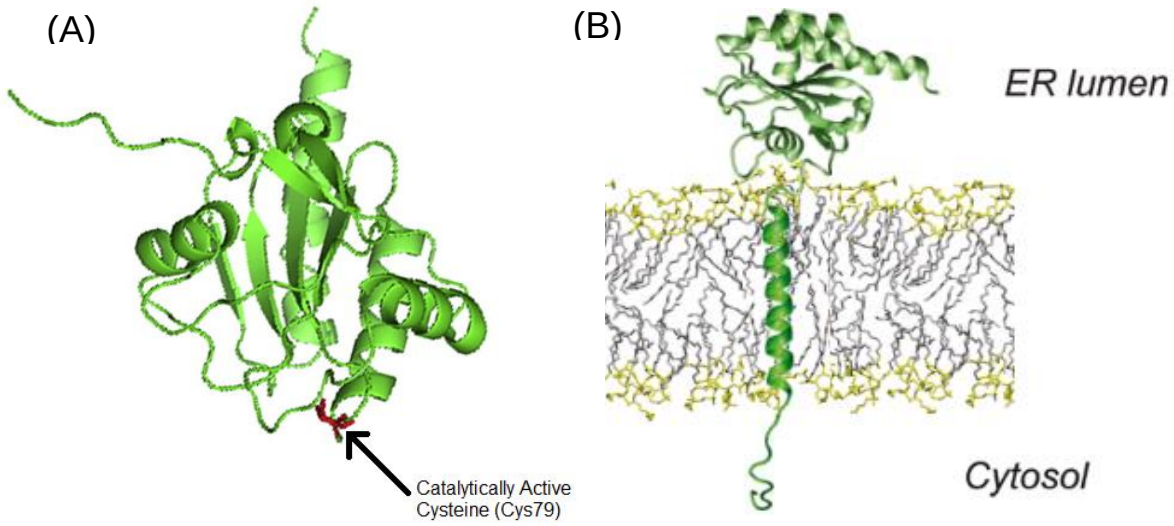

Fig 1.7. Crystal structure of GPx8
(A) The crystal structure of a molecule of GPx8 absent of transmembrane domain with catalytically active cysteine C79 shown in red. Figure adapted from Nguyen, V. D., et al[47]. (B) Crystal structure of GPx8 in the ER membrane with light green transmembrane domain cytosolic tip. Figure adapted from Morikawa, K., et al[58]

1.2.5. Mechanism of hydrogen peroxide detoxification by glutathione peroxidases 7 and 8

Although both GPx7 and GPx8 have very low levels of peroxiredoxin activity with GSH, they do have much higher levels of PDI peroxidation with GPx7 having at least a 95 times greater activity with PDI as a substrate compared with GSH and GPx8 has at least 250 times greater activity[47], although there is some dispute regarding this finding[50]. GPx7 and GPx8 therefore utilise H_2O_2 to oxidise reduced PDI detoxifying H_2O_2 while also enabling PDI to continue to perform OPF. Despite the lower specificity of GPx7 and GPx8 for GSH over PDI there is still competition between these two substrates[52] and therefore the rate of PDI oxidation is determined by the concentration of GSH. It has been shown that GPx7 and GPx8 have differing specificities for different members of the human PDI family, with the highest activity being in PDI, ERp72 and ERp46 while ERp57 and P5 had lower activities[47].

There are currently two proposed models for the mechanism of GPx7 activity: a single-cys-mechanism and a 2-cys-mechanism[39], based on current evidence the single-cys-mechanism is the favoured model. In the 2-cys-mechanism it was

suggested that reduction of substrates was dependent upon an intramolecular disulphide bond between C86 and C57 within GPx7 that forms in oxidative conditions and thereby acting as a sensor for oxidative stress[59]. In support of this mechanism a disulphide bond was identified between these two cysteines using mass spectrometry[59]. However, a GPx7^{C86A} mutant exhibited WT like activity suggesting the single-cys-mechanism over the 2-cys-mechanism[39], it was also demonstrated that the disulphide bond between C86 and C57 is only present in the oxidation of GPx7 and when there is an absence of reducing substrate[39].

The single-cys-mechanism is the current proposed model for both GPx7, it is likely that GPx8 operates in a similar way, as both of these proteins have a peroxidatic cysteine(C_P), C57 for GPx7 and C79 for GPx8[47], but are absent of a resolving cysteine(C_R)[50] and have closely related amino acid sequence homology (Fig 1.6.).

The single-cys mechanism suggests that the C_P[50] is responsible for both the oxidation of H_2O_2 and the oxidation of PDI, interacting preferably with the *a* domain of PDI[39]. The initially reduced GPx7 of GPx8 catalyses the conversion of H_2O_2 to H_2O and an –SOH (sulfenic acid) group attached to C_P[39][50]. It is suspected that the conserved catalytic tetrad is responsible for enabling hydroxylation of the thiol of C_P through oxidation of the thiol group by glutamine allowing the formation of sufenic acid[52][53]. The liberated proton can interact with the hydroxyl group formed from the splitting of H_2O_2 forming H_2O.

In the presence of a reducing substrate such as PDI or GSH a reduced thiol group from either of these substrates interacts with the C_P-SOH group yielding H_2O and forming a disulphide bond between the thiol of the reducing agent and the thiol of the C_P[39][50]. The next step in the mechanism is a reduction of the C_P by a second reduced thiol group, in the case of PDI this is from the second cysteine in the CXXC domain while in the case of reduction by GSH a second molecule of GSH is used to reduce C_P[39] (Fig 1.8). This results in formation of the oxidised state of the PDI active site which is then able to catalyse OPF, or in the case of GSH reduction a molecule of glutathione disulphide (GSSG) is formed[39] (Fig 1.8). This therefore couples the detoxification of H_2O_2 to OPF through the re-oxidation of PDI.

In the case where there is no available reducing substrates C86 of GPx7[39] or C108 of GPx8 (Fig1.2) could have a role in generating a stable form of hydroxylated proteins in the absence of reducing substrates[39]. GPx7 and GPx8s detoxifying

effects on H_2O_2 would lead to increased generation of sulfenic acid (-SOH) due to there being no reducing substrates to accept the electrons from reduced GPx7[39] and GPx8. The –SOH group on C57 could therefore react with the –SH group on C86 or C108 for GPx7 and GPx8 respectively. This would yield one molecule of H_2O and a disulphide bond between C57 and C86 for GPx7 or C79 and C108 for GPx8 (Fig1.5.). Therefore both C86 and C108 for GPx7 and GPx8 respectively are auto-oxidative cysteines (C_{AO}). Sulfenic acid is an oxidising agent and can cause oxidative damage to either nearby protein or itself if it is not immediately reduced by either PDI or GSH, this results in C_{AO} being critical in removing these sulfenic groups detoxifying itself[39]. Another advantage of this mechanism of action is that in an absence of reducing substrate GPx7 and GPx8 are capable of reducing an equimolar amount of H_2O_2 before becoming inactive which would reduce the oxidative stress on the ER. The C_{AO} in GPx7 also prevents the formation of significantly less active GPx7 homodimers resulting from a disulphide bond bridging two C57s[39].

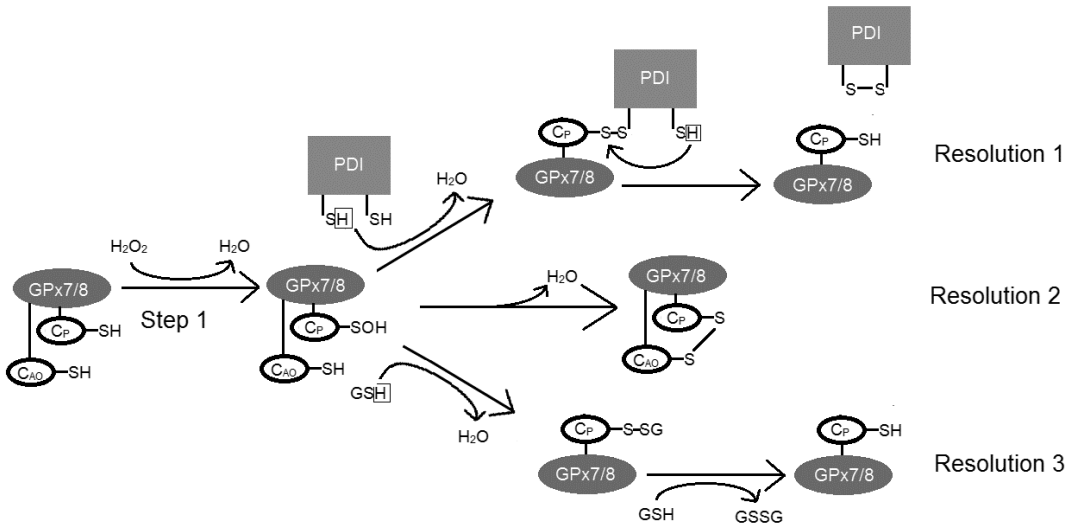

Fig 1.8. The single-cys model for GPx7 and GPx8 activity with the three suggested resolutions of the sulfenic acid produced by H_2O_2 detoxification.
A simplified mechanism for the detoxification of H_2O_2 by GPx7 and GPx8, the initial step is conversion of H_2O_2 to H_2O using C_P resulting in the thiol of C_P becoming hydroxylated to a sulfenic acid group (Step1). In order to resolve this sulfenic acid group there are three potential pathways. In presence of substrate GPx7 or GPx8 can couple the removal of the sulfenic acid group to PDI (Resolution 1) or GSH (Resolution 3) oxidation in a two-step process. The first oxidises C_P forming a disulphide bond between the target protein and C_P yielding H_2O_2. The second step is a reduction event of C_P by a second reduced thiol. In the absence of utilisable substrate an intramolecular bond can be formed with the auto-oxidative cysteine (C_{AO}) removing the sulfenic acid group but inactivating the protein (Resolution 2).

The salvage and detoxification of Ero1p generated H_2O_2 by GPx7 and GPx8 occurs near instantly[39][57], this is a result of both GPx7 and GPx8 associating with Ero1p directly[56]. GPx7 and GPx8 bind to the side furthest from the catalytic site and FAD cofactor of Ero1p[60] to a region of the peptide containing two regulatory cysteines C208 and C241 (Fig 1.9.). This regulatory cysteine pair prevents entry of oxygen to the FAD cofactor and GPx7 and GPx8 binding when they are in the oxidised form[61]. When Ero1p is reduced by PDI, however, this disulphide is broken and hence allows entry of oxygen which then can then be reduced to H_2O_2 by the FAD cofactor[61] (Fig 1.9.). The breakage of this disulphide bond also allows docking of the GPx8 or GPx7 proteins[61], which due to its proximity to the site of formation of H_2O_2 rapidly catalyses conversion to H_2O and a sulfenic acid group on C_P.

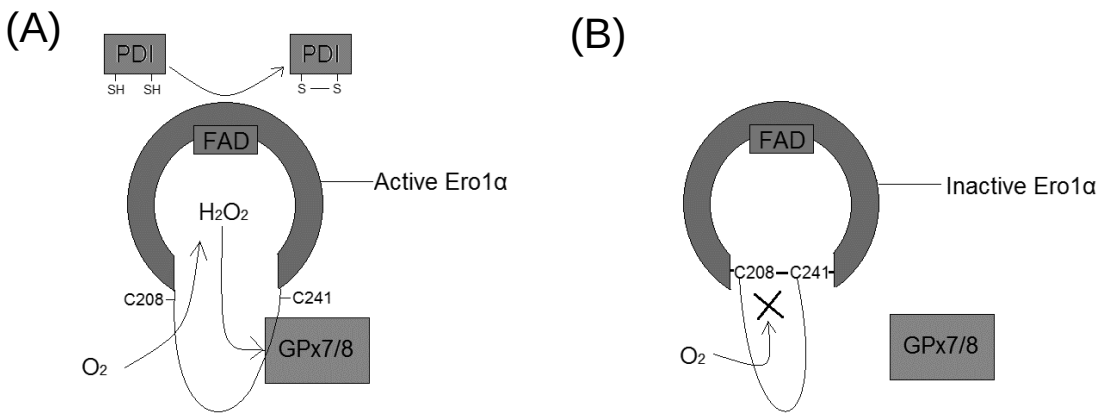

Fig 1.9. The regulation of Ero1α by the C208/C241 cysteine pair
Entry of oxygen to the FAD cofactor of Ero1α is controlled by a C208/C241 regulatory disulphide bond. A) In abundance of substrate Ero1α is active and the C208/C241 cysteine pair is reduced, this allows oxygen to accept protons from reduced FAD forming H_2O_2. C208/C241 in the reduced state also allows binding of GPx7 and GPx8 to Ero1α. This allows rapid degradation of H_2O_2. B) In the absence of substrate the C208/C241 disulphide bond is formed preventing entry of oxygen to FAD and inhibiting GPx7 and GPx8 binding. Figure adapted from Ramming, T., et al.[61].

1.3 Localisation of proteins to the endoplasmic reticulum in yeast

1.3.1 Endoplasmic reticulum signal sequences

Nascent peptides that require posttranslational modifications typically enter the ER co-translationally and for which require a signal recognition particle (SRP), this transports the peptide with associated ribosome to the Sec61 ER membrane

translocon. The nascent protein then enters the ER as it is being translated before cleavage of the SRP[62].

Traditionally a pre-pro secretion signal from the yeast was used for the expression of non-native proteins, this consisted of a pre region of a 19 residue signal sequence terminating in a peptidase cleavage site followed by the pro region, a 66 residue region followed by a Kex2 endoprotease cleavage site and ending in an EAEA 4 residue peptide, removed by Ste13[63]. This sometimes leads to unintended products due to incomplete cleavage by Ste13 or Kex2[63].

Use of an Ost1 pre-sequence MATα pro-sequence hybrid resulted in increased efficiency of foreign protein expression, the Ost1 pre-sequence is suitably hydrophobic to enable co-translational translocation[63]. Addition of the MATα pro-sequence results in increased export to the ER through binding of the pro-sequence to Erv29[63],a chaperone involved in packaging of nascent proteins into COPII vesicles for export to the golgi apparatus[64].

1.3.2 Endoplasmic reticulum retention sequences

The ER retention of proteins is mediated through their C-terminus, at which the 4 residue sequence resides: KDEL, among others, for animals[65] while yeast exclusively utilises HDEL. The protein responsible for recognition of this HDEL sequence is Erd2p, an integral membrane protein with 7 helical transmembrane domains[66][67]. The N terminal domain of Erd2p is located within the lumen while the C terminal domain is located in the cytoplasm[67]. Residues in transmembrane domains 1, 2, 5 and 6 are important in facilitating ligand binding and hence it is likely that these residues form a hydrophobic pocket, in which the highly polar HDEL residue can bind[67]. In the human KDEL receptor 4 residues are key in substrate binding, Arg5, Asp50, Tyr162 and Asn165 and all are located luminally[66], there is likely to be some variation in binding mechanism due to yeast only being able to utilise the HDEL tetrapeptide despite the only alteration to that of human KDEL sequence is a substitution of the charged residue Histidine for the charged residue Lysine. Nonetheless, the Asp50 residue is conserved in all known Erd2 sequences, with the exception of in *K. lactis*[66], it is therefore likely that this contacts the first residue of the ER retention sequence[67].

Nascent proteins destined for ER retention are first transported into the Golgi to allow for post-translational modifications to take place before retrieval back into the ER through a salvage compartment on the cis side[68]. This occurs through binding of the HDEL sequence to Erd2p in the Golgi Apparatus, the receptor:HDEL-protein complexes are gathered into COPI coated vesicles and through retrograde vesicular protein transport the vesicles dock with the tSNARE Ufe1p with other components that enables receptor mediated retrieval of HDEL proteins[69]. An Asp193 residue of transmembrane domain 7 is required for this retrograde transportation mechanism of the receptor-ligand complex[BN].

1.4 Aims of the project

The aims of the project was to increase the rate of OPF in *S. cerevisiae*. As many pharmaceutical products require disulphide bond formation in a biological system increasing the rate of OPF in yeast would generate an efficient factory at producing these biopharmaceuticals. To increase OPF *in vivo* two main avenues were pursued, the first was to investigate a potential mutation that resulted in retained viability of a Δ*pdi1* strain, as this would likely supplement OPF and hence be a key target for upregulation to assist disulphide bond formation. Furthermore the functions of the yPDI homologues are still largely unknown and so a mutation that results in upregulation in one or more of these homologues as a result of a Δ*pdi1* may shed light upon their function and would form a better model for OPF in yeast

The second approach was through expression of recombinant GPx7 and GPx8 in yeast. As control of levels of ER ROS is dependent upon inactivation of Ero1p[24] it is therefore a limiting factor on OPF of high expression proteins, such as biopharmaceuticals. The work of Zito, E., has shown that expression of the mammalian ER localised PRxIV in yeast can reoxidise yPDI[70]. Therefore GPx7 and GPx8 may alleviate ROS stress associated with OPF as well as increasing the rate of OPF through coupling of PDI through coupling the degradation of H_2O_2.

Chapter 2 - Materials and Methods

2.1 Materials

2.1.1 Yeast and bacterial strains

2.1.1.1 *Saccharomyces cerevisiae* strains

Table 2.1.1.1: Strains of *S. cerevisiae* used in the project

Strain name	Genotype	Summary
BY4741	*MATα his3Δ0, leu2Δ0 met15Δ0 ura3Δ0*	Parent strain
2736	*MATα, ade2-1, ura3-1, leu2-3, trp1-1, his3-11, -15, pdi1::HIS3* + [*GAL1-PDI1-URA3*-CEN]	Δ*pdi1* genomic deletion strain with viability maintained by the *PDI1* containing plasmid
DN5	*MATα/α, his3/his3, leu2/leu2, ura3/ura3, trp1/trp1, pdi1::HIS3/pdi1::HIS3*	Cross of 2736 and JML3, use of 5FOA to cure strain of *pdi1* containing plasmid (Natalia 1994). Viable PDI-deficient strain
Δcox4	Δ*cox4::HIS*	Deletion of COX4 gene encoding cytochrome c oxidase subunit IV. Decreased H_2O_2 production removal.
Ski4		Super secretor of killer toxin carrying a

		mutation in the *SKI4* gene
S6	Wild type	Strain sensitive to killer toxin

2.1.1.2 *Escherichia coli* strains

Table 2.1.1.2 Strains of *E.coli* used in the project

Strains	Production
Z-Competent™ *E.coli* cells, DH5α *E.coli* strain	Prepared by G. Staniforth (School of Biosciences, Kent) using Z-Competent™ *E.coli* Transformation kit (G-Biosciences)
Top 10 Competent *E.coli* cells, commercially available Top 10 Competent *E.coli* cells.	Prepared by E. Kazana (School of Bioscience, Kent), competency induced using KOAc, $CaCl_2$, $MnCl_2$ and $MgCl_2$.

2.1.2 Media Recipes

All media sterilised in a Classic Prestige Medical (Quirumed) autoclave prior to use.

Table 2.1.2 Recipes for media used in the project

Medium	**Recipe**
YPD	2% D-Glucose Anhydrous, 1% Yeast Extract, 2% Bactopeptone, (+2% Agar for solid medium)
Synthetic Defined Drop Out Medium	2% D-Glucose Anhydrous, 0.67% YNB w/o amino acids, 0.16%(-Leu) / 0.195%(-Ura) / 0.155% (-Leu –Ura) Synthetic Complete Drop-Out Mixture, (+2% Agar for solid medium)
5FOA Medium	2% D-Glucose Anhydrous, 0.67% YNB w/o amino acids, 0.2% Complete SC Mixture, 5FOA added by filter sterilsation to a final concentration of 5.74mM post autoclaving and once medium had cooled to ~60˚C. Plates stored at 4˚C.
LB with Ampicillin	1% Tryptone, 0.5% Yeast Extract, 1% NaCl, (+2% Agar for solid medium) and autoclaved. For solid medium ampicillin added to a final concentration of 100µg/ml once medium had cooled to ~55˚C. For liquid medium ampicillin added to a final concentration 100µg/ml of immediately prior to use.

Prior to plating cells onto agar plates they were dried in a drying oven for ~10 min at ~65˚C.

2.1.2.1 Making killer toxin assay solid medium

2.1.2.1.1 Base Agar

0.5% (w/v) Yeast Extract, 0.5% (w/v) Bactopeptone, 1.5% (w/v) Agar, 0.05M Citric Acid and 0.1M Na_2HPO_4 in 90% of total intended volume distilled water (dH_2O), adjusted to pH 4.6-4.8 with HCl and then autoclaved. 4% D-Glucose Anhydrous added by filter sterilisation post autoclaving and once medium has cooled to ~55˚C filter sterilised Methylene Blue added to a final concentration of 0.375mM. 20mL added to each 8.5cm diameter plate and left to solidify.

2.1.2.1.2 Top Agar

Made in an identical fashion to Base Agar but without the addition of methylene blue. O/N culture of S6 yeast strain diluted to OD_{600} 0.1 and regrown to OD_{600} 0.4-0.5 and added to Top Agar to a cell density of $5x10^6$ cells/ml. ~5ml of Top Agar poured over solidified Bottom Agar giving a total plate media volume of ~25ml of Killer Toxin Assay agar. Made on day of assay.

2.1.3 Chemicals used

Table 2.1.3 A list of chemicals used the project and their manufacturer

Chemical Used in Media	Manufacturer
D-Glucose Anhydrous	Fisher Scientific
Yeast Extract	Fisher Scientific
Bacto™ peptone	Fisher Scientific
Granulated Agar	Fisher Scientific
YNB w/o Amino Acids	Fisher Scientific
Synthetic Complete Drop-Out Mixtures	Formedium
Complete SC Mixture	Formedium

Citric Acid	Sigma-Aldrich
Na_2HPO_4	Sigma-Aldrich
Methylene Blue	Sigma-Aldrich
Tryptone	Fisher Scientific
NaCl	Melford

2.1.4 Oligonucleotide sequences

Table 2.1.4 The sequence of oligonucleotides used for polymerase chain reactions

Name	**Sequence**
KpnI_GPx7_F	CCCGGTACCATGCATCACCATCACCACCATATG
SacI_GPx7_R	CCCGAGCTCTTATTATAAGTCTTCTCGCTTCAGTAG
KpnI_GPx8_F	CCCGGTACCATGCATCACCATCACCACCATGAGCCTCTTGCAGCTTACCC
SacI_GPx8_R	CCCGAGCTCTCATAGATCCTCTTTCTTTTTTATGATC
BamHI_GPx7_F	CCCGGATCCATGCATCACCATCCCACCATATGCAGCA
XbaI_GPx7_R	CCCTCTAGATTATTATAAGTCTTCTCGCTTCAGTAG
BamHI_GPx8_F	CCCGGATCCATGGAGCCTCTTGCAGCTTAC
XbaI_GPx8_R	CCCTCTAGATCATAGATCCTCTTTCTTTTTTATGATC
-983_pdi1_1F	CGTTCTCATCGTCTAGCAAATCATCGGG
-972_pdi1_1R	GCGACGCTTTGTTTGACCTCAGGG
-500_pdi1_2F	CATTAGTGCCCACCGTTTGAGCGTG
-504_pdi1_2R	CTCAGTCTCCAAAGGGCAAAGAAACCC

All oligonucleotides were designed during this project and produced by Eurofins Genomics, for more information see section 2.2.10.

2.1.5 Antibodies used

Table 2.1.5 The suppliers of the antibodies used during this product and the dilution at which they were used

Antibody	Supplier	Dilution
Yeast PDI	Antibody made Capra Sciences against antigen purified by Beal, D. M. (School of Biosciences, Kent)	1/1000
Monoclonal anti-polyHistidine-Peroxidase clone HIS-1 IgG_{2a}	Sigma-Aldrich	1/1000
Monoclonal HA-probe IgG_{2a}	Santa Cruz Biotechnology	1/200
Yeast PGK	Antibody made by York Biosciences against purified PGK1 purchased from Sigma Aldrich	1/5000
Anti Gaussia Luciferase IgG	New England Biosciences	1/1000
Anti Rabbit IgG-Peroxidase	Sigma Aldrich	1/5000
Anti Mouse IgG-Peroxidase	Sigma Aldrich	1/2500

2.1.6 Plasmids used

Table 2.1.6 The name and details of plasmids used during this project

Plasmid Name	Backbone	Insert Details	Size (bp)	Source
pUKC3400	pBEVY-L 2 Micron	GPx7 with signal sequence (residues 2-19) replaced with 6xHis Tag. 5' *Kpn*I and 3' *Sac*I restriction sites.	7570	This Project
pUKC3401	pBEVY-L 2 Micron	Native GPx8. 5' *Kpn*I and 3' *Sac*I restriction sites	7684	This Project
pUKC3402	p6431 CEN	Native GPx7. 5' BamHI and 3' XbaI restriction sites	6580	This Project
pUKC3403	p6431 CEN	Native GPx8. 5' BamHI and 3' XbaI restriction sites	6676	This Project
pUKC3404	pTH644-L CEN	GPx7 with original human leader sequence with HA tag and Yeast ER retention signal	~7494	This Project
pUKC3405	pTH644-L CEN	GPx8 with original human leader sequence with HA tag and Yeast ER retention signal	~7560	This Project
pUKC3406	pTH644-L CEN	GPx7 with Yeast Ost1 pre-sequence and Yeast MAT pro-sequence with	~7584	This Project

		HA tag and Yeast ER retention signal		
pUKC3407	pTH644-L CEN	GPx8 with Yeast Ost1 pre-sequence and Yeast MAT pro-sequence with HA tag and Yeast ER retention signal	~7623	This Project
pKEHS780	pET-23 *E.coli* vector	GPx7 with signal sequence (residues 2-19) replaced with 6xHis Tag	~4200	Ruddock, L (Biocenter Oulu and Fauculty of Biochemistry and Molecular Medicine, University of Oulu)[(AC)]
Human GPx8 cDNA clone	pUC57 *E.coli* vector	Native GPx8	~3415	FlareBio CSB-CL848417HU1
pVT100U-K1	pVT100U 2 Micron	Killer Toxin	7995	-
GLuc Plasmid	pBEVY-U	Gaussia Luciferase with pre-pro MATα factor for intracellular localisation	-	Josse, L. D. (School of Biosciences, Kent)

2.1.6.1 Cloning vector maps

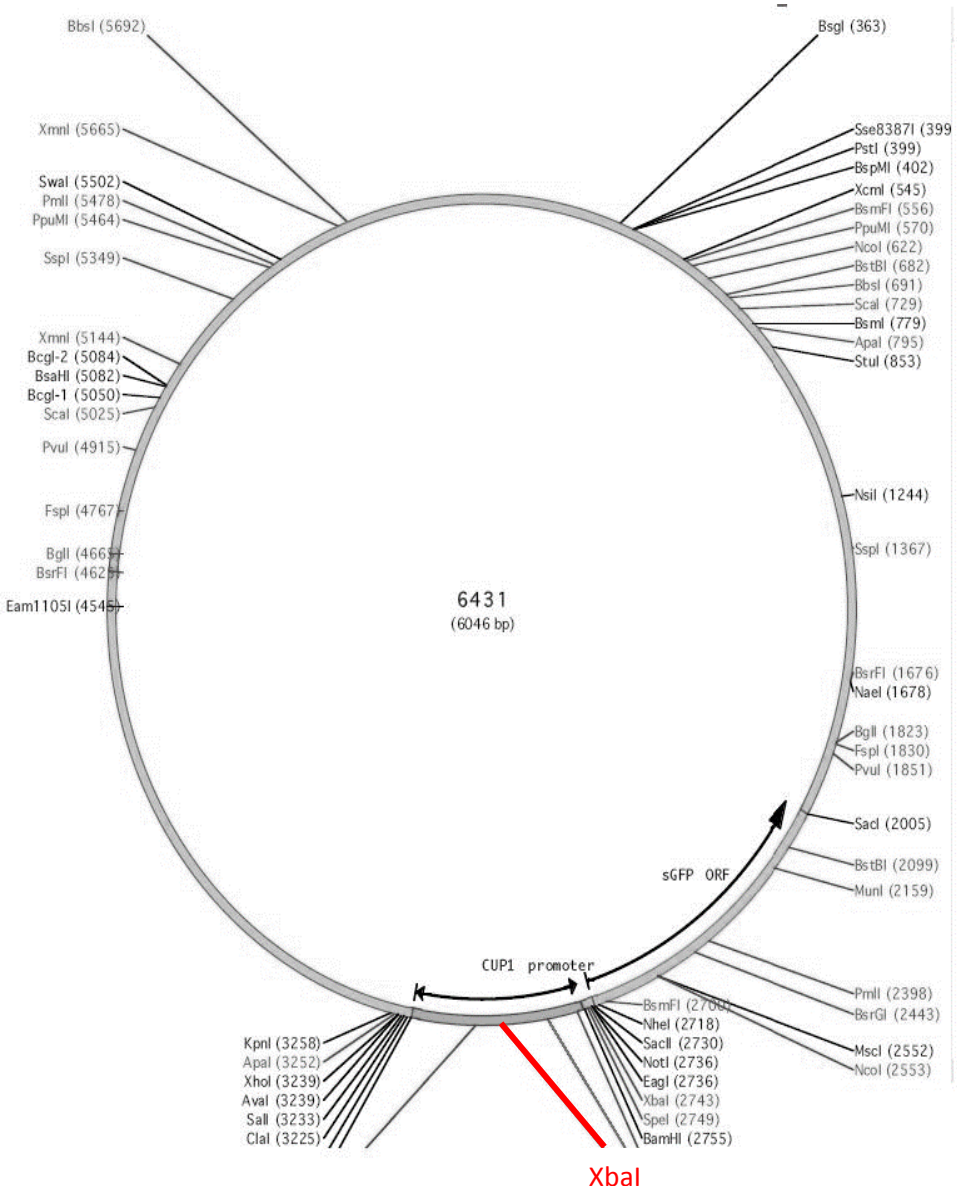

Fig 2.1. Plasmid map of p6431

Plasmid map of p6431 plasmid for GFP fusion, sites of interest including the CUP1 promoter and sGFP ORF included as well as restriction sites. The previously second XbaI restriction site present in the CUP1 promoter is shown in red. Map from Serio, T. (Molecular and Cellular Biology, The University of Arizona).

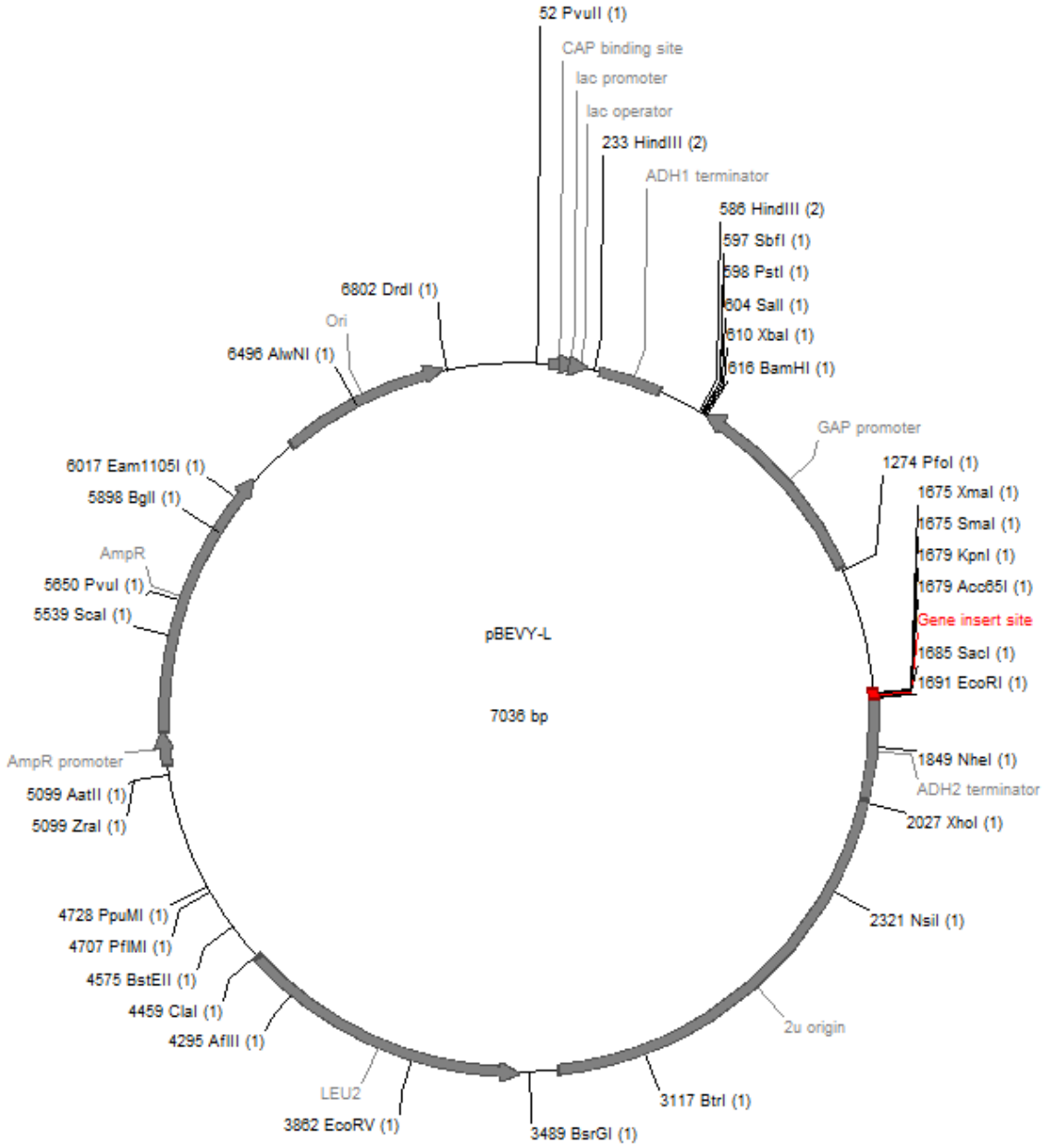

Fig 2.2. Plasmid map of pBEVY-L
Plasmid map of pBEVY-L plasmid backbone[71] for native GPx7 and GPx8, the gene insert site for which is shown in red. AmpR, GAP and lac promoter regions, selection markers AmpR and LEU2, ADH1 and ADH2 terminators and 2µ origins shown in dark grey. Common restriction sites of the vector shown.

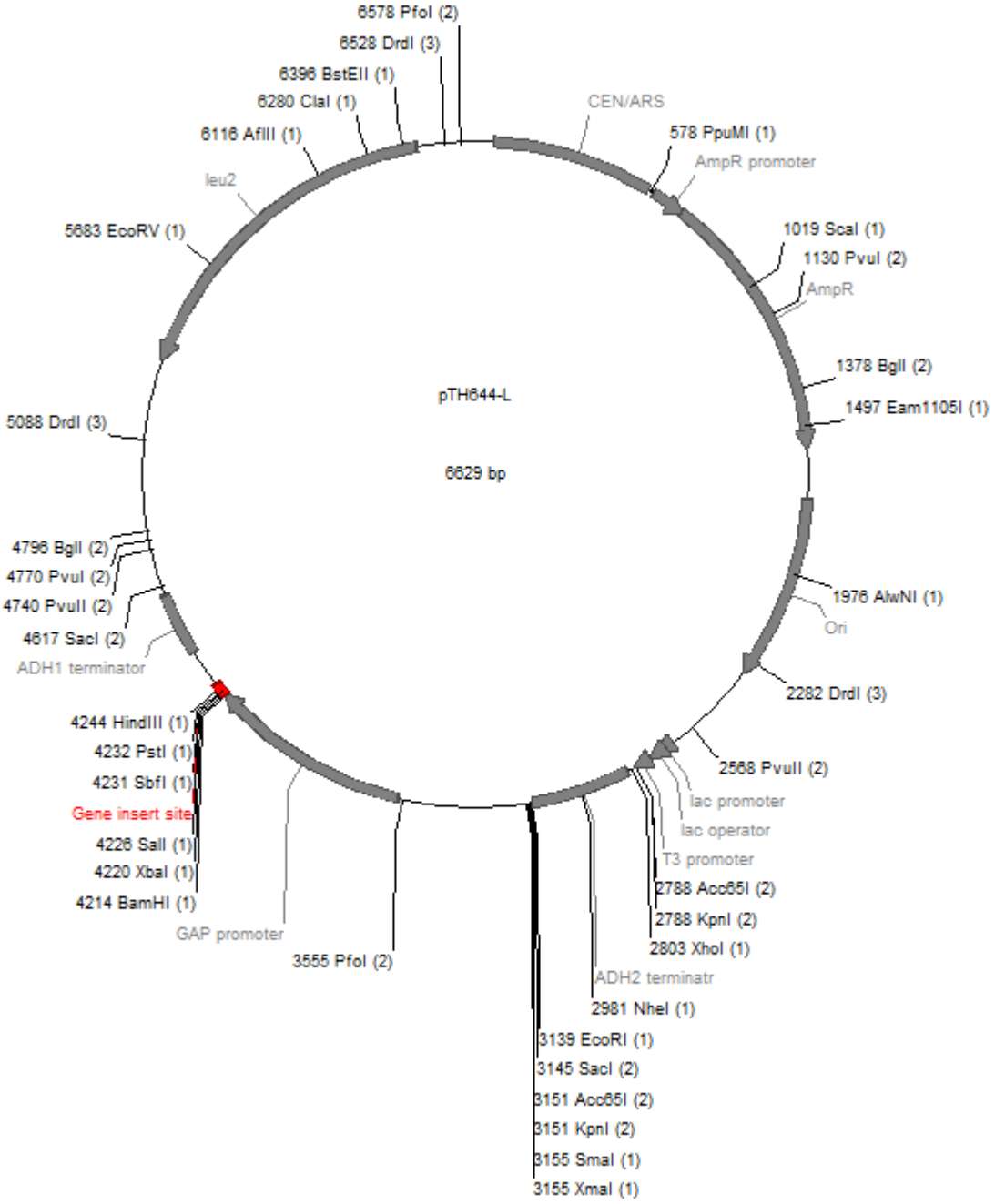

Fig 2.3. Plasmid map of pTH644-L
Plasmid map of pTH644-L plasmid backbone[72] for GPx7 and GPx8 constructs, the gene insert site for which is shown in red. AmpR, GAP and lac promoter regions, selection markers AmpR and LEU2, ADH1 and ADH2 terminators and CEN/ARS origins shown in dark grey. Common restriction sites of the vector shown.

All plasmid maps were made using ApE, A Plasmid Editor, software by Davis, M. W., (Deparment of Biology, University of Utah).

2.2 DNA techniques

2.2.1 DNA extraction from *E.coli*

A QUIprep Spin Miniprep Kit (Quigen) was used to extract plasmid DNA from *E.coli* as per the protocol supplied by the manufacturer. RNA was degraded through addition of RNAse prior to lysis using an alkaline based buffer. Successful lysis was confirmed through a colour change of sample using LyseBlue (Quigen). The sample was then neutralised using guanidine hydrochloride and adjusted to high salt content with potassium acetate[73] to facilitate DNA binding to a QuiaPrep silica gel membrane. Salts are washed from the DNA sample bound to the gel silica membrane with a solution of 70% ethanol with Tris-HCl, the DNA was then eluted using 50µL 10mM Tris-Cl and stored at -20˚C

2.2.2 Extraction of genomic DNA from yeast

Using a Epicentre Masterpure Yeast DNA purification kit genomic DNA extracts of yeast cultures were prepared, as was performed as per the manufacturers protocol. A *S. cerevisiae* culture grown for 16-18hr shaking incubation at 30˚C was pelleted at 13,000RPM and resuspended in Yeast Lysis Buffer (Epicentre) and incubated at 65˚C for 15 min. Protein was precipitated from the DNA sample using MPC Protein Precipitation Reagent (Epicentre) and pelleted along with cellular debris. DNA containing supernatant was removed and precipitated using isopropanol, the DNA was pelleted and washed in 70% ethanol before resuspension of the DNA in 30 TE µL buffer (10mM Tris-HCl, 1mM disodium EDTA) and stored at -20˚C.

2.2.3 Methods of quantification of DNA concentrations

2.2.3.1 NanoDrop

The $OD_{260}/OD_{280}/OD_{230}$ of DNA samples were measured using a NanoDrop Microvolume Spectrophotometer. A 2µL volume of each sample was measured against an elution buffer blank.

2.2.3.2 Spectrophotometry

DNA samples were diluted 50-fold in MilliQ H_2O in a UV Cuvette (BrandTech Scientific, Inc.) and OD_{260}/OD_{280} measured. Likewise the elution buffer was diluted 50-fold with MilliQ H_2O and was used as the blank.

2.2.3 *E.coli* transformation with plasmid DNA

2.2.3.1 Z-Competent™ *E.coli* cells

Z-Competent™ *E.coli* Cells prepaed by G.Staniforth (School of Biosciences, Kent) and stored at -80˚C, were defrosted on ice and 2µL of plasmid DNA added to each 20µL sample. The samples were mixed and left for 5 - 15 min on ice before plating onto LB + Ampicillin plates and incubated overnight (~16-18 hr) at 37˚C.

2.2.3.2 Top10 *E.coli* cells

Top10 *E.coli* Cells prepared by E.Kazana (School of Biosciences, Kent) were thawed on ice from a -80˚C stock, 2µL of plasmid DNA was added to a 100µL aliquot and left on ice for 30 min. Cells were then heat shocked at 42˚C for 60 sec, put back on ice for 2 min for recovery and then 900µL of LB medium was added to the aliquot and incubated for 1 hr at 37˚C. 50 µL of the sample was plated onto the LB+Ampicillin agar and incubated overnight (~16-18hrs) at 37˚C.

2.2.4 Yeast transformation

A yeast culture grown in YPD medium for ~16-18hrs in a shaking incubator at 30˚C was pelleted, the supernatant was removed and resuspended in 240µL 50% PEG (Sigma Aldrich), 36µL 1M LiAc, 34µL dH_2O, 10µL ssDNA , 2.5µL 14.3M β-mercaptoethanol (Sigma Aldrich) and ~0.25µg plasmid DNA. Samples were then incubated for 30 min at 30˚C and then for a further 30 min at 42˚C. The cells were pelleted at 2000 rpm for 5 min, the supernatant removed and the cell pellet resuspended in 100µL in sterile dH_2O(sdH_2O) and plated onto solid selective medium (table2.1.2). Culture grown for ~3-5 days at 30˚C and colonies replated onto fresh selective medium before use.

2.2.5 Standard polymerase chain reaction

Polymerase chain reactions (PCR) was performed with Taq polymerases from either from New England Biolabs® Inc. (NEB) or Invitrogen were used and hence conditions specific to these enzymes were needed. For both enzymes a Bibby Scientific™ Techne™ TC-312 Thermal Cycler was used with lid heating to 105˚C.

2.2.6.1 NEB Taq polymerase

The reaction mix for a PCR reaction using the NEB OneTaq Hot Start DNA polymerase was:

- 5µl 5x standard taq reaction buffer
- 0.5µl 10mM dNTP's
- 0.5µl 100µM forward primer
- 0.5µl 100µM reverse primer
- ~0.2µg target DNA

The thermocycling conditions used were:

- Initial denaturation (94˚C for 30 sec),
- 25-35 cycles of denaturation (94˚C for 30 sec),
- annealing (~5˚C lower than primer melting points for 45 sec),
- extension (68˚C for 1 min/kb) followed by
- a final extension step (68˚C for 5 min).

2.2.6.2 Invitrogen Taq polymerase

The reaction mix for a PCR reaction using the Invitrogen Taq polymerase was:

- 2.5µl 10x PCR buffer minus Mg^{2+},
- 0.5µl 10mM dNTP mixture,
- 0.75µl 50mM $MgCl_2$,
- 0.5µl 10µM forward primer,
- 0.5µl 10µM reverse primer,
- ~0.2µg target plasmid DNA
- 18µl MilliQ H_2O to make a ~25µl reaction mix.

The thermocycling conditions used were:

- initial denaturation (94˚C for 3 min),
- 25-35 cycles of denaturation (94˚C for 45 sec),
- annealing (~5˚C lower than primer melting points for 30 sec)
- extension (72˚C for 1min/kb) followed by
- a final extension step (72˚C for 10 min).

2.2.7 Gradient polymerase chain reaction

PCR reaction mixes were prepared as described above but using a BioRad C1000 ThermoCycler PCR to carry out the reactions. All reactions were performed simultaneously with different annealing temperatures to identify the optimal conditions for amplification. Annealing temperatures set provided 8 different temperature points in a range of 5˚C from 54˚C to 59˚C.

2.2.8 Agarose gel electrophoresis

A 1% (w/v) agarose (Melford) solution in 1 x TAE (40mM Tris Base, 1mM EDTA, 4mM acetic acid) was microwaved for ~1 min to dissolve the agarose and left to cool to ~60˚C. SybrSafe DNA stain (Invitrogen) was then added to a final concentration of 0.002% (v/v). The solidified agarose gel was then transferred to a gel tank and submerged in 1 x TAE. DNA Gel Loading Dye (6x) (ThermoFisher Scientific) was added in a 1:5 ratio to DNA samples, 6µl of which was then loaded into the agarose gel wells, gel run at 80-100V until the dye front was ~2cm from gel end. Gels were then imaged using a Syngene G:Box using blue light excitation of the SybrSafe dye at a 500nm wavelength. Images were captured using GeneSys software.

2.2.9 Restriction Enzyme Digests

~0.2µg of plasmid DNA or ~0.2µg of PCR product was incubated with 1µL of each fast digest restriction enzyme (ThermoFisher Scientific) required with 10x fast digest buffer diluted to 1x and made up to 20µL (for plasmid DNA) or 30µL (for PCR products) with nuclease-free H_2O. Restriction digest mixes incubated at 37˚C for 20 min.

2.2.10 Oligonucleotide primer design

Oligonucleotide primers were designed complying with the following specifications wherever possible: 40-60% GC content, 18-30 nucleotides long and T_m of 65˚C to 75˚C and with the forward and reverse primers having T_m within 5˚C of each other. Hairpin formation, complementarity and self-annealing regions were avoided. The Oligocalc online resource[74] was used to identify self-complementarity and T_m of oligonucleotides.

2.2.11 Plasmid construction

PCR-generated DNA products were double restriction digested along with the target plasmids. Any small oligonucleotides released from these restriction digests were removed using a PCR purification or Agarose Gel purification kits (i.e. ThermoFisher Scientific GeneJET PCR Purification Kit or GeneJET Gel Extraction Kit respectively, performed as per kit protocol). The DNA concentration of these linear target plasmids and inserts with cohesive ends was quantified (see 2.2.3). For the ligation reaction 10-100ng of vector DNA was typically used and the insert mass required in the ligase reaction was determined using the following calculation:

$$Insert\ Mass\ (ng) = 5\ x\ \frac{Insert\ Length\ (bp)}{Vector\ Length\ (bp)} x\ Vector\ Mass\ (ng)$$

The insert and vector DNA at the calculated masses was incubated with 4µl of 5x Rapid Ligation Buffer and 1µl T4 DNA ligase (5U/µL) from a ThermoFisher Scientific kit and nuclease-free H_2O added up to 20µl final volume. Each ligation mix was incubated at 22˚C for 15 min. A control was run alongside each ligation reaction in which no DNA insert was added to the mix to determine the level of vector recircularization without insert inclusion.

2.3 Protein techniques

2.3.1 Cell lysates

Overnight (~16-18hrs growth) cell cultures were diluted in fresh medium to OD_{600} 0.1 and regrown for ~4hrs to OD_{600} ~0.5. The log phase cells were then pelleted, the medium removed and the cell pellet washed in 1 ml ice cold sdH_2O prior to resuspension in 200µL lysis buffer (100mM NaOH, 50mM EDTA, 2% (v/v) SDS, 2% (v/v) β-mercaptoethanol) (Sigma-Aldrich), prepared on day of lysis. The sample was then boiled at 95˚C for 10 min, 5 µL 4 M acetic acid (Fisher Scientific) added and the sample boiled again at 95˚C before addition of 50µL blue buffer (250 mM Tris HCl pH 6.8, 50% (v/v) glycerol, 0.05% Bromophenol Blue (Fisher Scientific) and storage at -80˚C.

2.3.2 Protein precipitation from culture medium

2.3.3 Protein gel electrophoresis

NuPAGE™ 4-12% Bis-Tris 10 wells Gels (ThermoFisher Scientific)were used for protein gel electrophoresis with 1 x NuPAGE™ MOPS SDS running buffer (50mM MOPS, 50mM Tris Base, 0.1% SDS, 1mM EDTA, pH 7.7). 5µL of PageRuler Prestained Protein Ladder (ThermoFisher Scientific) was loaded into lane 1, 10µL of each sample was loaded into remaining lanes using gel loading tips. 180V was applied to the gel and run until the dye front had reached the bottom of the gel. The gel cassette was opened, well dividers removed and membrane removed to be transferred to PVDF membrane.

2.3.4 Western blot

2.3.4.1 Transfer

An Invitrogen Semi-Dry Blotter was used for the transfer of proteins from the SDS-PAGE onto a PVDF membrane. The PVDF membrane was cut to 7.5cm by 8.5cm: the size of the SDS-PAGE gel. The membrane was then soaked in pure methanol (Thermo Fisher Scientific) for 2 min before being rinsed in dH_2O and then placed into 1x NuPAGE™ Transfer Buffer (ThermoFisher Scientific) with the SDS-PAGE gel for 10 min. The transfer stack consisted of 5mm transfer paper on the top and bottom sandwiching PVDF membrane beneath the SDS-PAGE gel. The blotter was run for 45 min at 20V.

2.3.4.2 Imaging

After transfer, the PVDF membrane was then placed in 10mL of 5% Oxoid skim milk solution in PBS (Oxoid) to block for 30 min. The milk solution was then removed and 10ml of 5% Oxoid skim milk solution in PBS with primary antibody diluted to the manufacturer's suggestion was then added. This was placed onto a belly dancer shaker overnight (~16-18hrs) at 4˚C. If an HRP conjugate was used the membrane was washed thrice in 10ml of PBS for 10 min per wash before exposure. If a secondary antibody was required then peroxidase-conjugate secondary antibody with specificity to the primary antibody in 5% Oxoid skim milk PBS solution diluted to manufacturer's suggestion was added and incubated for 2 hr at room temperature on a belly dancer shaker. Solution 1 (4.3ml dH_2O, 0.5ml 1M Tris pH 8.5, 50µl luminol

[Sigma-Aldrich] and 22µl *p*-Coumaric Acid) and solution 2 (4.5ml dH_2O, 0.5ml 1M Tris pH 8.5, 3.2µL 30% H_2O_2) were prepared in 15mL falcon tubes and stored wrapped in aluminium foil to protect these light sensitive solutions from exposure.

The solution present on the membrane was poured off and solution 1 and solution 2 of the ECL solution combined and poured onto membrane and agitated gently for 1 min. The membrane was then removed with tweezers from the solution and placed on the inner plastic sleeve of the exposure cassette. The outer plastic sleeve was placed on top of the membrane and Amersham Hyperfilm ECL (18x24cm) placed on top of plastic sleeve. The cassette was fastened shut for the duration of the exposure before running the film through the Optimax 2010 Film Processor.

An alternate method of imaging western blots was also used i.e. using a Syngene G:Box with GeneSys Software.

2.4 *In vitro* oxygen consumption assay

A Digital Model 10 oxygen electrode (Rank Brothers Ltd) was used to assay for ambient levels of oxygen within a sample (Fig 2.4.). A water circulator was used to heat the cell containing the oxygen electrode to 25˚C with an initial heating period of 10 min being used to ensure the cell was maintained at a constant 25˚C. A saturated KCl solution was added onto the electrode with PTFE film placed over the top and sealed. Polarising volts were adjusted to 0.6V and the electrode reading adjusted to zero before the electrode was plugged in and the magnetic stirrer added. An Elman's assay was performed on GSH to assay for levels of free thiols[75] from which the volume of GSH required to reach a final concentration of 40mM free thiol GSH could be calculated. The reaction mix was as follows:

- O_2 Buffer (100mM Tris, 50mM NaCl, pH 8),
- 5µM PDI
- 10µM Ero1p
- 50µM GPx7 or 50µM GPx8 when required
- dH_2O added to give a final volume of 600µL per reaction.

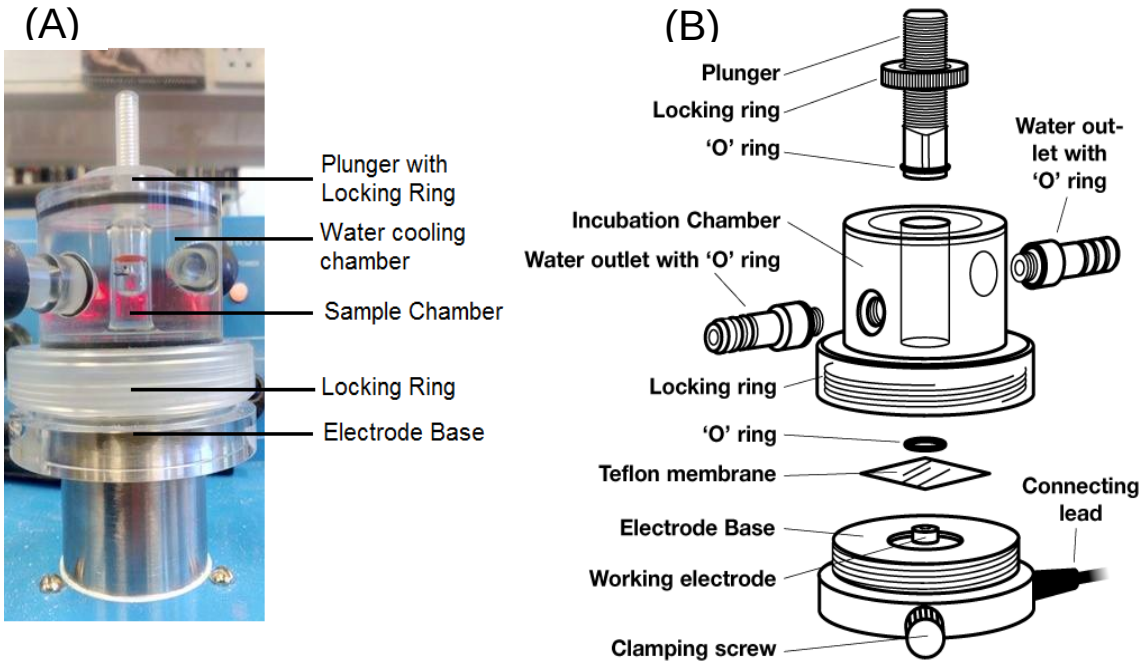

Fig 2.4. Diagram of components of the oxygen electrode used for the oxygen consumption assay
The externally visible set up (A), and deconstruction of components (B) of the oxygen electrode. Key components indicated including the sample chamber, water cooling system and electrode base Image (B) from manufacturers website (Rank Brothers Ltd, rankbrothers.co.uk/prod1.htm).

Each reaction mix was added to the oxygen electrode cell and magnetic stirrer turned on and left until the electrode reading stabilised. At this point the electrode reading was adjusted to 100 and electrode reading recording started. After 100 sec 12µL Ero1p (µg) was added and the reaction left to continue until after rate of consumption of oxygen had begun to decline. Using PicoLog data logging software a graph was generated of the ambient levels of oxygen in the system with time, from which the rate of oxygen consumption was calculated.

2.5 Yeast techniques

2.5.1 Spontaneous generation of Δ*pdi1* mutants

A cell count was performed on a culture yeast strain 2736 after overnight growth (16-18hrs) using a haemocytometer to determine cell density. To establish the rate of spontaneous mutation generating viable Δ*pdi* mutants, ~8x10^5 cells were plated onto 5FOA plates (table 2.1.2) and incubated for ~10 days at 30˚C.

2.5.2 Generation of Δ*pdi1* mutants through mutagenesis

This was performed identically to 2.4.1, however, the resulting plates were then exposed to 30μW/cm^2 of radiation for 20 sec prior to incubation. The dosage was determined using a radiometer. All agar plates were then wrapped in aluminium foil to prevent exposure to light which could induce photoreactivation and hence result in DNA repair[76].

2.5.3 Producing -80˚C glycerol stocks

0.5ml of an overnight (~16-18hrs) YEPD-based culture of yeast was added to 0.5ml 50% glycerol, mixed thoroughly and added to a 1.8ml Nunc® CryoTube cryogenic vial and stored at -80˚C. When required a small portion of the frozen sample was removed without defrosting and added to suitable agar plate or liquid medium to prevent multiple freeze thaw cycles of the cell stock.

2.5.4 Measuring growth in liquid medium

Overnight cultures (~16-18hrs) were diluted to OD_{600} ~ 0.1 and a volume consistent for all samples to be measured was then transferred to a sterile 96 well microwell plate. Where required a drug was added to each sample to the required final concentration. Absorbance at OD_{600} was measured for ~3 days at 30˚C using a SPECTROstar Nano Microplate Reader (BMG Labtech) with double orbital shaking.

2.5.5 Spectrophotometry

1ml of a culture was added to a Sarstedt polystyrene and acrylic 1ml cuvettes and the OD_{600} measured. If the absorbance reading was higher than 1.0 the culture was diluted with identical sterile medium to give a reading less than 1.0.

2.5.6 Replica plating

Yeast cultures were diluted with appropriate liquid medium to OD_{600} 0.1. 100μl of culture was added to different wells of a sterile 96-well microwell plate, a sterile replica plater was placed into the wells and agitated for a few sec before being transferred to an agar plate dependent upon the assay where the replica plater was moved in a small circular motion on the surface of the agar plate to ensure complete cell transfer. The agar plates were incubated at 30˚C for 3-5 days.

2.5.7.1 Cell counts using a haemocytometer

A sample of a culture was added to a haemocytometer to completely cover both grids before the cover slip replaced. Five 62.5µm squares were counted in each grid and the average taken to estimate the cell numbers/mL in the culture. If the cell density was too high to count, the culture was diluted by a factor of 10 in sdH_2O and recounted.

2.5.8 Fluorescence analysis of cells by flow cytometry

Overnight cultures (~16-18hrs) were diluted to OD_{600} ~ 0.5 in sdH_2O, pelleted and transferred to appropriate fresh medium with or without 2mM H_2O_2 and incubated at 30˚C for 2 hrs. The medium was then removed and cells washed before resuspension in YPD with or without 10µM 2', 7'-dichlorodihydrofluorescein diacetate (H_2DCFDA) and incubated for a further 3 hr. 10µl of the sample was then added to 1ml of PBS in a BD Falcon 5ml Polystyrene Tube and attached to the sample injection port (SIP) of the flowcytometer (Fig 2.5). Cell fluorescence was measured through excitation of cells at 490nm and detection through an emission at 517-527nm by the primed fluorescent H_2DCFDA dye. A histogram plot of cellular fluorescence and a dot plot of forward and side scatter were generated using BD

CellQuest™ Pro Analysis software. The basal fluorescence was established by adding a line at which ~50% of the cells were more fluorescent and ~50% of the cells were less fluorescent on the histogram for culture incubated in the absence of H_2DCFDA dye(Fig 2.6.). The change in the percentage of the population of more fluorescent cells as a result of addition of H_2DCFDA was measured (Fig 2.6.).

2.5.9 Killer toxin assay

Strains transformed with pVT100U-K1 plasmid were grown overnight (~16-18hrs) in selective medium and diluted to OD_{600} 0.2 before regrowth in fresh selective medium to OD_{600} 0.7-0.8. All cell cultures were adjusted to this OD_{600} with sdH_2O. Cultures added in 20µl aliquots to sterile Grade AA 6mm Whatman discs placed on Killer Toxin Assay agar (see 2.1.2.1). Cultures were incubated at ~20˚C overnight (16-18hrs), the area of the zones of clearing around the 6mm Whatman discs formed as a result of killer toxin secretion were measured using ImageJ software.

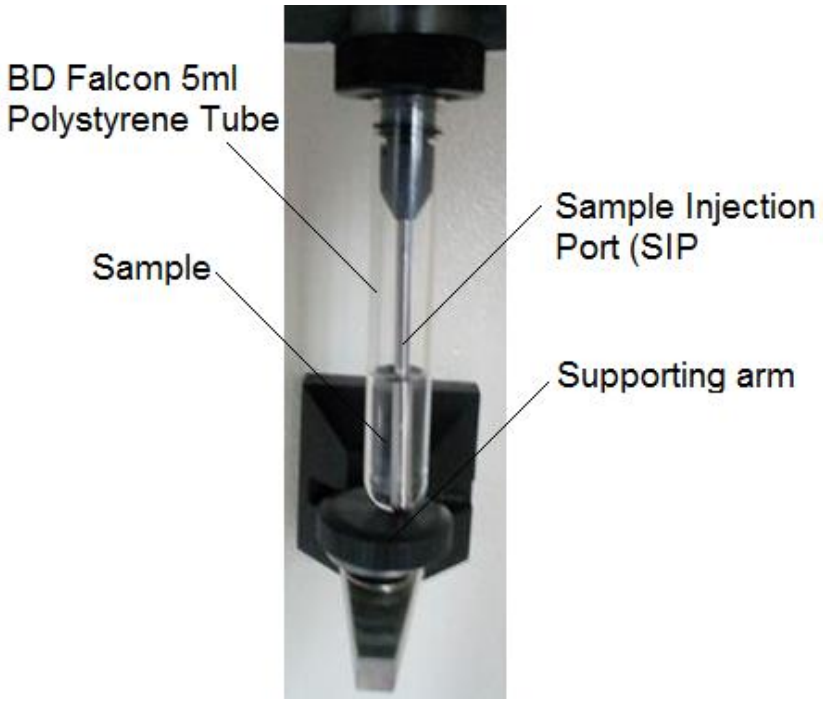

Fig 2.5. Sample Injection Port of the flow cytometer
1ml of PBS and culture in a BD Falcon 5ml Polystyrene Tube is held in place by the supporting arm allowing the sample injection port (SIP) to uptake cells measurement via suction.

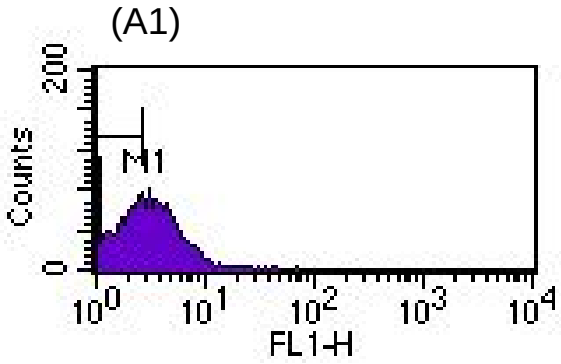

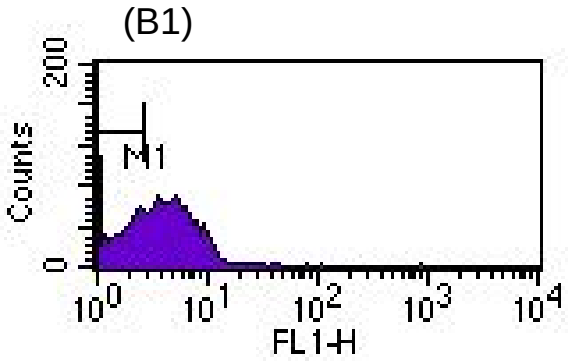

(A2)

Percentage of cells within the M1 region (%)	Percentage of cells outside of M1 region (%)
50.1	49.9

(B2)

Percentage of cells within the M1 region (%)	Percentage of cells outside of M1 region (%)
22.9	77.1

Fig 2.6. Histogram of flow cytometry to show change in percentage of fluorescent cells from as a result of addition of H_2DCFDA dye
The M1 region set to contain 50% of the cells of the population to determine basal levels of fluorescence (A1)(A2). As a result of addition of H_2DCFDA there is a shift in increase in percentage of fluorescent cells in the population which can be seen by shift of the hisogram (B1), the change in percentage of cells outside of the M1 region from the basal levels of fluorescence can therefore be measured to calculate change in percentage of fluorescent cells in the population (A2)(B2).

Chapter 3 – Results

3.1 Screen for viable Δ*pdi1* mutants

As *PDI1* is an essential gene in yeast a knock-out of this gene ordinarily results in cell lethality[4]. Therefore if a strain remained viable following a *PDI1* knock out it would indicate a suppressor of Δ*pdi1* lethality, termed *supX.* The mutation s*upX* is suspected to be upregulation of one of the nonessential yPdi1p homologues, Mpd1p or Mpd2p, as these have been shown to be able to restore viability to Δ*pdi1* strains[4]. Therefore viable Δ*pdi1* strains are to be created and the *supX* mutation identified.

Selection for 2736 strain that had lost the *PDI1 URA3* plasmid was performed using 5-FOA[77] and hence select for viable Δ*pdi1* strains of yeast. The *URA3* gene encodes for a protein called orotidine-5'-monophosphate decarboxylase (ODCase)[78], this converts orotidine-5'-monophosphate (OMP) to uridine-5'-monophosphate (UMP) which is then utilised for RNA production[79]. 5-FOA is an OMP homologue and is converted to 5-FU by ODCase and orotate phosphoribosyltransferase (OPRTase), 5-FU can be misincorporated into DNA and RNA resulting in interference of their processing and ultimately cell death[78] (Fig 3.1.).

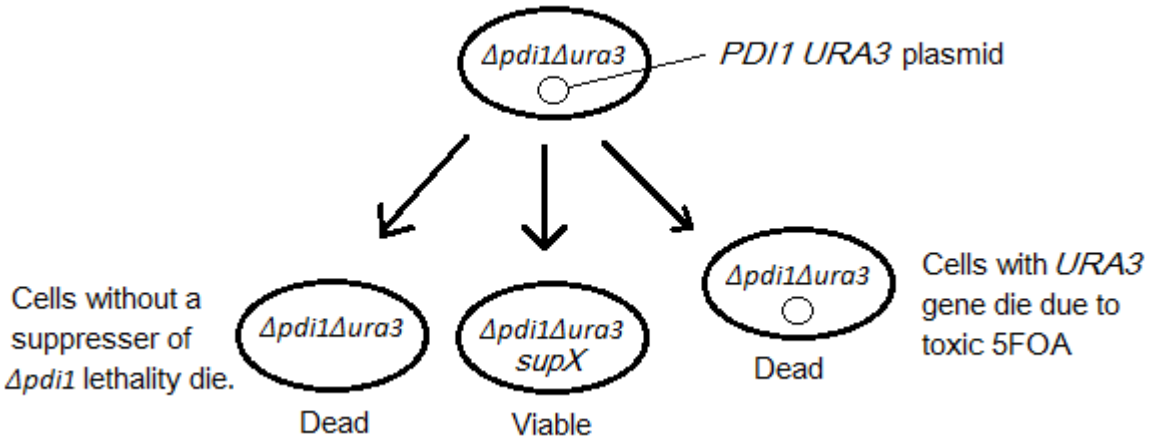

Fig 3.1. The possible fates of 2736 strain yeast plated onto 5FOA
When the *URA3 PDI1* plasmid carrying strain 2736 is plated onto 5-FOA there were three possible proposed outcomes. If the cell retains the plasmid is dies due to conversion of 5-FOA to the toxic compound 5-FU by ODCase, if the cell loses the plasmid but does not have the *supX* mutation it dies through Δ*pdi1* lethality. Only if the cell has both lost the plasmid and has *supX* mutation does it survive to form a colony on 5-FOA plates.

Colonies of 2736 strain yeast that emerge following plating onto 5-FOA medium should therefore be Δ*pdi1* Δ*ura3* and *supX* as any cells that retain the plasmid will be killed by the conversion of 5-FOA to the toxic compound 5-FU. Strains that have lost the plasmid but do not have *supX* will be killed by Δ*pdi1* lethality.

3.1.1 Duration of ultraviolet radiation exposure for a 50% kill rate

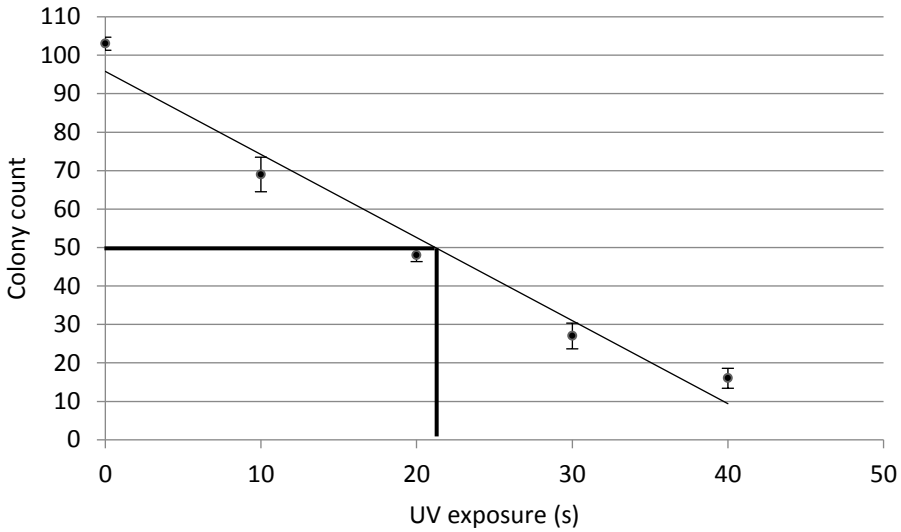

Fig 3.2. Colony count on YNB-Ura as a result of exposure to a range of durations of UV exposure.
~100 CFUs of 2736 strain yeast on YNB-Ura solid medium were exposed to a range of durations of 30mW/cm^2 UV radiation from 0s to 40s in 10s intervals followed by 3 days incubation. The number of colonies at each exposure were counted and plotted, the resulting line of best fit indicates that 20s exposure leads to 50% kill rate.

To increase the frequency of viable Δ*pdi1* mutants UV mutagenesis was used to increase the rate of mutation. UV causes mutations by UV photons are absorbed by the double bonds of pyrimidines, resulting in their breakage, if two adjacent pyrimidines are hit by UV light they are able to dimerise through reformation of the broken disulphide bonds forming a cyclobutane ring connecting the two nucleotides[80][81]. This nucleotide dimer is misincoporated as a single nucleotide during DNA replication resulting in frame-shift mutations. To find a 50% kill rate and therefore an appropriate induction of mutation without excessive cell lethality[82] ~100 colony forming units (CFU) were exposed to 30mW/cm2 UV radiation for 0s to 40s in 10s intervals performed in triplicate. A line of best fit was used to indicate that the duration of UV exposure that resulted in a ~50% kill rate was ~20s (Fig 3.2.).

This duration of UV exposure was used in all subsequent mutagenesis events to generate Δ*pdi1* strains. Potential Δpdi1 mutants emerged on 5-FOA solid medium through either spontaneous generation, a mutation rate of ~1.9x10^{-6}, or through UV-induced mutagenesis, at a mutation rate of ~4.3x10^{-6}, and were replated onto fresh 5-FOA solid medium to confirm absence of 5-FOA-mediated cytotoxicity.

3.1.2 Growth of potential viable Δ*pdi1* mutants on YNB–Ura solid medium

Growth on 5-FOA should result in selection for Δ*ura3* strains, to confirm this cell suspensions of putative Δ*pdi1* mutants were inoculated on YNB–Ura solid medium to confirm lack of growth as a result of loss of the *PDI1*-containing plasmid. Initially 3 mutants generated through mutagenesis (designated PDIMR2-PDIMR4) and 5 mutants spontaneously generated (designated PDISR2-PDISR7) were tested on YNB-Ura by adding 5µL of a cell culture of OD600~0.1

Fig 3.3. Growth of potential Δ*pdi1* mutants on YNB-Ura solid media
5µL of cultures of potential Δ*pdi1* mutants PDIMR2-4, PDISR2 and PDISR4-7 at OD_{600} 0.1 were added to YNB-Ura medium as well as to 5-FOA as a growth control.

All but 2 strains, PDISR5 and PDISR6, were able to grow i.e. were Ura+ with little to no impediment of growth on YNB-Ura medium (Fig 3.3.). Peculiarly, DN5, a homozygous *ura3/ura3* diploid heterozygous strain with both reverting Δ*ura3-1*[83] and non-reverting Δ*ura3-52*[83][84] alleles, was also able to grow on YNB-Ura (Fig 3.3). As YNB–Ura plates from the same batch had been used for other purposes confirming that the medium was not defective, a fresh stock culture of DN5 was made.

A further 12 mutants (PDIMR17, PDIMR19 and PDIMR21-30) were obtained after UV mutagenesis in identical fashion to those prior. This was to screen enough viable 5-FOA resistant mutants to find a successful Δ*pdi1 supX* mutant and to be confident, if no successful Δ*pdi1* mutants are found, that it is due to *supX* not being a mutation

that can occur rather than from small sampling numbers. These mutants were tested for growth on YNB-Ura using replica plating (Fig 3.4).

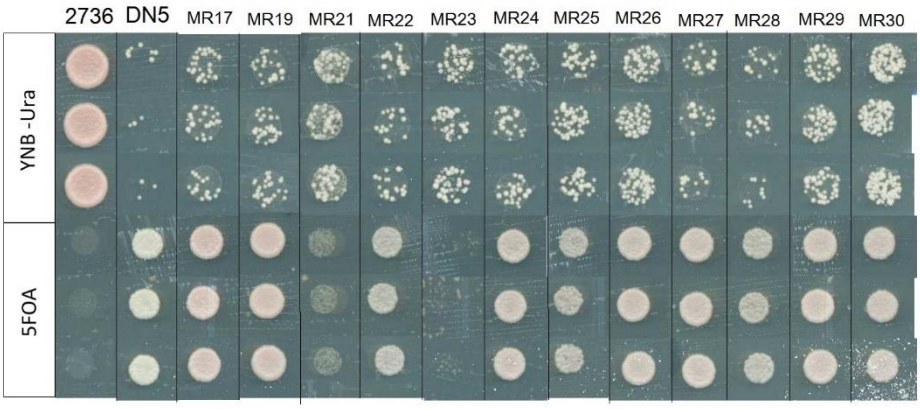

Fig 3.4. Growth of potential Δ*pdi1* mutants on YNB-Ura solid media
Cultures of potential Δ*pdi1* mutants PDIMR17,19 and PDIMR21-30 at OD_{600} were added to YNB-Ura medium via replica plating as well as to 5-FOA as a growth control.

The potential Δpdi1 mutant strains showed growth of a fraction of the population of plated cells, suggesting reversion of the *ura3-1* mutation in the 2736 strain (Fig 3.4.). This occurred at a much higher frequency than seen with the *ura3-1/ura3-52* diploid DN5. Growth on YNB-Ura also occurred at much lower rate than mutants PDIMR2-4, PDISR2 and PDISR4-7 (Fig 3.3), however, this may have resulted from addition of 5µL of OD600 0.1 culture resulting in a much higher CFU number being added than through replica plating.

Therefore, as there is papillae growth of PDIS/MRx mutant on YNB-Ura medium, it suggests that the *ura3-1* mutation of the PDIS/MRx mutants is able to revert to *URA3* at a much higher frequency than that of DN5.

3.1.3 Assaying for absence of protein disulphide isomerase in the potential Δ*pdi1* mutants

Despite growth of PDIS/MRx mutants on YNB-Ura it appears that the mutants are reverting to the WT *URA3* gene, and hence may still have lost the *URA3* plasmid, and with it *PDI1*. Therefore in order to determine whether potential Δpdi1 strains were still expressing yPdi1p a western blot was performed.

For controls the Pdi1p positive strain 2736 was used, as well as the ∆pdi1 strain: DN5. Purified yPDI, a gift from Beal. D.M. (School of Biosciences, Kent) and Pdi1p positive control cell extracts (a gift from G. Staniforth, School of Biosciences, primary antibodies for yPdi1p and phosphoglycerate kinase (PGK), the latter as a loading control.

The initial collection of potential ∆*pdi1* mutants was tested first (PDIMR2-4, PDISR2 and PDISR4-7) (Fig 3.5.).

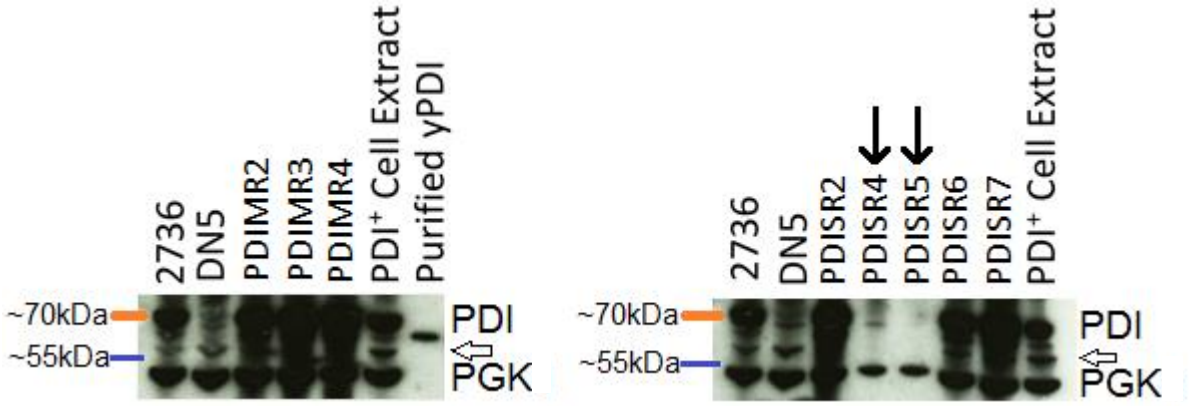

Fig 3.5. Western blot for expression of Pdi1p in ∆*pdi1* mutants
Expression of Pdi1p in potential ∆*pdi1*mutants PDIMR2-4, PDISR2 and PDISR4-7 using an anti-yeast Pdi1p antibody as well as a PGK antibody as a loading control. Pdi1p expressing strain 2736 and ∆*pdi1* strain DN5 were used as controls as well as a Pdi1p positive cell extract and purified yeast Pdi1p. Bands for PDI and PGK are indicated on the right of the blot, with the unknown band indicated by a white arrow. The two strains not expressing PDI are indicated by black arrows

The results indicated that all the of the potential ∆pdi1 knock out strains were still expressing Pdi1p, with the exception of PDISR4 and PDISR5. These two mutants also exhibited less intense bands for PGK. This was a result of the two strains having impaired growth rates and so PDISR4 and PDISR5 were lysed at the lower cell concentration of OD600 0.138 ml^{-1} and OD600 0.129 ml^{-1} respectively rather than OD600 ~0.5ml^{-1} for all other strains. The PDISR4 and PDISR5 mutants also appeared to lack a second band between the band for yPdi1p and the band for PGK that was present in all of the other lysates (Fig 3.5.). The identity of this protein is unknown, but is likely the result of non-specific binding of either the PGK or yPdi1p antibodies to an unrelated protein or a truncated form of one of these proteins. The band for PGK appeared to migrate slower in PDISR4 and PDISR5 compared to the other PDIS/MRx mutants and the controls, however, this may have been the result of distortion of the gel when transferring. Purified yPdi1p migrated further than the

Pdi1p expressed in the yeast strains as it was isolated from E.coli cells and hence was not glycosylated. Despite the promising result of having generated two Δpdi1 mutants, neither could be revived from glycerol stocks held at -80oC and so new mutants were made through UV mutagenesis and screened for expression of Pdi1p (Fig 3.6.).

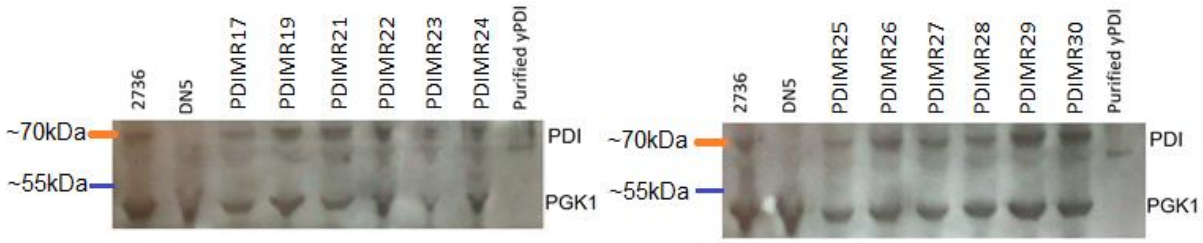

Fig 3.6. Western blot for expression of Pdi1p in Δ*pdi1* mutants
Expression of Pdi1p in potential Δ*pdi1*mutants PDIMR17, PDIMR19 and PDIMR21-30 using an anti-yeast Pdi1p antibody as well as a PGK antibody as a loading control. Pdi1p expressing strain 2736 and Δ*pdi1* strain DN5 were used as controls as well as a Pdi1p positive cell extract and purified yeast Pdi1p. The bands for PDI and PGK are indicated to the right of the blot.

The western blot for PDIMR17, 19 and PDIMR21-30 indicated that all of these strains still produced Pdi1p (Fig 3.6.).

As all but two of the PDIS/MRx mutants remained expressers of PDI (Fig 3.5, Fig 3.6) it is clear that the *PDI1* gene is retained despite selecting against *URA3* cells. This suggests that the plasmid is either being retained, or the plasmid version of *PDI1* is integrating into the genome.

3.1.4 Growth of putative mutants in YPD liquid medium

The growth curves in YPD medium of strains PDIMR2-4, PDISR2 and PDISR4-7, were measured, as viability retained by *supX* in a Δ*pdi1* strain would be expected to result in a growth defects and hence an observable change to the growth curve[4].

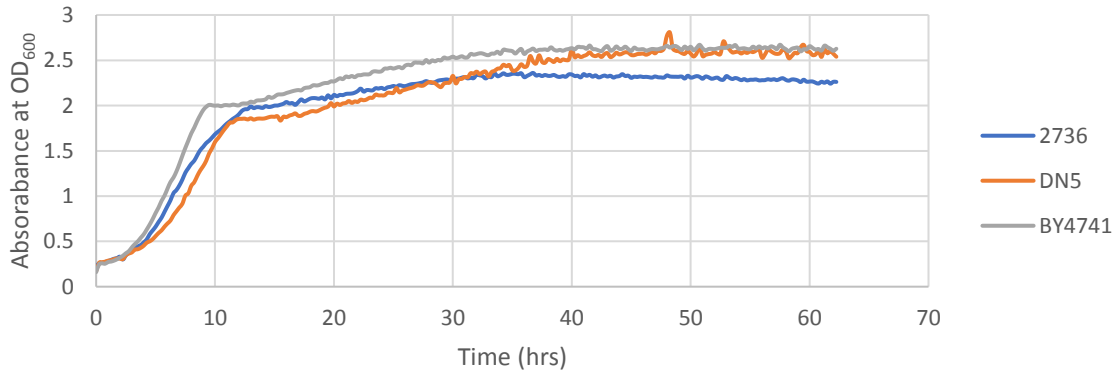

Fig 3.7. Growth of BY4741, 2736 and DN5 in YPD liquid medium
Change in absorbance over time indicating growth in YPD liquid medium of 2736 (blue), DN5 (orange) and BY4741 (grey),

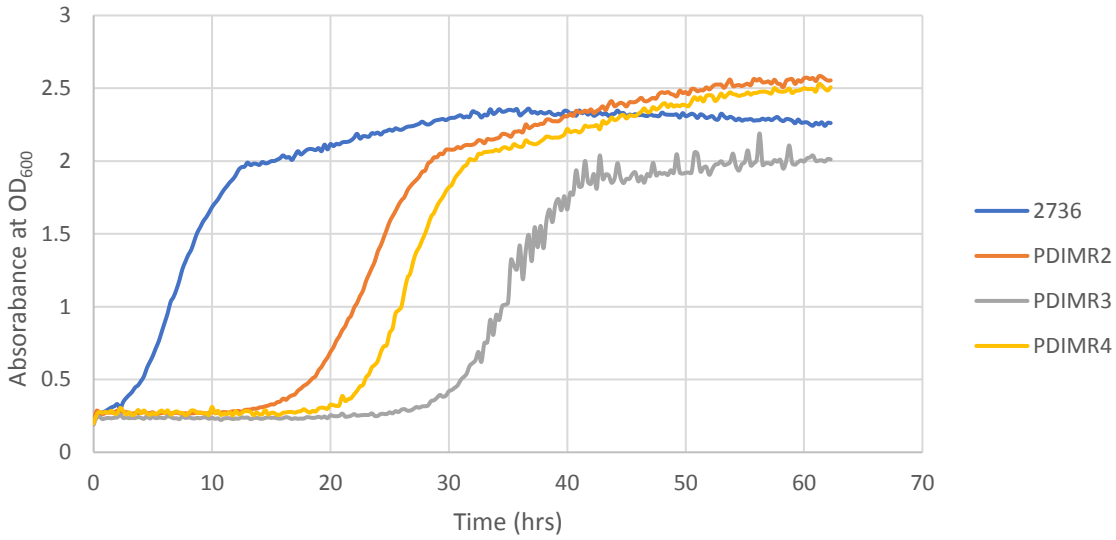

Fig 3.8. Growth of 2736 and UV mutagenesis generated potential Δ*pdi1* mutants in YPD liquid media
Change in absorbance over time indicating growth in YPD liquid medium of 2736 (blue) as a control, and mutants PDIMR2 (orange), PDIMR3 (grey) and PDIMR4 (yellow).

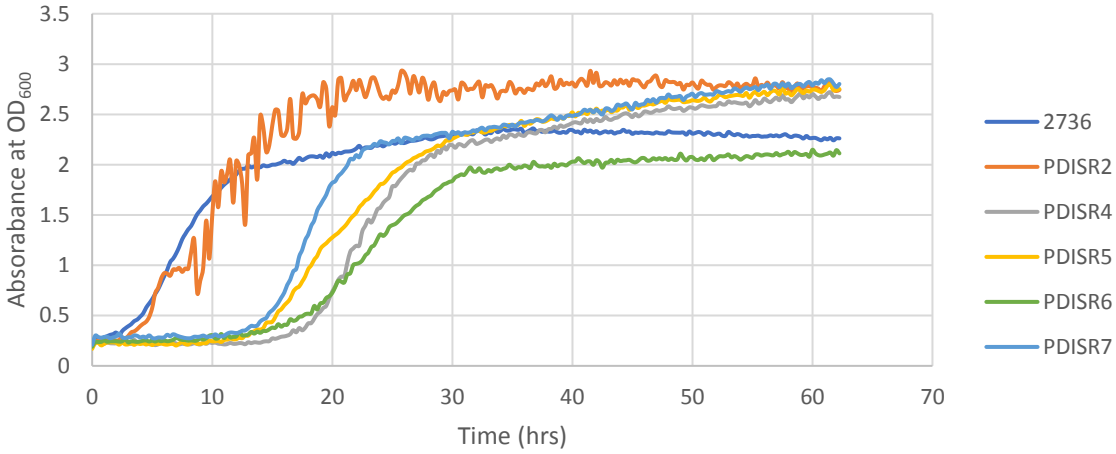

Fig 3.9. Growth of 2736 and spontaneously generated potential Δ*pdi1* mutants in YPD liquid media
Change in absorbance over time indicating growth in YPD liquid medium of 2736 (blue) as a control, and mutants PDISR2 (orange), PDISR4 (grey). PDISR5 (yellow), PDISR6 (green) and PDISR7 (light blue).

The sporadic growth curve of PDISR2 is indicative of contamination (Fig 3.9), as many bacterial strains form aggregates, the presence of which would result in artificially high absorbance readings. All other mutants, however, had growth curves absent of this sporadic spiking, suggesting that only PDISR2 was affected by contamination (Fig 3.7. – 3.9.). The PDIS/MRx mutants all had a longer lag phase than the parent strain, which entered log phase at 4.25 hrs. The duration of lag

phase varied considerably between mutants ranging from 14.5 hrs for PDISR7 to 31.25 hours for PDIMR3. The maximum growth rate of the 2736 parent strain control was 0.179hrs^{-1} while the PDISMRx mutants exhibited maximum growth rates ranging between 0.2hrs^{-1}, for PDISR7, and 0.095hrs^{-1} for PDISR6 (Fig 3.8., Fig 3.9.). For all of the PDISMRx mutants, with the exception of PDISR6 and PDIMR3, the maximum biomass exceeds that of 2736 (Fig 3.8., Fig 3.9.). 2736 parent strain control had a maximum absorbance at OD_{600} ~2.3, while all PDISRx mutants and all PDIMRx mutants reached maximum absorbances of OD_{600} ~2.8 and OD_{600} ~2.5 respectively, with the obvious exceptions of PDISR6 and PDIMR3. This maximum absorbance for the PDIS/MRx mutants was at 62hrs, the final data point of the experiment, and hence the maximum biomass may have increased if the experiment was to continue for longer.

An analysis of growth in liquid culture analysis was only performed on early various PDIS/MRx mutants. For PDIMR17, 19 and PDIMR21-M30 growth curve analysis was not performed, as once it was established that they remained producers of PDI no further time was invested in characterising these mutants.

A consistent trend from all of the PDIS/MRx mutants is an increased lag phase compared with the 2736 parent strain control, this indicates that the mutation that provides resistance to 5-FOA is detrimental to the cells. There is, however, wide variation between PDIS/MRx mutants for both duration of lag phase and maximum growth rate, this indicates that the PDIS/MRx mutants do not have a conserved mutation between them that results in the 5-FOA resistance.

3.1.5 Polymerase chain reaction of genomic DNA to amplify *PDI1* gene and check for a recombination event

In order to check for recombination of the plasmid *PDI1* gene into the genome a PCR reaction was performed to amplify the genomic *PDI1* of PDIS/MRx mutants. If fragments generated from the PCR reaction were the same size as those for a 2736 parent strain control then it would suggest that the genomic disrupted *pdi1:his3* gene present in this strain is unmodified. If there has been a recombination event the *PDI1* DNA fragment would be expected to be smaller as it is absent of the *HIS3* disruption.

Oligonucleotide primers, -983_pdi1_F, -972_pdi1_R, -500_pdi1_F and -504_pdi1_R, complementary to ~1000bp and ~500bp up and down stream of the

PDI1 gene were designed and used with PCR in an attempt to amplify the *PDI1* gene region from the mutant strains. Initially genomic DNA was prepared from the 2736 strain and the sample run on an agarose gel to confirm presence of genomic DNA. This DNA was then used as a template for the PCR reaction at the calculated optimum conditions for primers with a melting temperature (Tm) of 60˚C, but was unsuccessful at amplifying the *PDI1* region. The presence of different DNA fragment generated by the reagents using in this PCR reaction confirmed that the PCR reaction mix was operational. A gradient PCR was also performed with a range of temperatures from 54˚C to 59˚C, this again was unsuccessful at amplifying any DNA.

The repeated failure of this PCR reaction at a range of different annealing temperatures suggests that the oligonucleotide primers used for amplification of *PDI1* are lacking in specificity for the upstream and downstream regions of the *PDI1* gene region.

3.2 The phenotypic impact upon expressing glutathione peroxidases 7 and 8 in yeast

S. cerevisiae is absent of ER resident peroxidases, therefore yeast strains were transformed with human proteins GPx7 and GPx8 in order to alleviate ROS stress. Both GPx7 and GPx8 couple the detoxification of H_2O_2 and it was therefore expected that expression of GPx7 and GPx8 in a yeast system would result in increased resistance to H_2O_2, through direct degradation of H_2O_2. It is predicted to also increase OPF of disulphide bonded proteins, through direct reoxidation of Pdi1p by GPx7 and GPx8, but also through alleviating Ero1p inactivation by H_2O_2 by detoxification of H_2O_2.

3.2.1 Construction of plasmids carrying *GPX7* and *GPX8* genes

In order to express GPx7 and GPx8 in yeast plasmids were designed and produced with *LEU2* selectable marker, allowing for simultaneous plasmid expression of pVT100U-KT and GLuc plasmid.

3.2.1.1 pBEVY-L vector carrying native *GPX7* and *GPX8*

As the initial vectors available containing human native GPx7 and GPx8 cDNA were *E.coli* vectors the gene had to be transferred to a yeast vector. To do this PCR was

performed on plasmids pKEHS780-hGPx7 and Human GPx8 cDNA clone with oligonucleotide primers (kpnI_GPx7_F and sacI_GPx7_R for GPx7 and kpnI_GPx8_F and sacI_GPx8_R for GPx8) to incorporate restriction sites 5' kpnI and 3' sacI, success of the PCR was confirmed using agarose gel electrophoresis (Fig 3.10.).

Restriction digests of the inserts and the target vector: pBEVY-L followed by a ligation to create the intended plasmids. Competent *E.coli* cells were used for cloning of the ligation product and following a plasmid DNA extraction insert positive vectors were identified through excision of insert (Fig 3.11., Fig 3.12.). The resulting plasmids with a pBEVY-L backbone (Fig 2.2.) and native *GPX7* and *GPX8* were named pUKC3400 and pUKC3401 respectively.

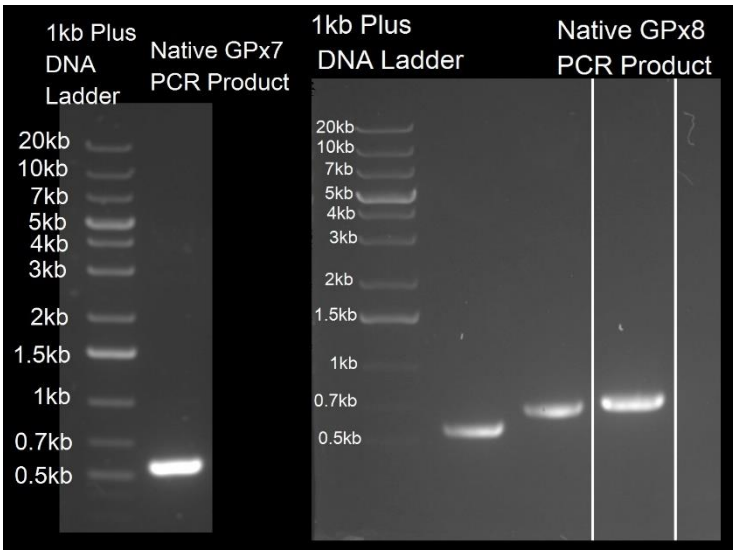

Fig 3.10. Agarose gel of *GPX7* and *GPX8* PCR generated DNA products for pBEVY-L backbone. Native *GPX7* (left) and Native *GPX8* (right), the native *GPX8* PCR generated DNA product (right) was ran alongside other PCR generated DNA products (GPx7 and GPx8 PCR products for ligation into p6431 vector) for economical use of agarose gel electrophoresis.

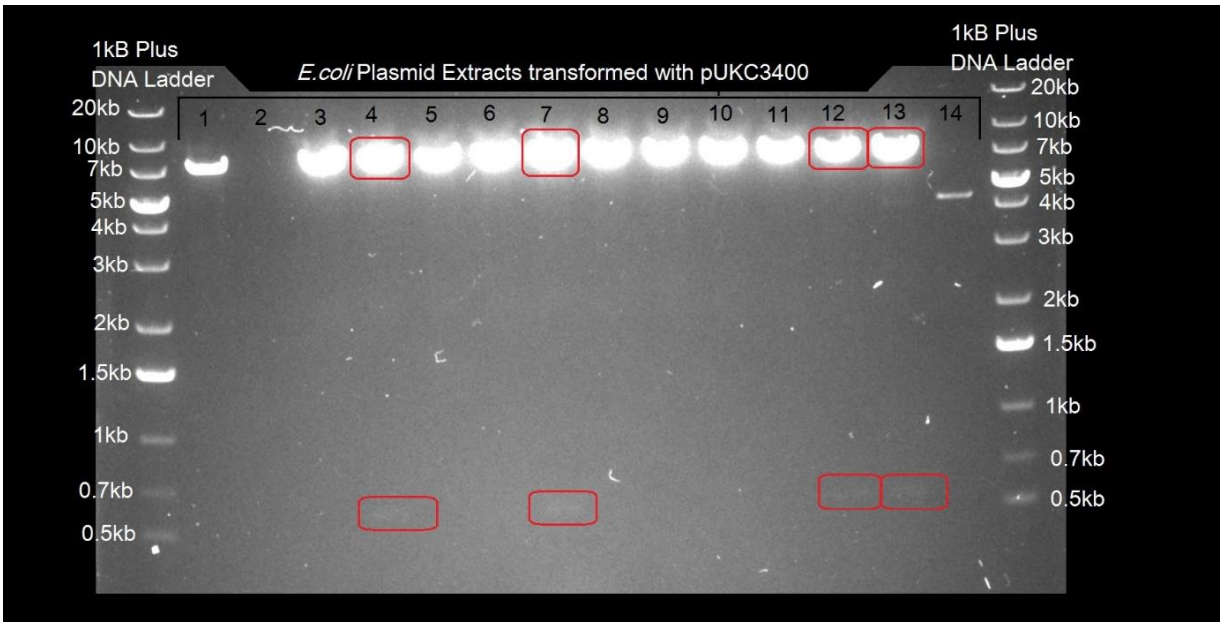

Fig 3.11. Restriction digests of plasmid extracts from *E.coli* cells transformed with pUKC3400.
14 digested plasmid extracts from *E.coli* run to identify insert positive vectors, the inserts and corresponding insert positive vectors indicated by red squares.

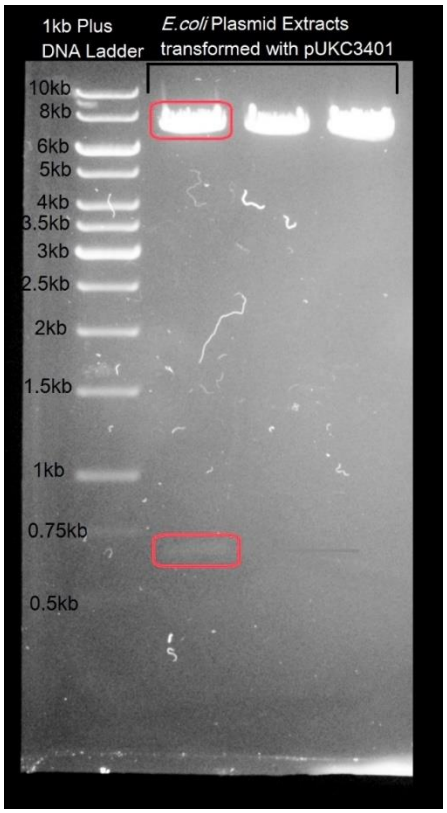

Fig 3.12. Restriction digests of plasmid extracts from *E.coli* cells transformed with pUKC3401.
Three digested plasmid extracts run to identify insert positive vectors, the insert and corresponding insert positive vectors indicated by red squares

3.2.1.2 Native *GPX7* and *GPX8* with a *GFP* fusion

Green Fluorescent Protein (GFP) is a chemiluminescent protein derived from *Aequorea victoria* jellyfish[85], the recombinant tagging of proteins of interest with GFP allows proteins localisation to be measured through fluorescence microscopy.

To identify intracellular localisation of GPx7 and GPx8 absent of yeast ER signal sequence or retention sequences fusion of GFP to GPx7 and GPx8 was attempted. For this the same initial vectors were used but with different oligonucleotide primers (BamHI_GPx7_F and XbaI_GPx7_R for *GPX7* and BamHI_GPx8_F and XbaI_GPx8_R for *GPX8*) to incorporate 5' BamHI and 3' XbaI restriction sites allowing recombination into a p6431 backbone (Fig 2.1). Successful PCR was confirmed (Fig 3.13.) and was purified by PCR purification prior to restriction digestion, ligation and cloning in competent *E.coli*. Restriction digests of plasmid extracts showed that no vectors contained inserts (Fig 3.14.).

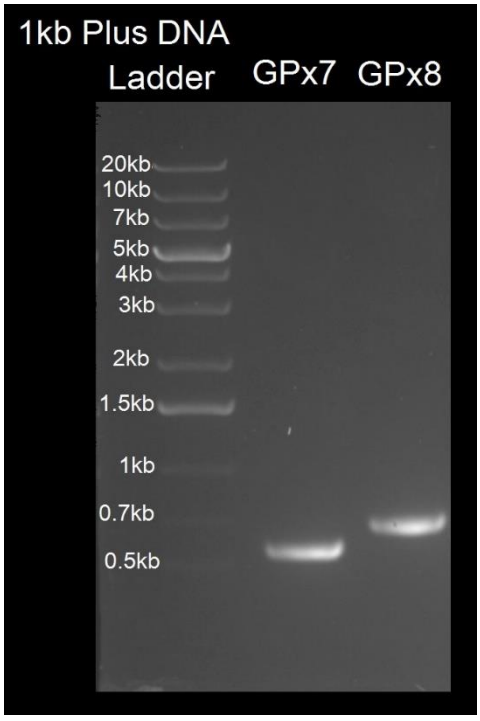

Fig 3.13. Agarose gel of *GPX7* and *GPX8* PCR generated DNA products for p6431.
Native *GPX7* (well 2) and *GPX8* (well 3) run on an agarose gel to confirm success of PCR prior to ligation into p6431 plasmid.

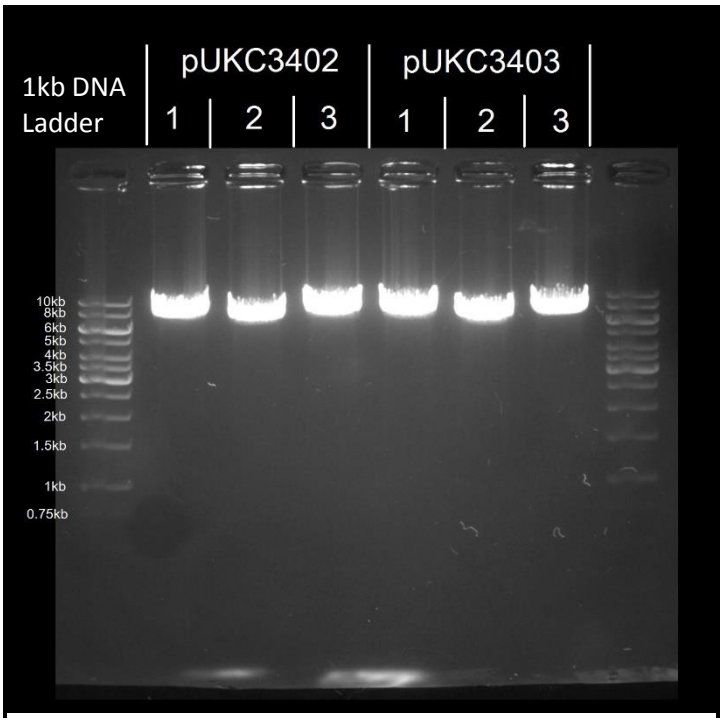

Fig 3.14. Restriction digests of plasmid extracts from *E.coli* cells transformed with pUKC3402 and pUKC3403.
Three plasmid extracts for both pUKC3402 (wells 2-4) and pUKC3403 (wells 5-7) plasmids restriction digested to identify successful integration of the gene. No inserts were seen.

A repeat of PCR and PCR purification was performed with 3 identical PCR reactions combined per gene amplified (Fig 3.15.), this was to ensure ample insert clones to maximise chances of ligation success. The PCR product was purified through gel extraction (Fig 3.16.).

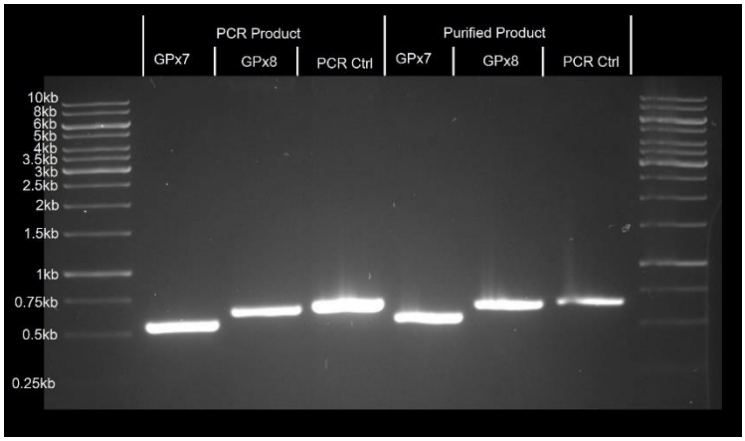

Fig 3.15. Native *GPX7* and *GPX8* PCR generated DNA products and purified PCR generated DNA products.
Following the unsuccessful previous attempt PCR was repeated with three fold as much PCR generated DNA product (wells 2-4) and purified PCR generated DNA products (wells 5-7) of *GPX7* (wells 2 and 5), *GPX8* (wells 3 and 6) and a PCR control of a reaction shown previously to work (*GPX8* for pBEVY-L) (wells 4 and 7).

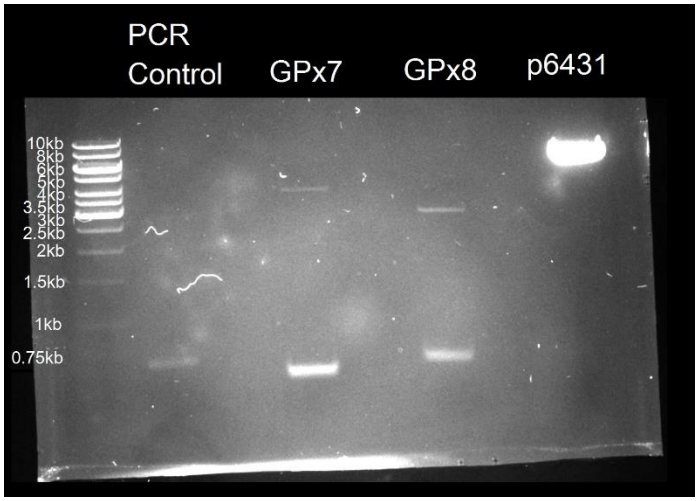

Fig 3.16. Restriction digests of native GPx7, GPx8, p6431 and PCR control for gel extraction and purification.
Using the restriction enzymes BamHI and XbaI *GPX7* (well 4), *GPX8* (well 6), p6431 (well 8) and PCR control (GPx8 for pBEVY-L) (well 2) were restriction digested in preparation for gel extraction and purification.

Multiple bands were seen in restriction digests of *GPX7* and *GPX8*, the expected bands of 534bp and 630bp respectively were present, although as the 0.5kb band of the DNA ladder was not visible this was approximated. An additional band at ~4kb for GPx7 and ~3kb for GPx8 was also present, only the insert was excised from the gel for gel purification.

Quantification of the concentration of DNA in the purified sample indicated there was very little DNA present, as well as significant contamination of the sample as indicated by the $OD_{260/230}$ ratios, all of which considerably lower than the ideal ratio of 2.0-2.2. The ideal ratio for $OD_{260/280}$ to indicate purity of DNA is 1.8, all of the samples, however, had ratios higher than this, typically a value lower than the ideal ratio is indicative of contamination (Fig 3.17.).

	Absorbance at different wavelengths					
Gel Purified product	OD_{260}	OD_{280}	OD_{230}	$OD_{260/280}$	$OD_{260/230}$	Concentration (ng/µl)
GPx7	0.329	0.166	0.967	1.98	0.34	16.4
GPx8	0.246	0.088	0.301	2.79	1.09	12.3
p6431	0.320	0.174	0.463	1.84	0.71	16.0

Fig 3.17. Absorbance of gel purified inserts *GPX7* and *GPX8* and linearised p6431 at OD_{260}, OD_{280} and OD_{230}
The absorbance of *GPX7*, *GPX8* and p6431 measured using a nanodrop spectrophotometer with the ratios of $OD_{260/280}$ and $OD_{260/230}$ along with the final DNA concentration to determine levels of purity of purified DNA.

3.2.1.3 pTH644 vector carrying *GPX7* and *GPX8* chimeric constructs

As human native GPx7 and GPx8 is absent of ER localisation signals it may not have been localising to the ER. Therefore chimeric gene constructs of *GPX7* and *GPX8* were made by von der Haar, T. (school of biosciences) by Gibson assembly with a pTH644-L plasmid backbone (Fig 2.3.). The first set of constructs were GPx7 and GPx8 with HA tags and a substitution of the KREDL and KDEL ER retention sequences of GPx7 and GPx8 respectively for a yeast HDEL ER retention sequence. These gene constructs with HDEL ER retention sequence in a pTH644-

L backbone (Fig 2.3.) were named pUKC3404 and pUKC3405 for GPx7 and GPx8 respectively. The second set of constructs had, HDEL yeast ER retention sequence, HA tag and an N-terminal Ost1 pre-sequence and MAT pro-sequence yeast ER signal sequence. These gene constructs with both HDEL ER retention sequence and yeast ER signal sequences in pTH644 were named pUKC3406 and pUKC3407 for GPx7 and GPx8 respectively.

3.2.1.3.1 *GPX7* and *GPX8* with native ER signal sequence but yeast ER retention sequence

In order to isolate the pUKC3404, pUKC3405, pUKC3406 and pUKC3407 plasmids for transformation into yeast they were extracted from transformed Top10 *E.coli* colonies present on LB + Ampicillin selective medium. This extraction was performed in duplicate, with the exception of pUKC3407 due to one of the replicates lacking viability during overnight growth. Agarose gel electrophoresis of a sample of double restriction digested plasmid extract confirmed integration of insert into the vector for all plasmids as two bands were seen in each of the samples, with the exception of the first duplicate of pUKC3404 which was not used. The expected sizes of DNA fragments of *GPX7* and *GPX8* with HDEL yeast ER retention

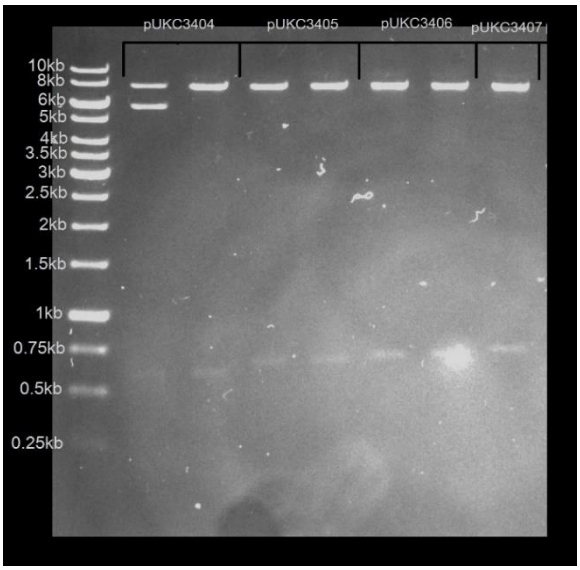

Fig 3.18. Restriction digests of plasmid extracts from *E.coli* cells transformed with pUKC3404, pUKC3405, pUKC3406 and pUKC3407.
Restriction digests using restriction enzymes BamHI and HindIII, the presence of correctly sized inserts were seen for all pUKC340x plasmids, with the exception of the first replicate for pUKC3404, with linearised pTH644-L plasmid at ~8kb seen in all samples.

sequence were 596bp and 662bp respectively, while the expected sizes of *GPX7* and *GPX8* with both ER retention sequence and ER signal sequence were 686bp and 725bp respectively. Use of the DNA ladder shows these inserts to be of correct size (Fig 3.18.).

In parallel to extraction of GPx7 and GPx8 constructs from pTH644-L plasmid the identical constructs were also cloned into pTH644-U, again constructed by von der Haar, T. (School of Biosciences, University of Kent), these plasmids were extracted from competent E.coli and inclusion of insert confirmed but were otherwise unused in this study.

3.2.2 Expression and cellular retention of glutathione peroxidases 7 and 8

Plasmids containing *GPX7* and *GPX8* genes were transformed into yeast and so the successful expression of these recombinant proteins had to be confirmed.

3.2.2.1 Native *GPX7* and *GPX8*

3.2.2.1.1 Confirming expression of glutathione peroxidases 7 and 8

Initially BY4741, 2736 and DN5 were all transformed with pUKC3400 and the expression of His-Tagged native *GPX7* protein tested for via western blot with a monoclonal anti 6xHis tag antibody, however, this showed that only 2736 and DN5 were successfully expressing GPx7 (Fig 3.19.). Alongside all western blots of His tagged GPx7 and GPx8 a control of purified His tagged GPx7 and GPx8, a gift from Beal, D. M. (School of Biosciences, University of Kent), was run. Initially 10µL of a 1/250 and a 1/500 dilution were used (Fig 3.19.) but was reduced to 5µL of a 1/500 dilution for all subsequent blots.

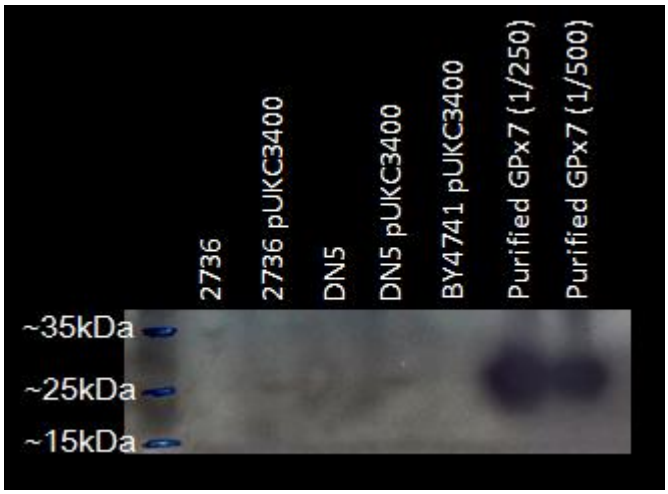

Fig 3.19. Western blot for the expression of native GPx7 in 2736, BY4741 and DN5 strains transformed with pUKC3400
A western blot to test for expression of His-tagged native GPx7 in 2736, DN5 and BY4741 strains transformed with pUKC3400 plasmid. 10µL of purified GPx7 at a 1/250 and 1/500 dilution was run alongside the lysates. Bands indicating expression of GPx7 were seen for 2736 and DN5 transformed with pUKC3400, but not for BY4741.

As a Pdi1p positive strain was required 2736 was chosen as the primary strain for initial investigations used for expression of GPx7 and GPx8. pUKC3401 was then transformed into 2736 once the plasmid had been constructed (Fig 3.20.).

Fig 3.20. Western blot for the expression of native GPx7 and GPx8 in 2736 transformed with pUKC3400 and pUKC3401
2736 strain was transformed with plasmids pUKC3401 and retransformed with pUKC3401. The expression of GPx7 and GPx8 was confirmed via comparison to 5µL 1/250 dilution of GPx7 and GPx8 purified protein.

Following preliminary investigations BY4741 and DN5 were later transformed, and 2736 retransformed, with the pUKC3400 and pUKC3401 plasmids. In the case of BY4741 both GPx7 and GPx8 were being expressed (Fig 3.21.), where as in DN5 it appears that either only GPx7 was being expressed (Fig 3.22.), or that GPx8 was at too low concentration to be seen. This is supported by the expression of GPx8 in both BY4741 and 2736 generated a weak signal (Fig 3.21.) and that DN5 is less efficient in the expression of recombinant proteins as a result of the *PDI1* knock out.

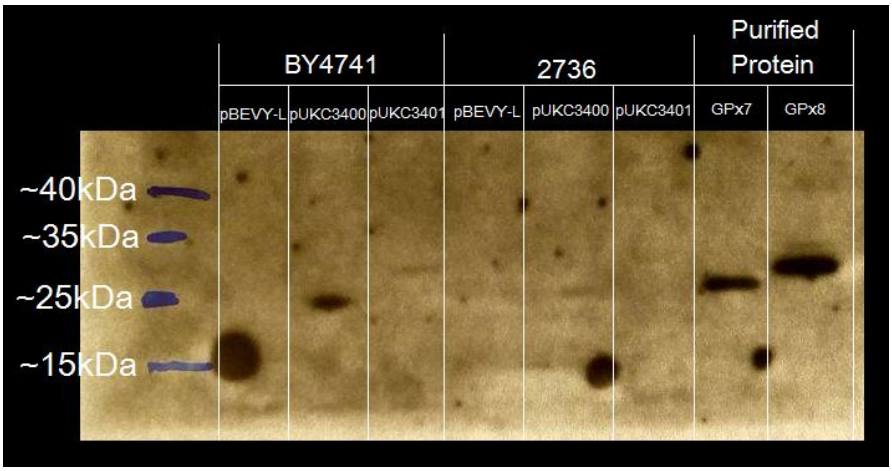

Fig 3.21. Western blot for the expression of native GPx7 and GPx8 in BY4741 and 2736 transformed with pUKC3400, pUKC3401
A western blot for expression of native GPx7 and GPx8 in strains BY4741 and 2736 resulting from a transformation with pUKC3400 and pUKC3401. Bands, albeit faint, were seen for both GPx7 and GPx8 in BY4741 and 2736.

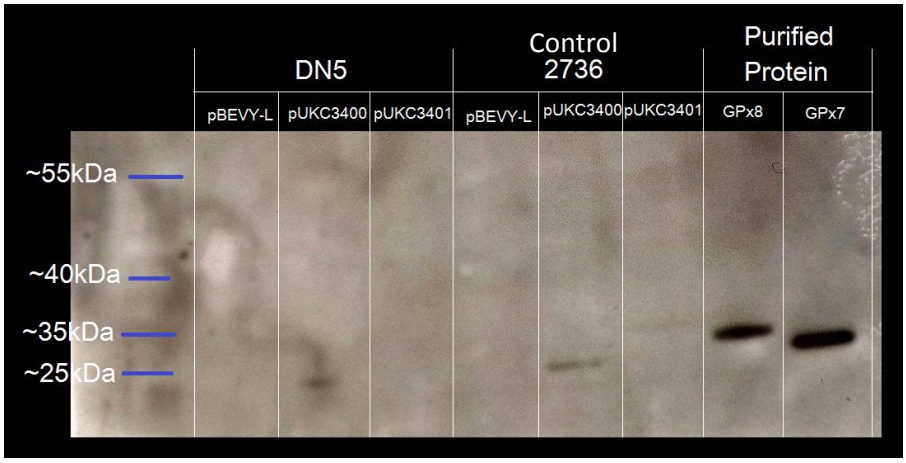

Fig 3.22. Western blot for the expression of native GPx7 and GPx8 in DN5 transformed with pUKC3400, pUKC3401
A western blot for expression of native GPx7 and GPx8 in DN5 transformed with pUKC3400 and pUKC3401. A faint band was seen for GPx7, but not for GPx8. An additional control of previously made 2736 lysates which were known to have shown presence of GPx7 and GPx8 via western blot (Fig 3.20.).

3.2.2.1.2 Cellular retention of native glutathione peroxidases 7 and 8

As the native GPx7 and GPx8 proteins were absent of yeast ER retention or signal sequences a western blot of protein precipitates from the medium was performed to investigate whether the majority of the GPx7 and GPx8 was being retained intracellularly or secreted. The blot, however, had too much background noise and neither control bands nor bands that would indicate secretion of GPx7 and GPx8 could not be seen as a result of this. Due to time constraints the blot was not able to be repeated.

3.2.2.2 BY4741 expressing glutathione peroxidases 7 and 8 constructs

3.2.2.2.1 Confirming expression of glutathione peroxidases 7 and 8 constructs

The expression of modified GPx7 and GPx8 proteins in transformed BY4741 was confirmed by performing a western blot using a monoclonal HA-probe antibody. The lysates of BY4741 transformed with pUKC3404, pUKC3405, pUKC3406 and pUKC3407 indicate that GPx7 and GPx8 with yeast ER retention sequence as well as with both yeast ER retention sequence and yeast ER signal sequence are being expressed (Fig 3.23.). The band for GPx7 with yeast ER retention sequence is very faint but can be seen at ~25kDa while the band for GPx8 with ER retention sequence is in between ~25kDa and ~35kDa (Fig 3.23.). The expression of GPx7 and GPx8 with both yeast ER retention sequence and ER signal sequence was confirmed by

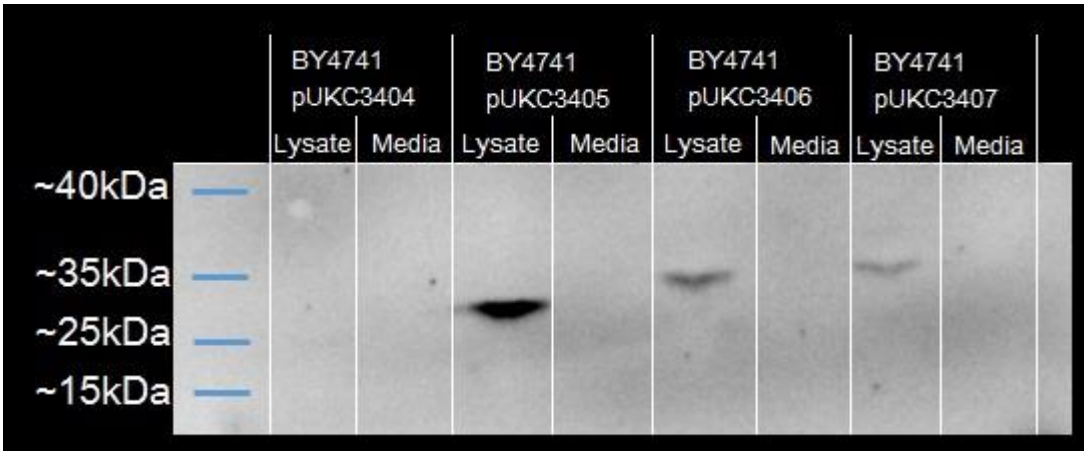

Fig 3.23. Western blot of BY4741 transformed with pUKC3404, pUKC3405, pUKC3406 and pUKC3407 lysates and protein precipitation from medium. Lysates and protein precipitates of medium from overnight growth were ran in parallel for BY4741 transformed with pUKC3404, pUKC3405, pUKC3406 and pUKC3407 to test for both expression and cellular retention of GPx7 and GPx8.

bands at ~35kDa for both GPx7 and GPx8, but with GPx8 having migrated slightly less (Fig 3.23.).

The theoretical molecular weights of each protein are 22kDa GPx7 and 25kDa for GPx8 with HDEL ER retention sequence, while GPx7 and GPx8 constructs with HDEL ER retention sequence and ER signal sequence is ~25kDa and ~28kDa respectively. Theorised molecular weights calculated using ExPASy Bioinformatics Resource Portal compute pI/Mw online resource (web.expasy.org/compute_pi/).

3.2.2.2.2 Cellular retention of glutathione peroxidases 7 and 8 constructs

To show whether presence of ER retention sequence and ER signal sequence was leading to successful intracellular retention protein precipitates from medium of BY4741 transformed with pUKC3404, pUCK3405, pUKC3406 and pUKC3407 after overnight (~16-18 hr) growth were ran alongside lysates. This indicated that the all of GPx7 and GPx8 constructs are being cellularly retained as no bands can be seen that would indicate secretion into the medium (Fig 3.23.). If secretion of these ER targeted proteins was occurring a dominant band would be expected as a result of secretion over a ~16-18 hour period.

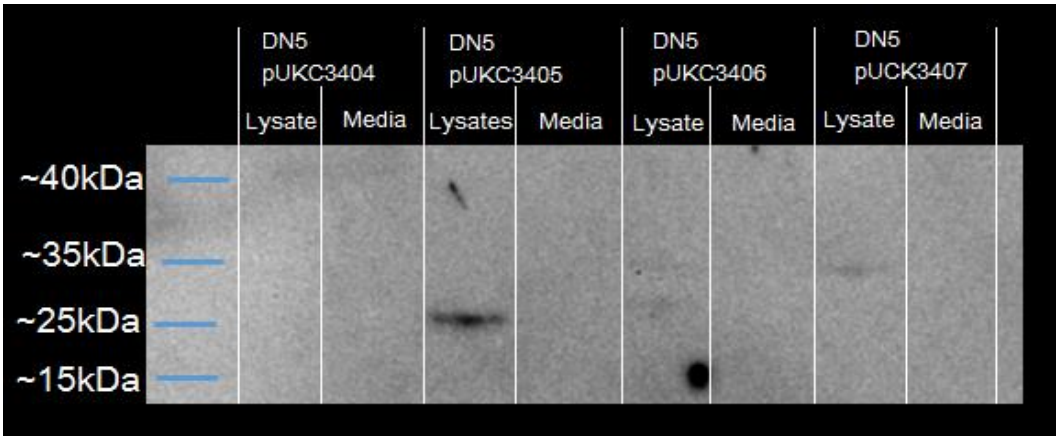

Fig3.24. Western blot of DN5 transformed with pUKC3404, pUKC3405, pUKC3406 and pUKC3407 lysates and protein precipitation from medium. Lysates and protein precipitates of medium from overnight growth were ran in parallel for DN5 transformed with pUKC3404, pUKC3405, pUKC3406 and pUKC3407 to test for both expression and cellular retention of GPx7 and GPx8 constructs.

3.2.2.3 A Δ*pdi1* strain expressing glutathione peroxidases 7 and 8 constructs

3.2.2.3.1 Confirming expression of glutathione peroxidases 7 and 8 constructs

To identify whether GPx7 and GPx8 constructs were being expressed in the Δ*pdi1* strain DN5 transformed with pUKC3404, pUKC3405, pUKC3406 and pUKC3407 a western blot was performed with a monoclonal HA-probe antibody. Bands can be seen for the GPx7 and GPx8 constructs expressed in DN5, with the exception of GPx7 with ER retention sequence only (Fig 3.24.).

When this plasmid was transformed into BY4741 and expression of GPx7 tested for the band was very faint (Fig 3.23.) and hence there may be expression but at too low levels to detect due to excess background noise from the blot. There appears to be two bands present for GPx7 with both yeast ER signal sequence and retention sequence, one at ~35kda, which was expected from the bands seen previously (Fig 3.23.), but an additional band just above the 25kda marker of the protein ladder was also seen.

3.2.2.3.2 Western Blot to assay for cellular retention of protein

To check for intracellular retention of GPx7 and GPx8 with ER retention sequence and ER signal sequences protein precipitates from medium of O/N (~16-18hrs) cultures for DN5 transformed with pUKC3404, pUKC3405, pUKC3406 and pUKC3407 shows absence in bands for suggests that there is not significant secretion of the protein and hence is retained intracellularly (Fig 3.23.).

3.2.3 Changes to sensitivity to hydrogen peroxide as a result of expressing glutathione peroxidases 7 and 8

Expression of GPx7 reportedly leads to reduced sensitivity to H_2O_2 in human tissue[86]. Therefore to investigate as to whether GPx7 and GPx8 confers increased resistance to H_2O_2 in a yeast system through intracellular H_2O_2 processing cells were exposed to a range of concentrations of H_2O_2. H_2O_2 is a redox reagent and causes damage to protein, lipids and nucleic acids[87], therefore it would be expected that cells more able to detoxify H_2O_2 would have increased growth rates. To test this hypothesis both growth analysis in liquid culture and sensitivity assays on solid medium were performed in presence of H_2O_2.

3.2.3.1 Growth in YNB-Leu liquid medium in presence of hydrogen peroxide

To investigate whether GPx7 and GPx8 mediate a resistance to H_2O_2 growth curves in 0mM-4mM H_2O_2 were performed.

3.2.3.1.1 BY4741 and 2736 expressing native glutathione peroxidases 7 and 8

BY4741 and 2736 each transformed with pBEVY-L empty vector control (Fig2.2.), pUKC3400 and pUKC3401 were grown in liquid YNB-Leu minimal medium to prevent plasmid loss with H_2O_2 concentrations ranging from 0mM to 4mM with 1mM intervals.

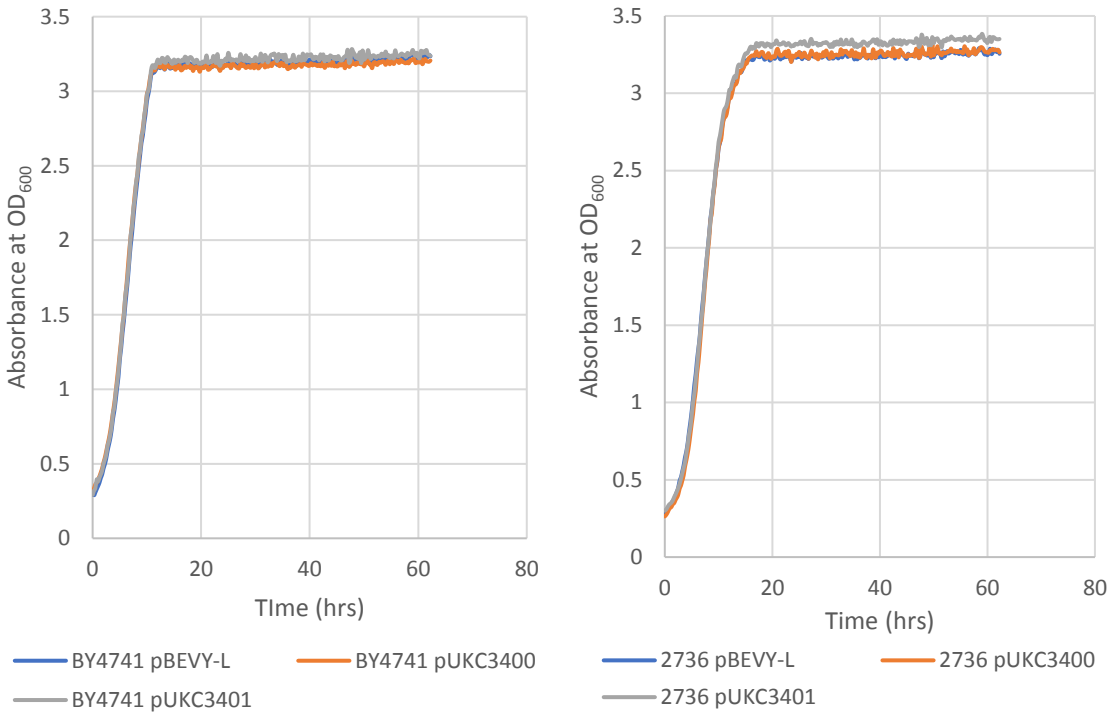

Fig 3.25. Growth of BY4741 and 2736 expressing native GPx7 and GPx8 in liquid medium in 0mM H_2O_2
Change in absorbance over time indicating growth in YNB-Leu liquid medium of BY4741 (left) and 2736 (right) expressing native GPx7 (orange) and GPx8 (grey), with each respective strain transformed with pBEVY-L empty vector as a control (blue) in the absence of external H_2O_2 induced stress.

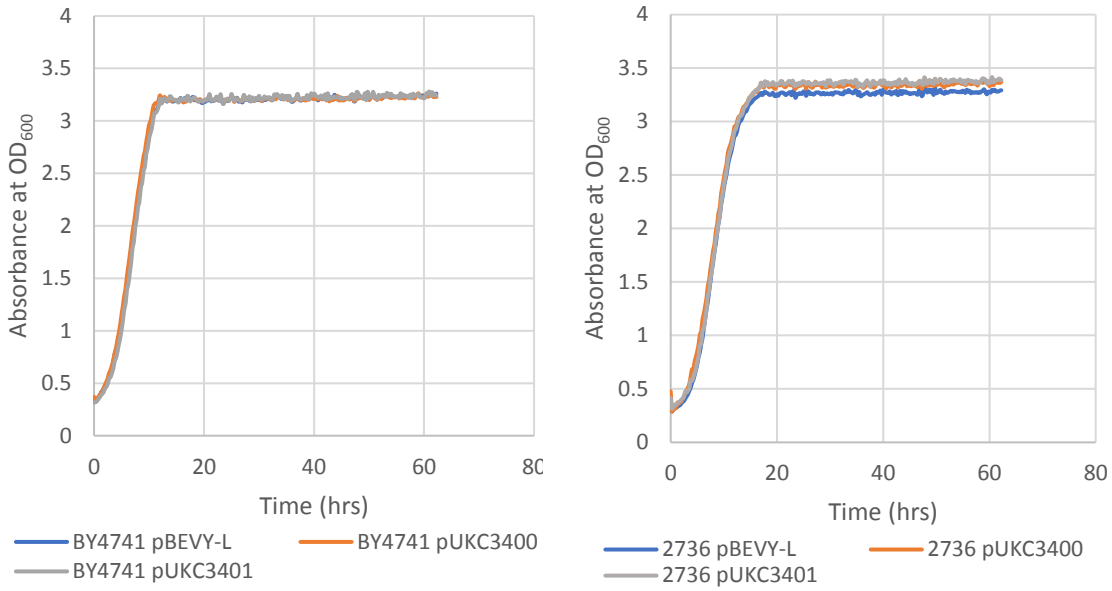

Fig 3.26. Growth of BY4741 and 2736 expressing native GPx7 and GPx8 in liquid medium in 1mM H_2O_2
Change in absorbance over time indicating growth in YNB-Leu liquid medium of BY4741 (left) and 2736 (right) expressing native GPx7 (orange) and GPx8 (grey), with each respective strain transformed with pBEVY-L empty vector as a control (blue) in 1mM H_2O_2.

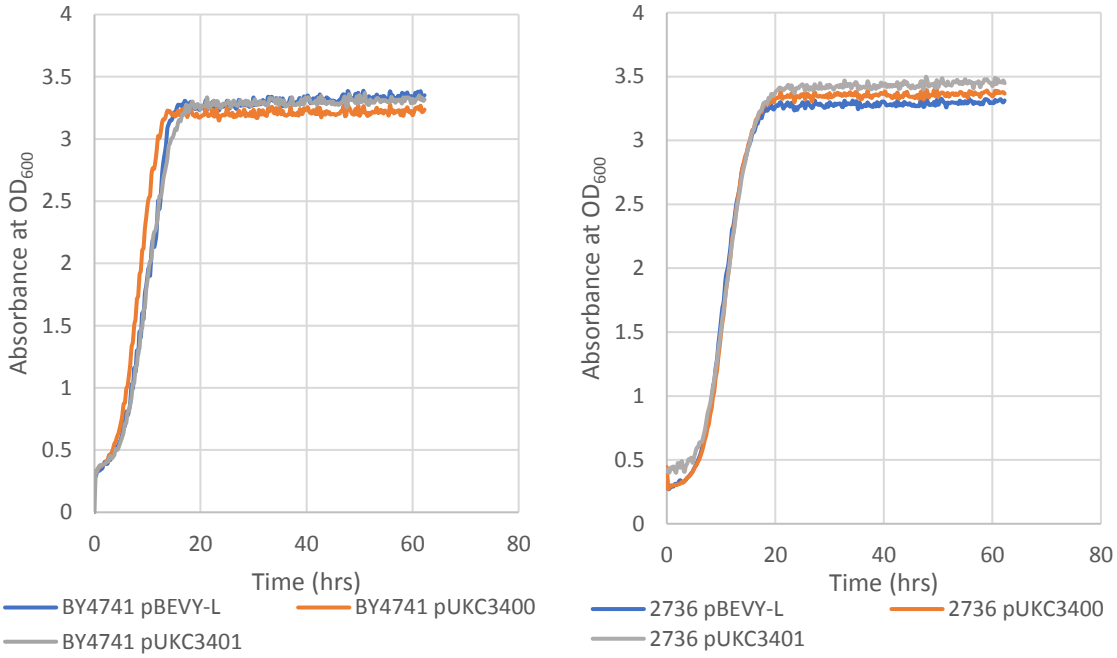

Fig 3.27. Growth of BY4741 and 2736 expressing native GPx7 and GPx8 in liquid medium in 2mM H_2O_2
Change in absorbance over time indicating growth in YNB-Leu liquid medium of BY4741 (left) and 2736 (right) expressing native GPx7 (orange) and GPx8 (grey), with each respective strain transformed with pBEVY-L empty vector as a control (blue) in 2mM H_2O_2.

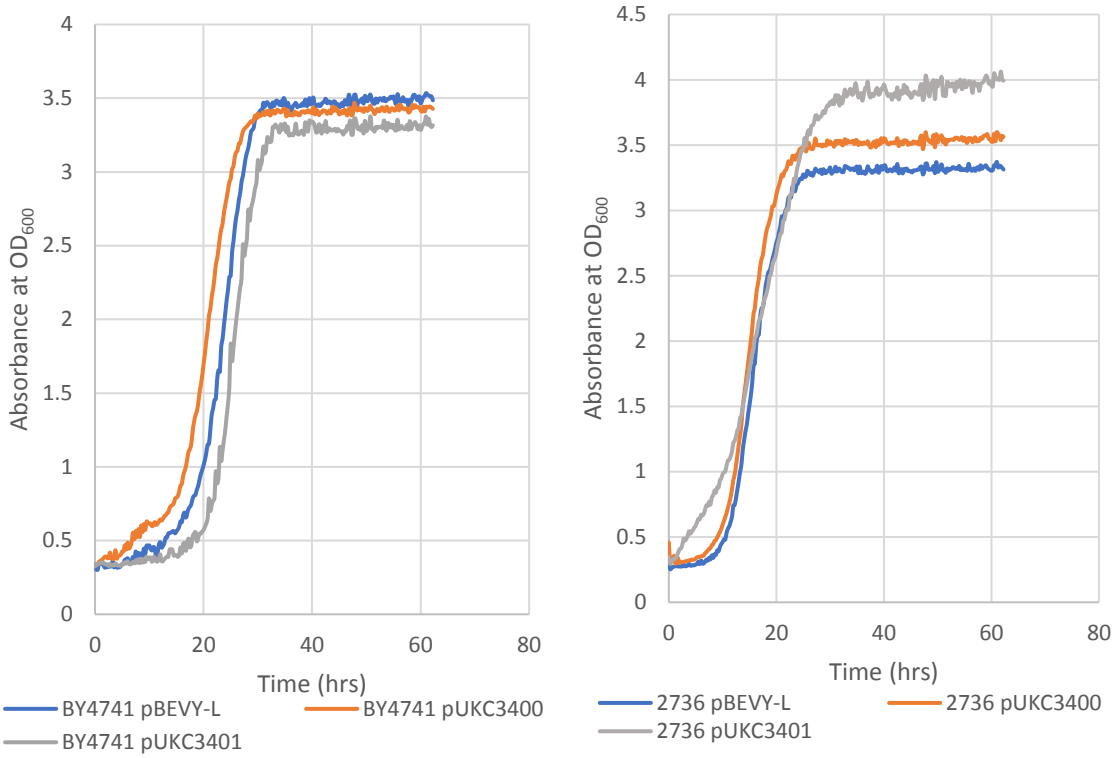

Fig 3.28. Growth of BY4741 and 2736 expressing native GPx7 and GPx8 in liquid medium in 3mM H_2O_2
Change in absorbance over time indicating growth in YNB-Leu liquid medium of BY4741 (left) and 2736 (right) expressing native GPx7 (orange) and GPx8 (grey), with each respective strain transformed with pBEVY-L empty vector as a control (blue) in 3mM H_2O_2.

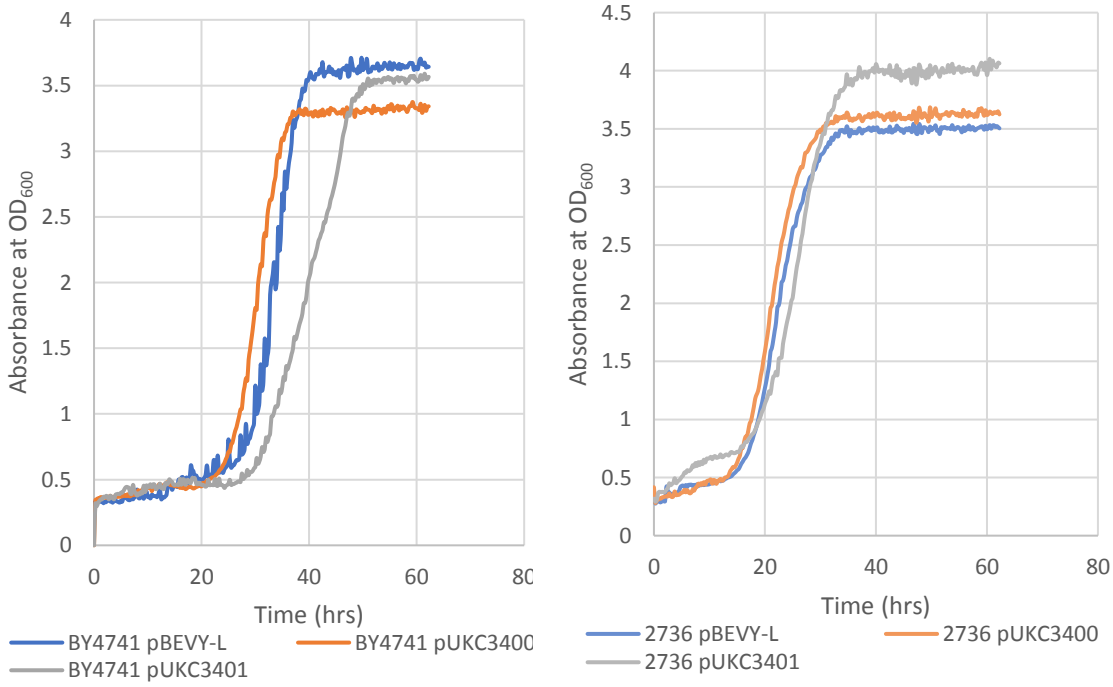

Fig 3.29. Growth of BY4741 and 2736 expressing native GPx7 and GPx8 in liquid medium in 4mM H_2O_2
Change in absorbance over time indicating growth in YNB-Leu liquid medium of BY4741 (left) and 2736 (right) expressing native GPx7 (orange) and GPx8 (grey), with each respective strain transformed with pBEVY-L empty vector as a control (blue) in 4mM H_2O_2.

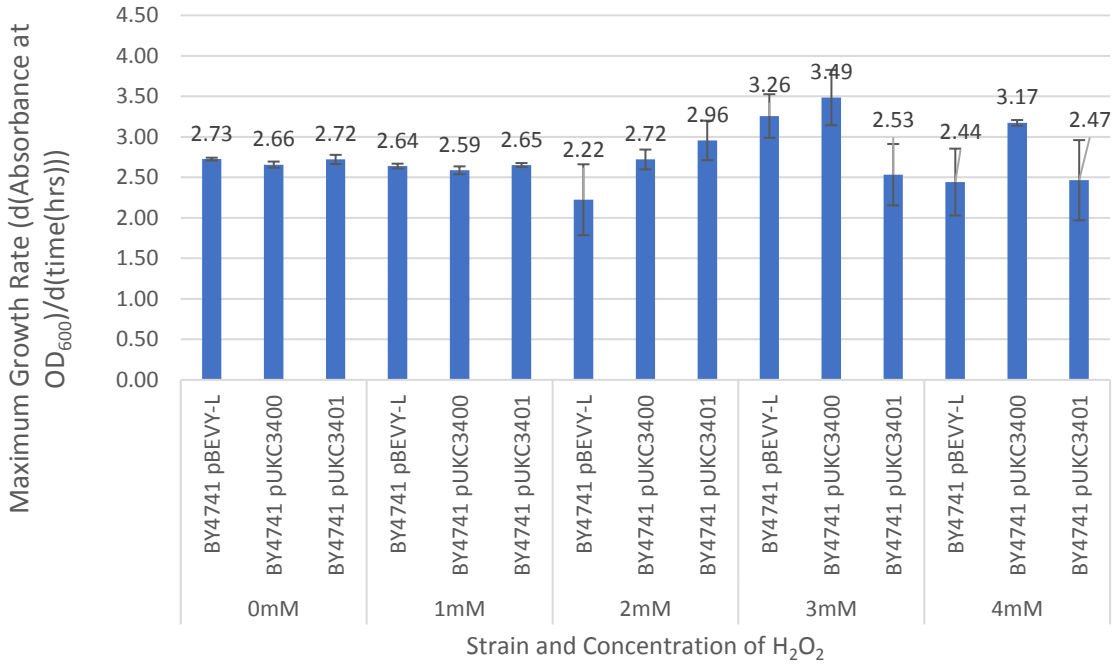

Fig 3.30. Maximum growth rate during log phase of BY4741 expressing native GPx7 and GPx8 in liquid medium at a range of H_2O_2 concentrations.
A bar chart of the maximum growth rates calculated from growth curves of BY4741 in YNB-Leu liquid medium expressing native GPx7 and GPx8 in H_2O_2 concentrations ranging from 0mM to 4mM. Experiment performed in triplicate with standard error bars.

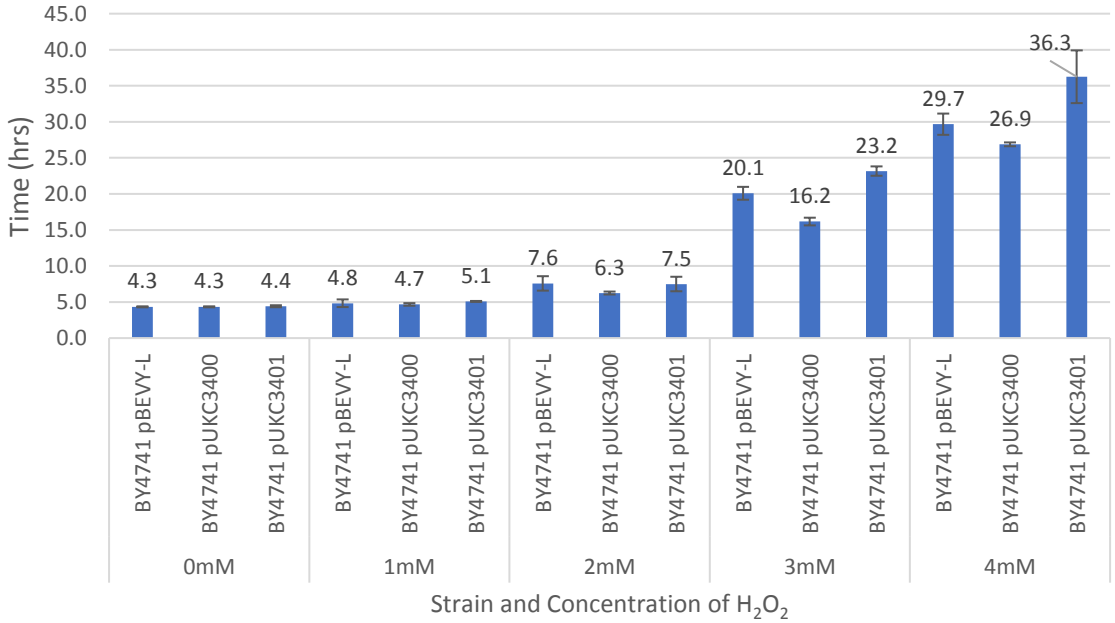

Fig 3.31. Duration of lag phase of BY4741 expressing native GPx7 and GPx8 in liquid medium at a range of H_2O_2 concentrations.
A bar chart of the duration of lag phase calculated from growth curves of BY4741 in YNB-Leu liquid medium expressing native GPx7 and GPx8 in H_2O_2 concentrations ranging from 0mM to 4mM.

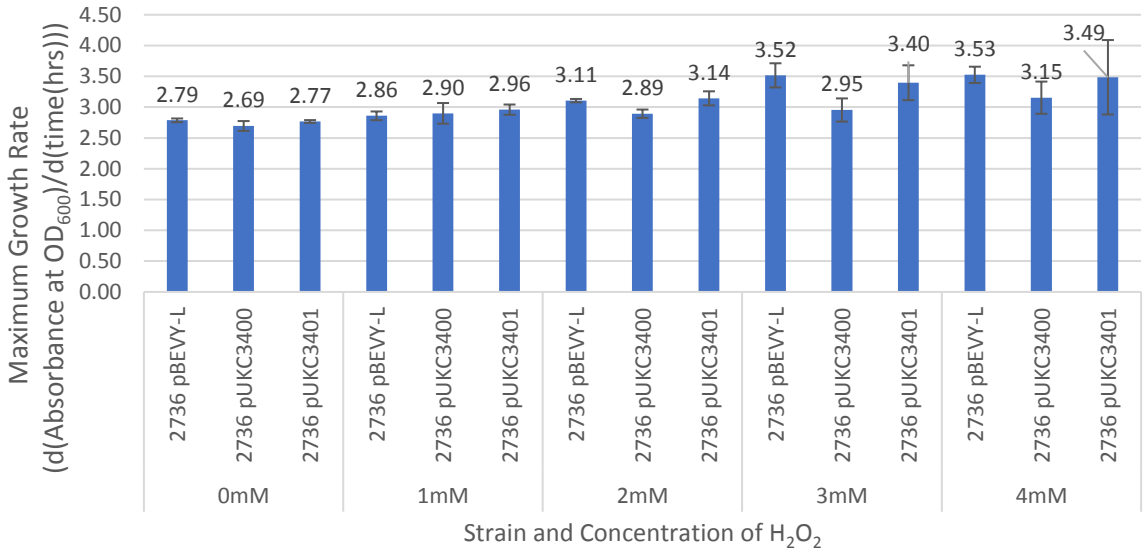

Fig 3.32. Maximum growth rate during log phase of 2736 expressing native GPx7 and GPx8 in liquid medium at a range of H_2O_2 concentrations.
A bar chart of the maximum growth rates calculated from growth curves of 2736 in YNB-Leu liquid medium expressing native GPx7 and GPx8 in H_2O_2 concentrations

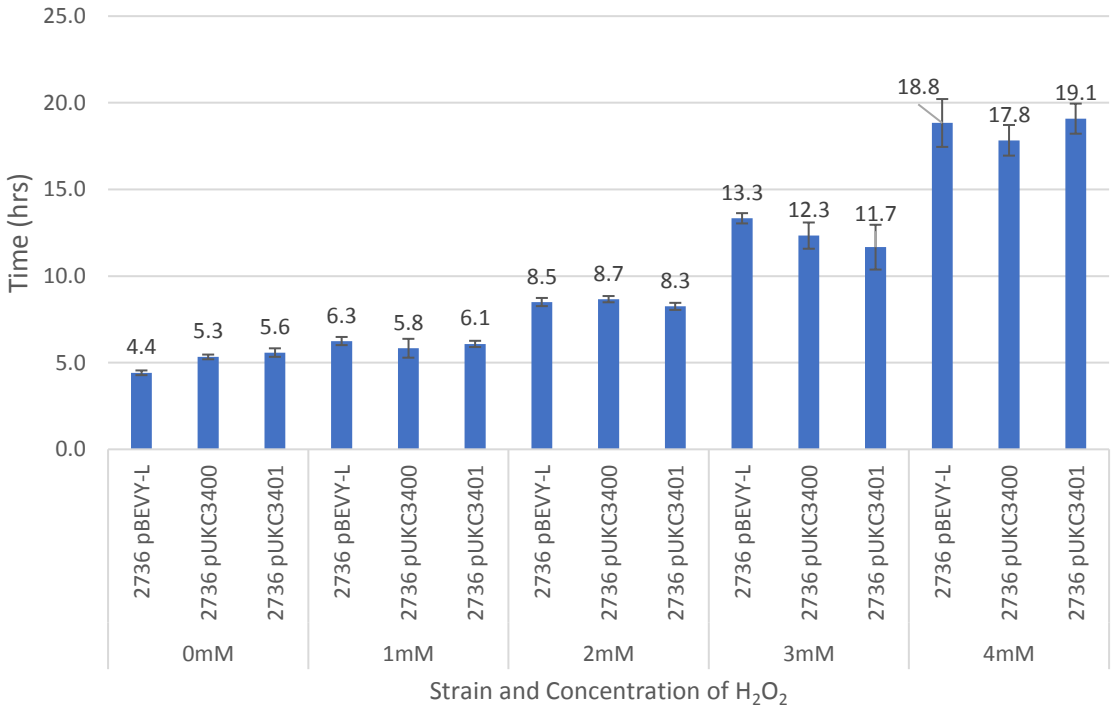

Fig 3.33. Duration of lag phase of 2736 expressing native GPx7 and GPx8 in liquid medium at a range of H_2O_2 concentrations.
A bar chart of the duration of lag phase calculated from growth curves of 2736 in YNB-Leu liquid medium expressing native GPx7 and GPx8 in H_2O_2 concentrations ranging from 0mM to 4mM.

Growth curves for BY4741 and 2736 show no significant changes as a result of expressing GPx7 or GPx8, particularly at low concentrations of H_2O_2 (Fig 3.24. – Fig 3.26.). Only once a concentration of 3mM H_2O_2 is reached is there some deviation between the growth curves of the control and strains expressing GPx7 or GPx8 (Fig 3.27.). In 2736 this discrepancy is more obvious as 2736 expressing GPx8 reaches stationary phase with an absorbance of OD_{600} ~4.0 in both 3mM and 4mM H_2O_2 (Fig 3.27., Fig 3.28.), this is higher than the 2736 control which reached stationary phase at an OD_{600} ~3.3 in 3mM H_2O_2 and ~3.5 in 4mM. 2736 expressing GPx7 also reaches stationary phase at an absorbance higher than that of the control with an OD_{600} of 3.5 in 3mM H_2O_2 and 3.6 in 4mM H_2O_2 (Fig 3.27., Fig 3.28.).

BY4741, however, in contrast to 2736, reaches stationary phase at a lower absorbance than the control when expressing GPx8 with an OD_{600} of ~3.3 at 3mM and ~3.5 at 4mM, compared with the control reaching stationary phase at OD_{600} ~3.5 and ~3.6 at 3mM and 4mM respectively (Fig 3.27., Fig 3.28.). BY4741 expressing GPx7 at 3mM reaches stationary phase at an absorbance very similar to that of the control, however, at 4mM stationary phase is only reached at OD_{600} ~3.3 (Fig 3.27., Fig 3.28.).

The most obviously affected strain from high concentrations of H_2O_2 was BY4741 expressing GPx8 at 4mM concentration (Fig 3.27.), however, this strain showed a large error bars and hence this result has low reliability (Fig 3.29., Fig 3.30.).

A chart of the maximum rates achieved during log phase growth and duration of lag phase shows that there are no statistically significant changes in maximum rate or duration of lag phase as a result of expressing GPx7 and GPx8, as P values of an unpaired two-tailed t-test were greater than the significant interval of 0.05. This was the case for any concentration of H_2O_2 for either BY4741 or 2736 as a result of expression of native GPx7 or GPx8 (Fig 3.29., Fig 3.31.), with the exception of 2736 in 0mM where there is a statistically significant increase in duration of lag phase, with an unpaired two-tailed t-test P value of 0.0177, lower than the significance interval of 0.05. The duration of lag phase increases in all strains as a result of increasing concentration of H_2O_2.

Therefore expression of native human GPx7 and GPx8 results in no statistically significant change in growth rates in PDI expressing strains BY4741 and 2736.

3.2.3.1.2 BY4741 expressing glutathione peroxidases 7 and 8 constructs

As there was no effect on growth rates from native human GPx7 and GPx8 the constructs of these genes with ER localisation signals were expressed in a PDI expressing strain. This was to investigate whether the resistance to H_2O_2 was a result of GPx7 and GPx8 not being localised to the ER. The change in sensitivity to H_2O_2 in liquid YNB-Leu medium of BY4741 transformed with pUKC3404, pUKC3405, pUKC3406 and pUKC3407 to H_2O_2 as a result of expressing GPx7 and GPx8 with ER localisation sequences was investigated. This was to check if the lack of statistically significant changes in H_2O_2 sensitivity for BY4741 and 2736 transformed with pUKC3400 and pUKC3401 were a result of the native GPx7 and GPx8 proteins not being resident in the ER.

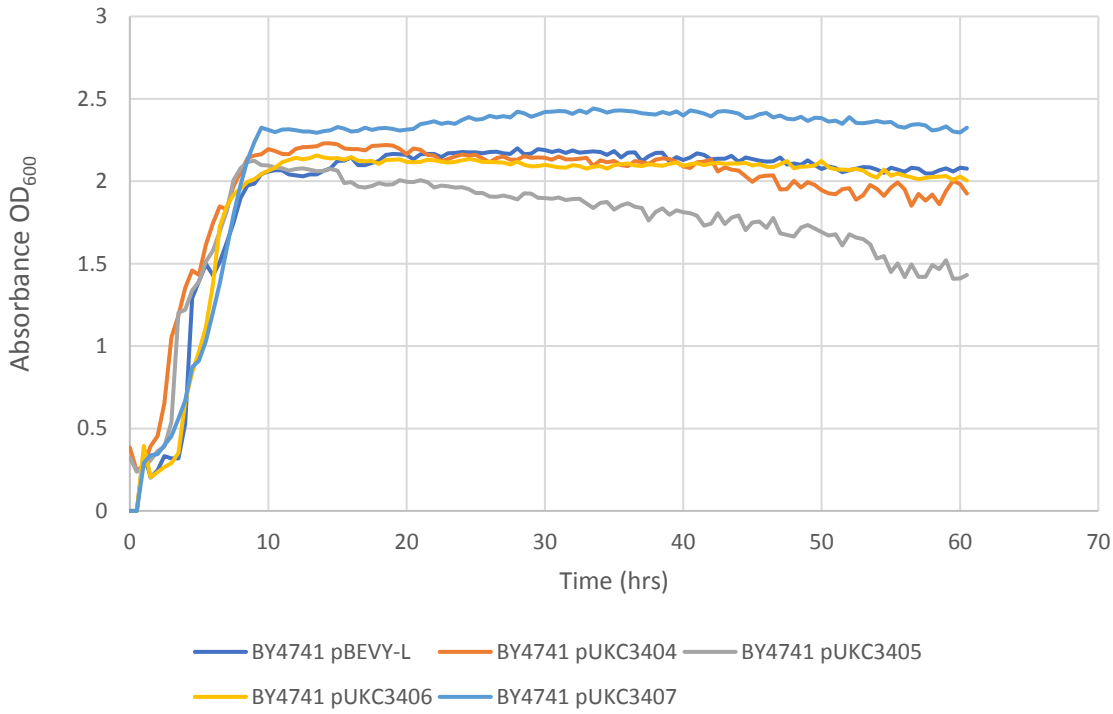

Fig 3.34. Growth of BY4741 expressing GPx7 and GPx8 constructs in liquid medium in 0mM H_2O_2
Change in absorbance over time indicating growth in YNB-Leu liquid medium of BY4741 expressing GPx7 and GPx8 with either an ER retention sequence only (orange and grey respectively), or both an ER retention sequence and ER signal sequence (yellow and dark blue respectively) in the absence of external H_2O_2 induced stress.

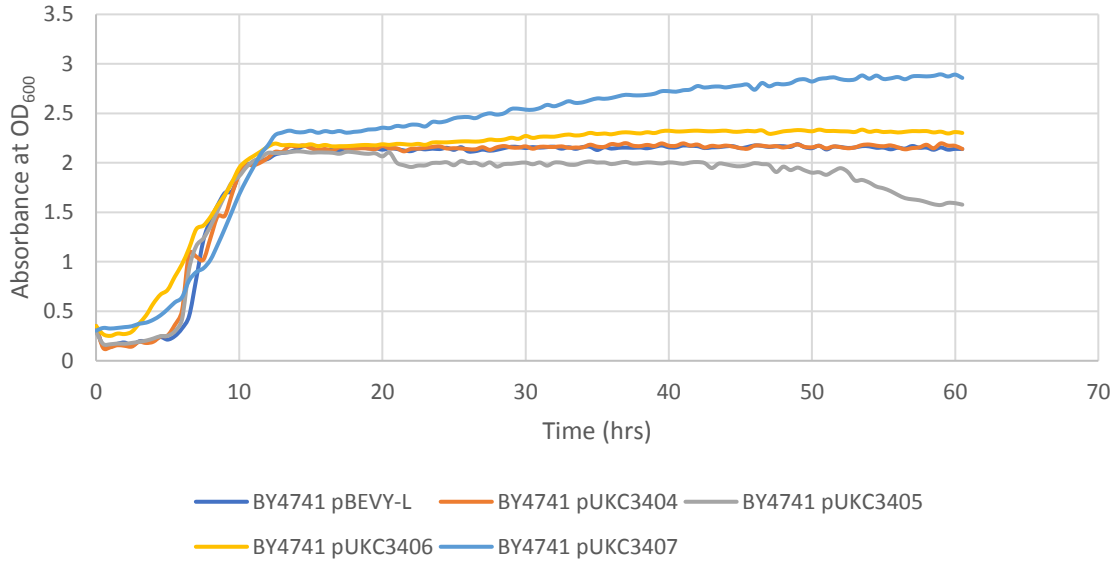

Fig 3.35. Growth of BY4741 expressing GPx7 and GPx8 constructs in liquid medium in 1mM H_2O_2
Change in absorbance over time indicating growth in YNB-Leu liquid medium of BY4741 expressing GPx7 and GPx8 with either an ER retention sequence only (orange and grey respectively), or both an ER retention sequence and ER signal sequence (yellow and dark blue respectively) in 1mM H_2O_2.

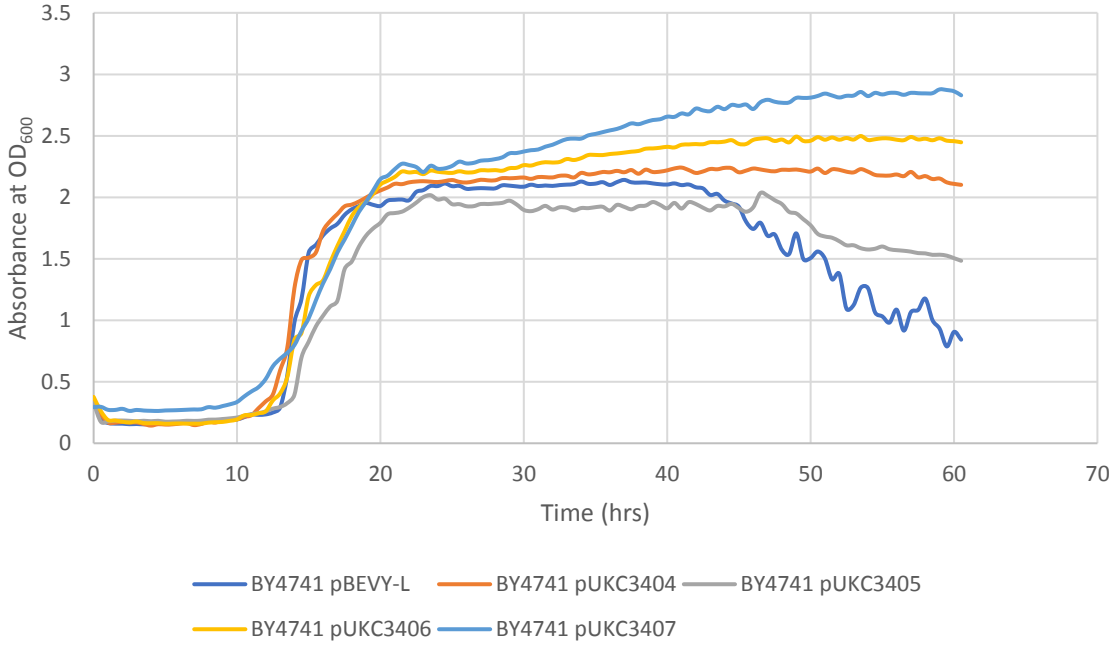

Fig 3.36. Growth of BY4741 expressing GPx7 and GPx8 constructs in liquid medium in 2mM H_2O_2
Change in absorbance over time indicating growth in YNB-Leu liquid medium of BY4741 expressing GPx7 and GPx8 with either an ER retention sequence only (orange and grey respectively), or both an ER retention sequence and ER signal sequence (yellow and dark blue respectively) in 2mM H_2O_2.

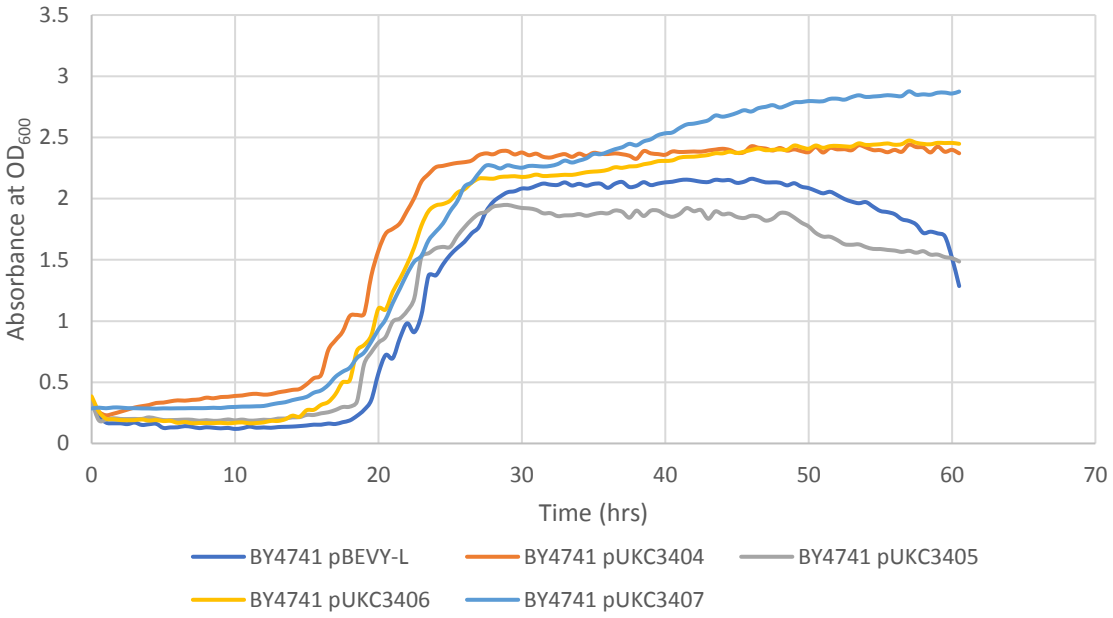

Fig 3.37. Growth of BY4741 expressing GPx7 and GPx8 constructs in liquid medium in 3mM H_2O_2
Change in absorbance over time indicating growth in YNB-Leu liquid medium of BY4741 expressing GPx7 and GPx8 with either an ER retention sequence only (orange and grey respectively), or both an ER retention sequence and ER signal sequence (yellow and dark blue respectively) in 3mM H_2O_2.

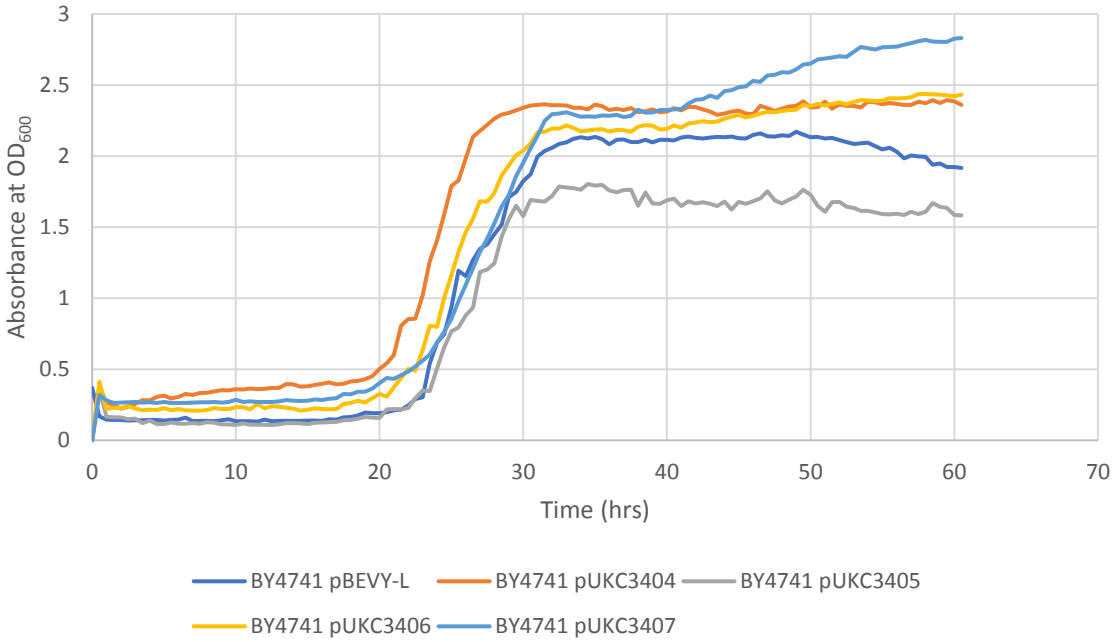

Fig 3.38. Growth of BY4741 expressing GPx7 and GPx8 constructs in liquid medium in 4mM H_2O_2
Change in absorbance over time indicating growth in YNB-Leu liquid medium of BY4741 expressing GPx7 and GPx8 with either an ER retention sequence only (orange and grey respectively), or both an ER retention sequence and ER signal sequence (yellow and dark blue respectively) in 4mM H_2O_2.

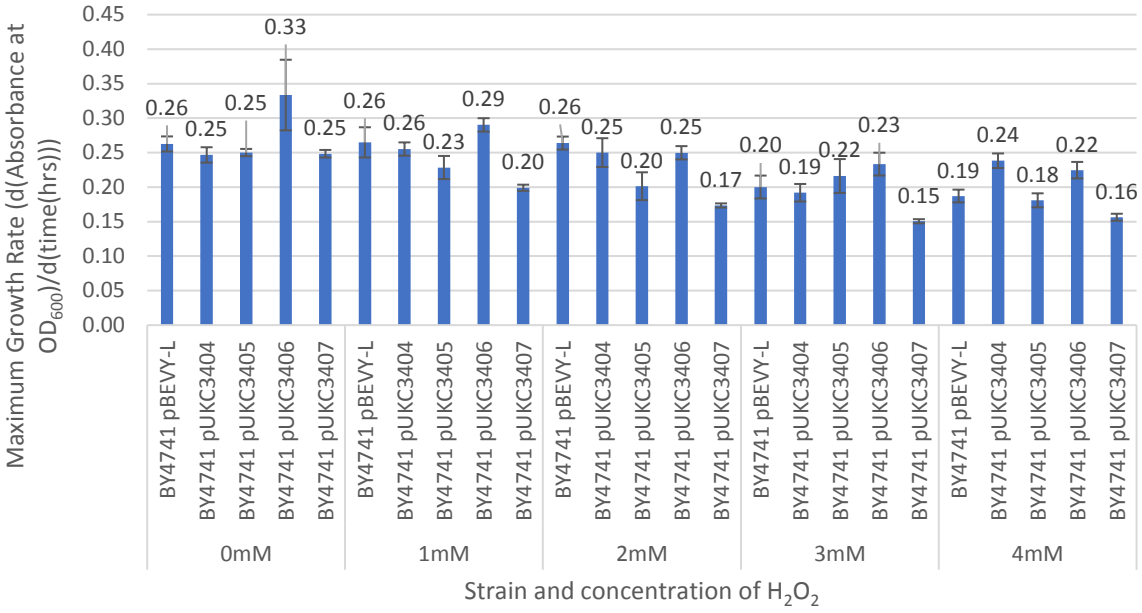

Fig 3.39. Maximum growth rate during log phase of BY4741 expressing GPx7 and GPx8 constructs in liquid medium at a range of H_2O_2 concentrations.
A bar chart of the maximum growth rates calculated from growth curves of BY4741 in YNB-Leu liquid medium expressing GPx7 and GPx8 constructs in H_2O_2 concentrations ranging from 0mM to 4mM with standard error bars.

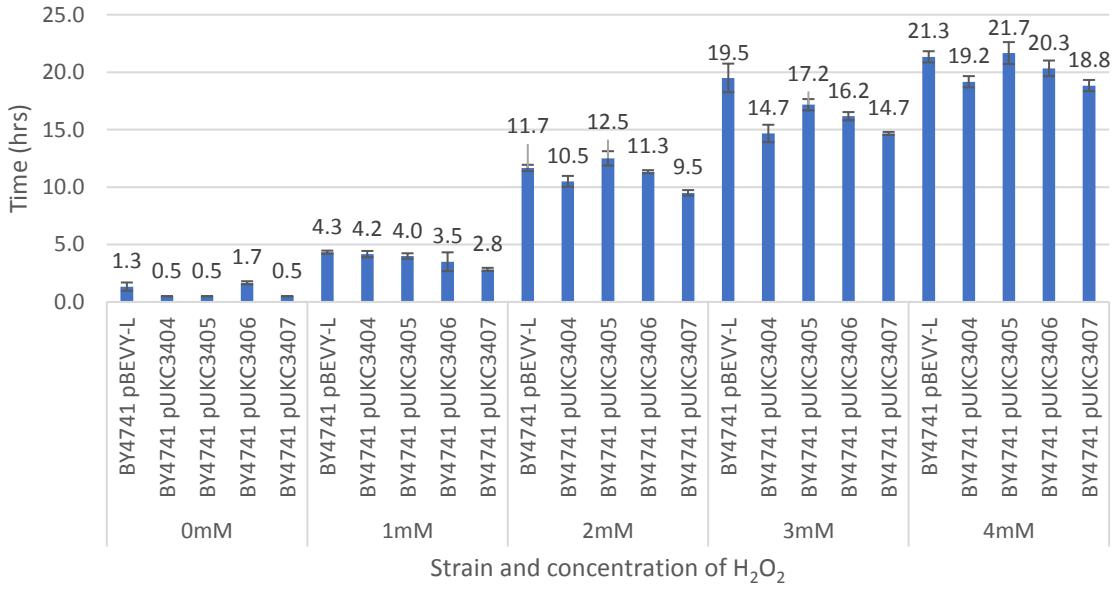

Fig 3.40. Duration of lag phase of BY4741 expressing native GPx7 and GPx8 in liquid medium at a range of H_2O_2 concentrations.
A bar chart of the duration of lag phase calculated from growth curves of BY4741 in YNB-Leu liquid medium expressing GPx7 and GPx8 constructs in H_2O_2 concentrations ranging from 0mM to 4mM with standard error bars

At all concentrations of H_2O_2 the duration of lag phase of BY4741 strain expressing the GPx7 and GPx8 constructs was very similar to that of the pBEVY-L empty vector control strain (Fig 3.40.). Across all concentrations pUKC3404 appeared to have a shorter lag phase than the control, however, this phenotype became more apparent at higher concentrations (Fig 3.40.) this finding, however, was not statistically significant, as the unpaired two-tailed t-test P values for BY4741 pUKC3404 at a range of concentrations when compared to the control were all greater than the significance interval of 0.05. The maximum growth rates also indicated no statistically significant changes as a result of expressing the GPx7 and GPx8 constructs, as again there were no two-tailed t-test P values less than the significance interval of 0.05, however, there was a general trend of all strains towards lower growth rate at higher concentration of H_2O_2 (Fig 3.39.).

One trend that was seen was that the different transformants reached stationary phase at different absorbances to each other. Consistent across all of the H_2O_2 concentrations BY4741 transformed with pUKC3407 reached stationary phase at the highest absorbance, while BY4741 transformed with pUKC3405 was the lowest. The second lowest was the BY4741 pBEVY-L control followed by pUKC3404 and pUKC3406 which reached stationary phase at similar absorbances (Fig 3.34. – Fig 3.38.). Likewise, it is the two strains that reached stationary phase with the lowest aborbances: BY4741 transformed with pUKC3405 and pBEVY-L that also enter decline phase earlier than the other strains (Fig 3.34. – Fig 3.38.). This indicates that these two strains may be more susceptible to growth inhibitions at lower nutrient availability and that BY4741 expressing GPx8 with both an ER retention sequence and an ER signal sequence is more resistant.

Nevertheless expressing GPx7 and GPx8 with ER localisation signals does not appear to have any effect on the sensitivity of BY4741 to H_2O_2.

3.2.3.1.3 A Δ*pdi1* strain expressing glutathione peroxidases 7 and 8 constructs

As the primary substrate for the GPx7 and GPx8 coupled detoxification of H_2O_2 is Pdi1p it was originally proposed that expression in a strain that expresses Pdi1p, such as BY4741 or 2736, would mediate *in vivo* H_2O_2 detoxification, while a Δ*pdi1* strain, such as DN5, would not. This would not result in an increased resistance to H_2O_2 that could be shown through growth curve analysis in liquid culture. However,

in light of the finding that GPx7 and GPx8 with ER localisation signals did not incur a detectable resistance to H_2O_2 in BY4741 the same would be expected of DN5.

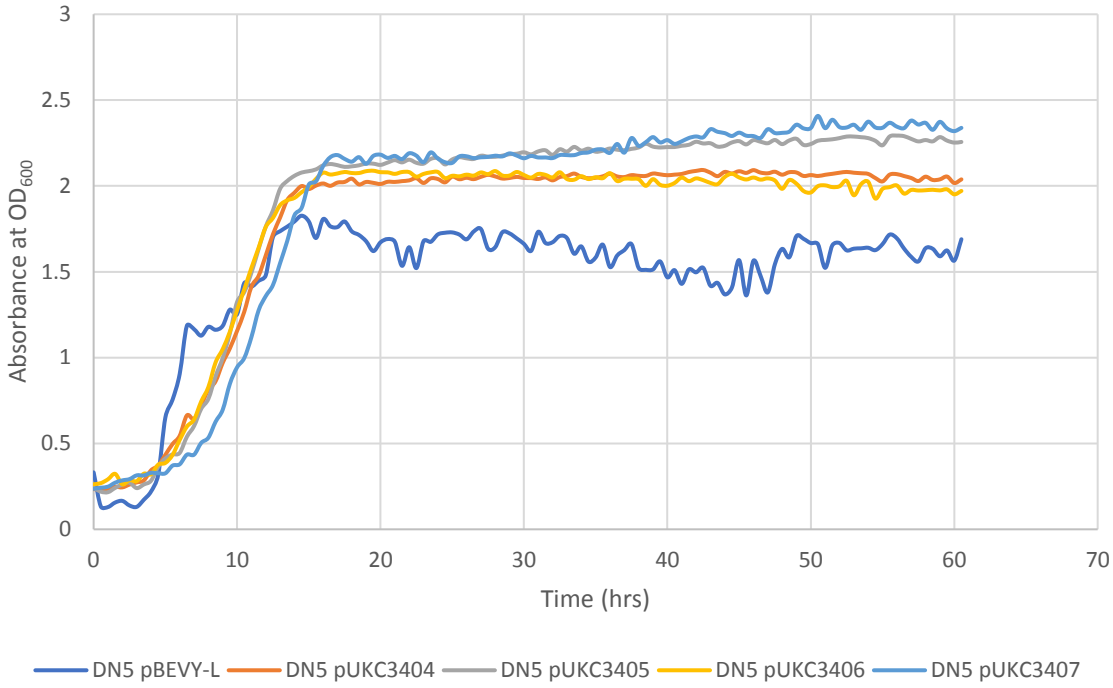

Fig 3.41. Growth of DN5 expressing GPx7 and GPx8 constructs in liquid medium in 0mM H_2O_2
Change in absorbance over time indicating growth in YNB-Leu liquid medium of DN5 expressing GPx7 and GPx8 with either an ER retention sequence only (orange and grey respectively), or both an ER retention sequence and ER signal sequence (yellow and dark blue respectively) in the absence of H_2O_2 induced stress.

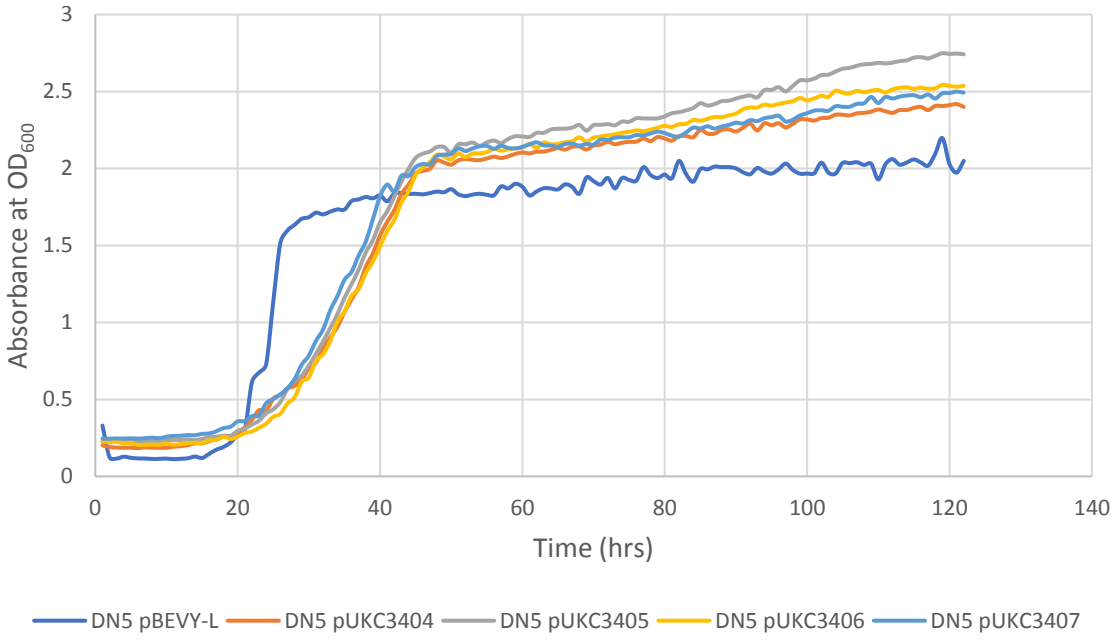

Fig 3.42. Growth of DN5 expressing GPx7 and GPx8 constructs in liquid medium in 1mM H_2O_2
Change in absorbance over time indicating growth in YNB-Leu liquid medium of DN5 expressing GPx7 and GPx8 with either an ER retention sequence only (orange and grey respectively), or both an ER retention sequence and ER signal sequence (yellow and dark blue respectively) in 1mM H_2O_2.

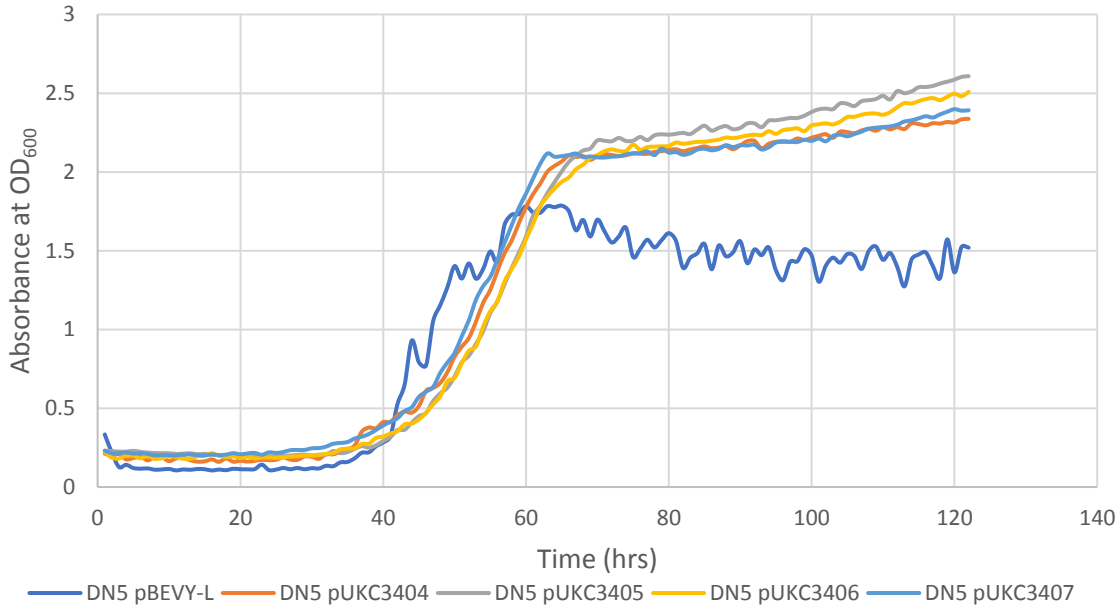

Fig 3.43. Growth of DN5 expressing GPx7 and GPx8 constructs in liquid medium in 2mM H_2O_2
Change in absorbance over time indicating growth in YNB-Leu liquid medium of DN5 expressing GPx7 and GPx8 with either an ER retention sequence only (orange and grey respectively), or both an ER retention sequence and ER signal sequence (yellow and dark blue respectively) in 2mM H_2O_2.

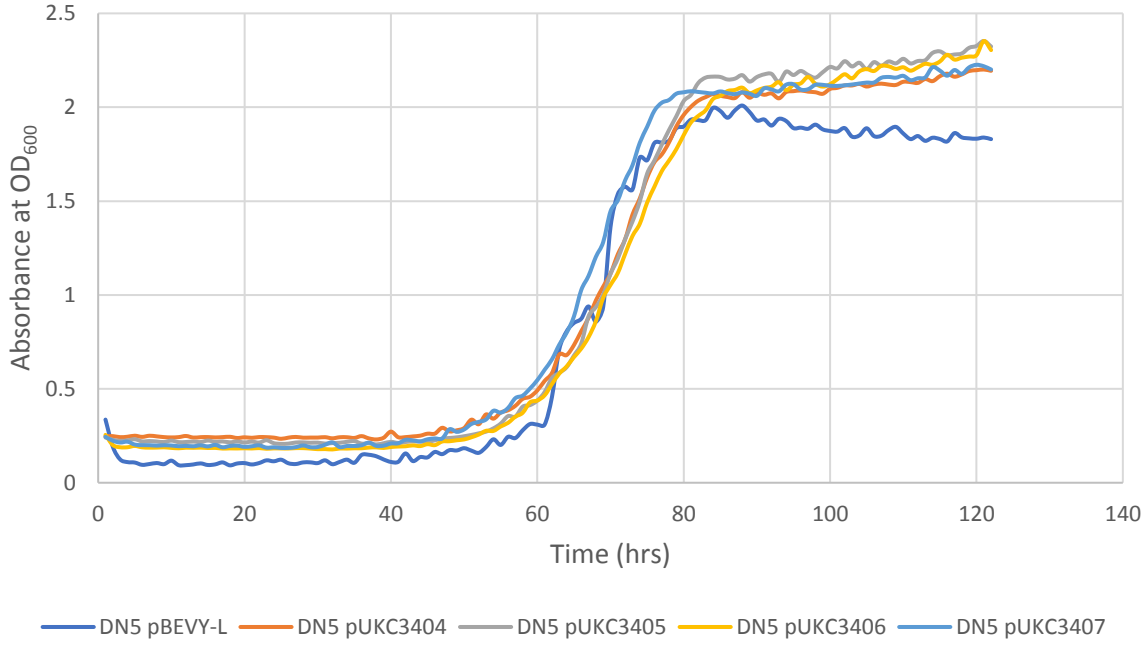

Fig 3.44. Growth of DN5 expressing GPx7 and GPx8 constructs in liquid medium in 3mM H_2O_2
Change in absorbance over time indicating growth in YNB-Leu liquid medium of DN5 expressing GPx7 and GPx8 with either an ER retention sequence only (orange and grey respectively), or both an ER retention sequence and ER signal sequence (yellow and dark blue respectively) in 3mM H_2O_2.

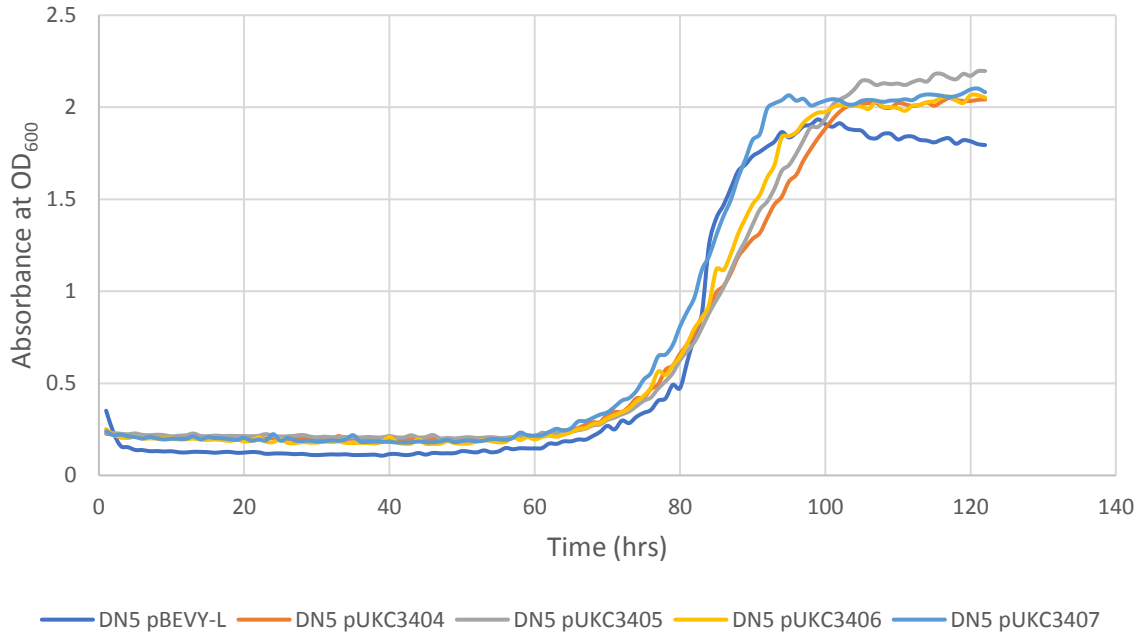

Fig 3.45. Growth of DN5 expressing GPx7 and GPx8 constructs in liquid medium in 4mM H_2O_2
Change in absorbance over time indicating growth in YNB-Leu liquid medium of DN5 expressing GPx7 and GPx8 with either an ER retention sequence only (orange and grey respectively), or both an ER retention sequence and ER signal sequence (yellow and dark blue respectively) in 4mM H_2O_2.

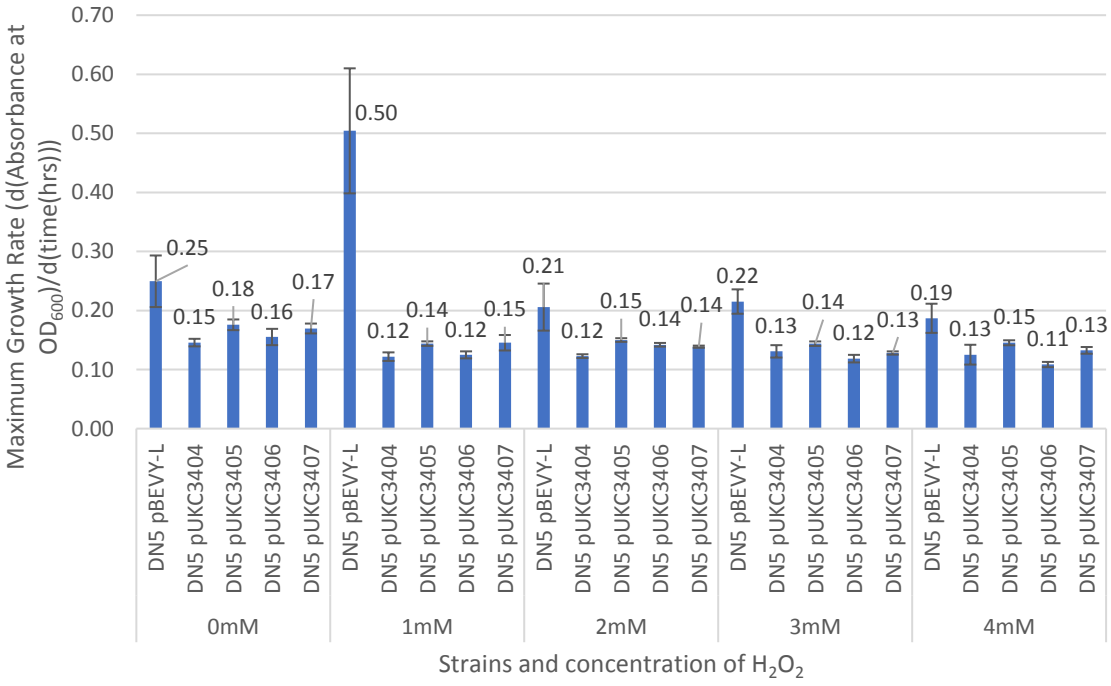

Fig 3.46. Maximum growth rate during log phase of DN5 expressing GPx7 and GPx8 constructs in liquid medium at a range of H_2O_2 concentrations.
A bar chart of the maximum growth rates calculated from growth curves of DN5 in YNB-Leu liquid medium expressing GPx7 and GPx8 constructs in H_2O_2 concentrations ranging from 0mM to 4mM with standard error bars.

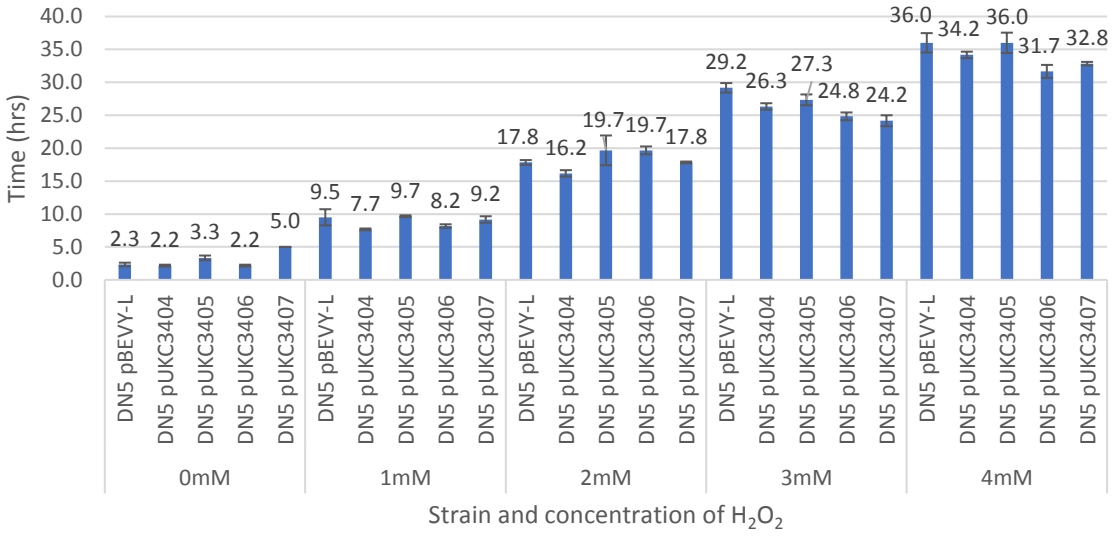

Fig 3.47. Duration of lag phase of DN5 expressing native GPx7 and GPx8 in liquid medium at a range of H_2O_2 concentrations.
A bar chart of the duration of lag phase calculated from growth curves of BY4741 in YNB-Leu liquid medium expressing GPx7 and GPx8 constructs in H_2O_2 concentrations ranging from 0mM to 4mM with standard error bars.

DN5 transformed with pUKC3404, pUKC3405, pUKC3406 and pUKC3407 all had growth curves very similar to each other (Fig 3.41. – Fig 3.45.) with minor variation between maximum growth rate during log phase (Fig 3.46.) and duration of lag phase (Fig 3.47.). The growth curves of the DN5 pBEVY-L empty vector control showed significant spiking at 0mM to 2mM H_2O_2 (Fig 3.41. – Fig 3.43.) When the individual repeats for 0mM to 2mM DN5 pBEVY-L control were examined there was a large degree of variability between repeats and hence resulting in the peculiar growth curves. The same trend was seen as with BY4741 where DN5 expressing the GPx7 and GPx8 constructs reached stationary phase at a higher OD_{600} than that of the control across all concentrations of H_2O_2 (Fig 3.41. – Fig 3.45.), again suggesting that there may be lessened inhibition to growth at lower nutrient availability as a result of expressing GPx7 and GPx8 constructs. Nevertheless there is no notable increased resistance to H_2O_2 in the Δ*pdi1* strain DN5 as a result of expressing GPx7 and GPx8 with ER localisation signals.

3.2.3.2 Growth on solid YNB-Leu medium with a range of hydrogen peroxide concentrations

To augment the data provided by the growth curves a sensitivity assay on was performed on solid YNB in 0mM to 4mM H_2O_2 to provide qualitative data regarding a possible change in resistance to H_2O_2 as a result of expressing GPx7 and GPx8.

3.2.3.2.1 2736 expressing native glutathione peroxidases 7 and 8

As this was a preliminary assay 2736 was used over BY4741, 2736 transformed with pUKC3400, pUKC3401 and pBEVY-L empty vector and hence expressing GPx7 and GPx8 without ER localisation sequences. The cultures serial dilutions from OD_{600} 0.1 to OD_{600} $1x10^{-4}$ were added to YNB-Leu solid medium with H_2O_2 concentrations ranging from 0mM to 4mM increasing in increments of 1mM (Fig 3.48.) to remain consistent with the concentrations used for assaying growth in liquid medium. Due to the temperature sensitivity nature of the H_2O_2 a 24 hour incubation period was used, as all 2736 strain yeast transformants in liquid culture at all concentrations of H_2O_2, with the exception of 4mM H_2O_2, had entered stationary phase growth within 24 hours, it was expected that some growth would be exhibited at all concentrations of H_2O_2 on solid medium.

There are no distinct changes in levels of growth between the control 2736 pBEVY-L strain and strains expressing GPx7 or GPx8 at both 0mM and 1mM H_2O_2 concentrations (Fig 3.48.). Despite a range of 0mM to 4mM H_2O_2 only data for 0mM and 1mM was included, as at 1mM H_2O_2 all strains exhibit dramatic growth inhibition (Fig 3.48.) and at 2mM, 3mM and 4mM no signs of growth were seen at all. This suggests greater inhibition of growth as a result of solid medium rather than liquid medium than was initially predicted. Therefore native human GPx7 and GPx8 do not result in increased resistance to H_2O_2 on solid YNB-Leu media.

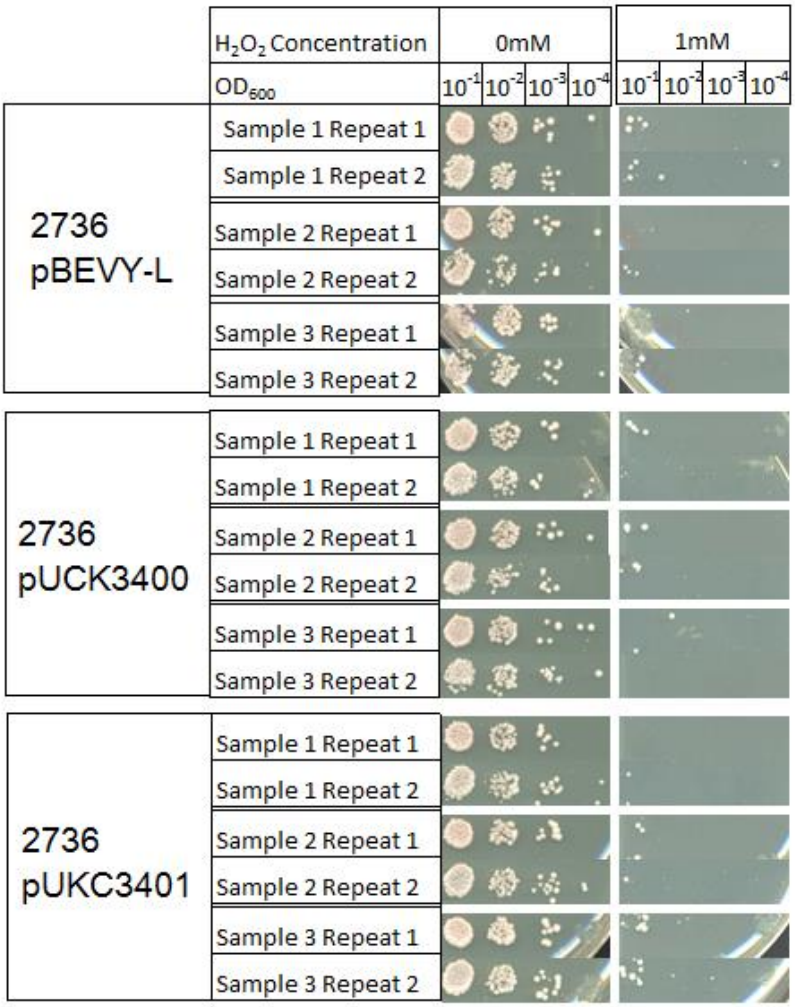

Fig 3.48. Growth of 2736 expressing native GPx7 and GPx8 at varying cell densities on solid YNB-Ura medium in 0mM and 1mM H_2O_2
2736 strain yeast transformed with pBEVY-L control, pUKC3400 and pUKC3401 plated onto YNB-Leu Agar by replica plating in 4 1/10 serial dilutions from OD_{600} 10^{-1} to OD_{600} 10^{-4} in biological triplicate and technical duplicate with H_2O_2 concentrations ranging from 0mM to 4mM in 1mM intervals. Data from 2mM-4mM omitted as no were colonies seen.

3.2.3.2.2 BY4741 expressing glutathione peroxidases 7 and 8 constructs

Due to low growth on 1mM H_2O_2 and non-existent growth on 2mM H_2O_2 for BY4741 mutants transformed with pUKC3400 and pUKC3401 (Fig 3.48.) the range of H_2O_2 concentrations was changed to 0mM to 2mM with 0.5mM intervals (Fig 3.49.). It was expected that subtle differences in sensitivity would become apparent with the smaller intervals

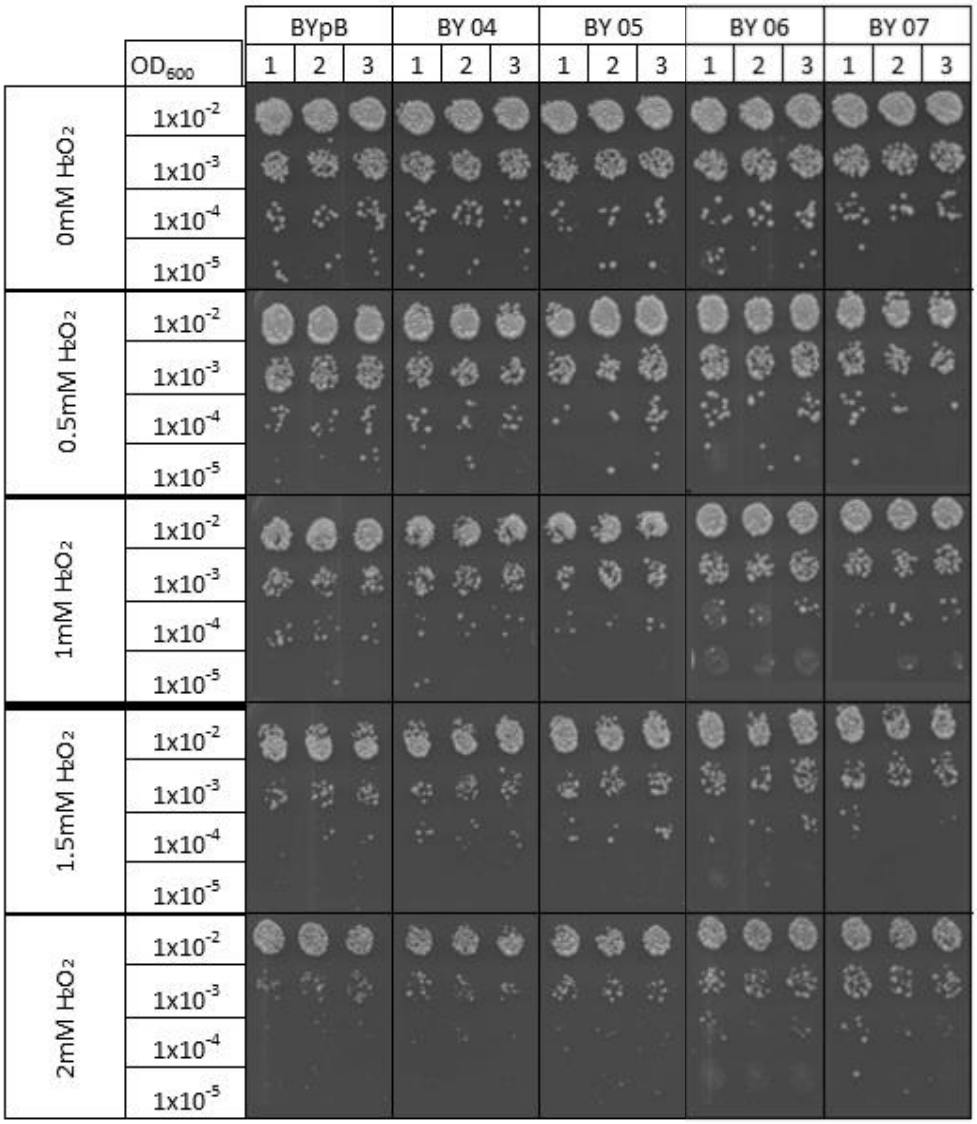

Fig 3.49. Growth of BY4741 expressing GPx7 and GPx8 constructs at varying cell densities on solid YNB-Ura medium in 0mM to 2mM H_2O_2
BY4741 strain yeast transformed with pBEVY-L control, pUKC3404, pUKC3405, pUKC3406 and pUKC3407 plated onto YNB-Leu Agar by replica plating in 4 1/10 serial dilutions from OD_{600} 10^{-2} to OD_{600} 10^{-5} in biological triplicate with H_2O_2 concentrations ranging from 0mM to 2mM in 0.5mM intervals.

At the highest H_2O_2 concentration of 2mM there was some inhibition of growth (Fig 3.49.) but not to the same extent as seen previously (Fig 3.48.). As such the differences in growth as a result of the 0.5mM intervals were small and the transformants were not tested at a concentration of H_2O_2 that was completely inhibitory to growth. Nonetheless, no obvious changes in resistance to H_2O_2 as a result of expressing GPx7 and GPx8 can be seen as a result of this assay (Fig 3.49.).

3.2.4 Changes in levels of intracellular hydrogen peroxide as a result of expressing glutathione peroxidases 7 and 8

A more direct approach to measure the intracellular levels of H_2O_2, and hence determine the H_2O_2 detoxification effects of GPx7 and GPx8, was to use flow cytometry. To determine intracellular levels of H_2O_2 H_2DCFDA was used, this is an intracellular molecular probe for ROS, the acetate group on the dye is cleaved by intracellular esterases which primes the dye and increases cellular retention, before becoming the fluorescent molecule 2',7' dichlorofluorescein through oxidation by ROS such as H_2O_2[88]. As H_2DCFDA is fluorescein derived the oxidised form has approximately the same excitation (492nm-495nm) and emission (517nm-527nm) spectra as fluorescein. This dye was used with flow cytometry to indicate the increase in percentages of fluorescent cells and hence efficiency of processing of intracellular ROS

3.2.4.1 Intracellular hydrogen peroxide in BY4741, 2736 and DN5 expressing native glutathione peroxidases 7 and 8

The increase in the percentage fluorescent cells as a result of addition of H_2DCFDA from basal levels measured in absence of the dye gave an indication of levels of intracellular ROS. Hence by comparing strains expressing GPx7 and GPx8 to the pBEVY-L control suggested the levels of H_2O_2 processing by these proteins. 2mM H_2O_2 stress was also induced to mimic the ROS conditions that would result from over expression of a disulphide bonded protein and to investigate whether GPx7 or GPx8 has effects on reducing these levels.

The first FACS analysis performed on 2736 transformed with pBEVY-L, pUKC3400 and pUKC3401 showed promising results as addition of H_2DCFDA dye to the control sample led to an increase in the percentage of fluorescent cells to 29.2% and then with the addition of 2mM H_2O_2 to the sample resulted in an even greater increase to 33.9% (Fig 3.50.). As a result of expressing GPx7 there was an increase to 14.8% in absence of H_2O_2 and 19.4% in presence of H_2O_2, having a two-tailed t-test P value of 0.0048 and 0.034 respectively, this was lower than the significance interval of 0.05 and hence a statistically significant decrease in the percentage of fluorescent cells by 14.4% and 14.5%. Due to the level of decrease resulting from expression of GPx7 being approximately the same in both presence and absence of H_2O_2 it suggests that GPx7 is operating at its maximum rate *in vivo* resulting in maximum

decrease in the percentage of fluorescent cells of ~14.5% over the 4 hour incubation time of the experiment.

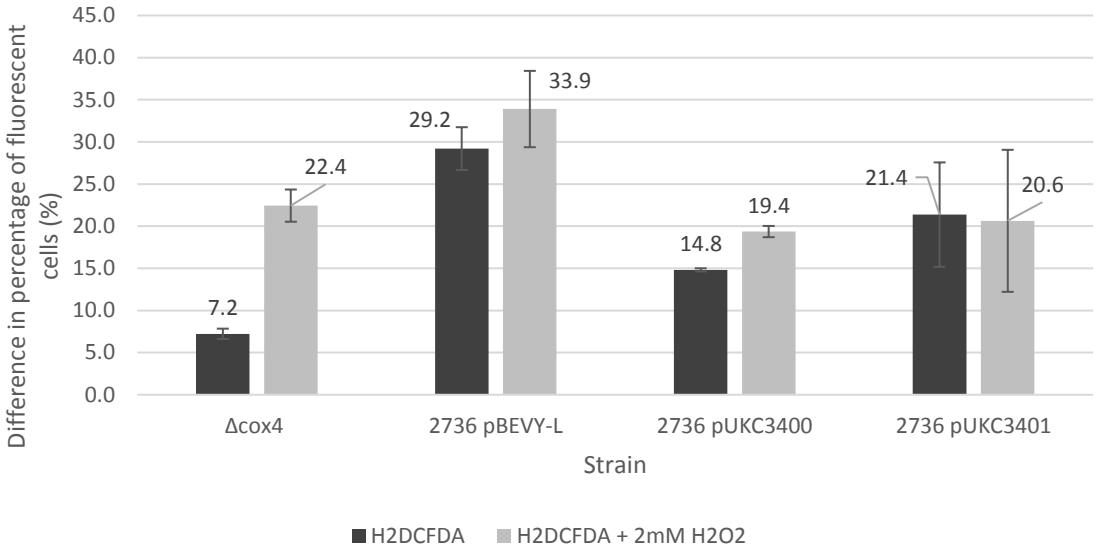

Fig 3.50. Percentage of fluorescent cells in populations of 2736 expressing native GPx7 and GPx8 in presence and absence of 2mM H_2O_2.
A population of 10,000 cells measured by flow cytometry with a baseline for each strain set at 50% fluorescent cells before the addition of H_2DCFDA ROS probe dye. The increase in percentage of fluorescent cells as a result of addition of just H_2DCFDA (black) and H_2DCFDA with 2mM H_2O_2 (grey) are shown for 2736 expressing native GPx7 and GPx8 with a pBEVY-L control and Δcox4 strain positive control. Experiment performed in biological triplicate with standard error bars are present for all samples

GPx8 only had a mean increase in the percentage of fluorescent cells to 21.4% in absence of H_2O_2, with an unpaired two-tailed t-test P value of 0.31, and 20.6% in presence of H_2O_2, with an unpaired two-tailed t-test P value of 0.24 (Fig 3.50.). Hence, this finding, was not deemed statistically significant, as both P values were higher than the significance interval of 0.05.

Following this encouraging result pUKC3400 and pUKC3401 plasmids were transformed into BY4741 and DN5 and 2736 was freshly transformed to perform repeats in identical conditions to the experiment prior.

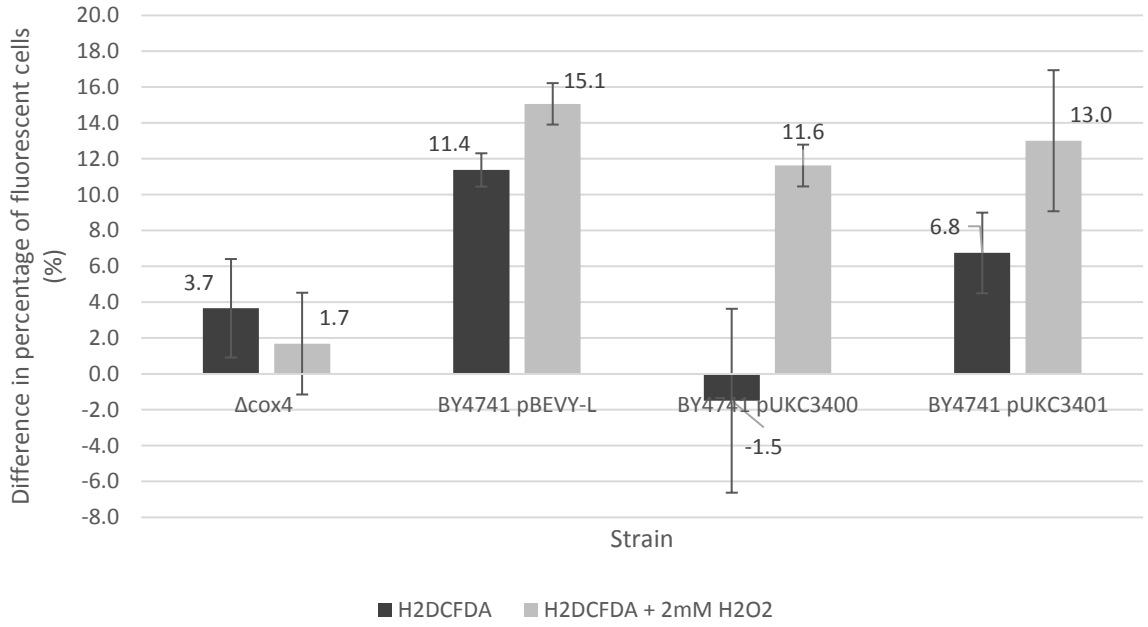

Fig 3.51. Percentage of fluorescent cells in populations of BY4741 expressing native GPx7 and GPx8 in presence and absence of 2mM H_2O_2.
A population of 10,000 cells measured by flow cytometry with a baseline for each strain set at 50% fluorescent cells before the addition of H_2DCFDA ROS probe dye. The increase in percentage of fluorescent cells as a result of addition of just H_2DCFDA (black) and H_2DCFDA with 2mM H_2O_2 (grey) are shown for BY4741 expressing native GPx7 and GPx8 with a pBEVY-L control and Δcox4 strain positive control. Experiment performed in biological triplicate with standard error bars are present for all samples

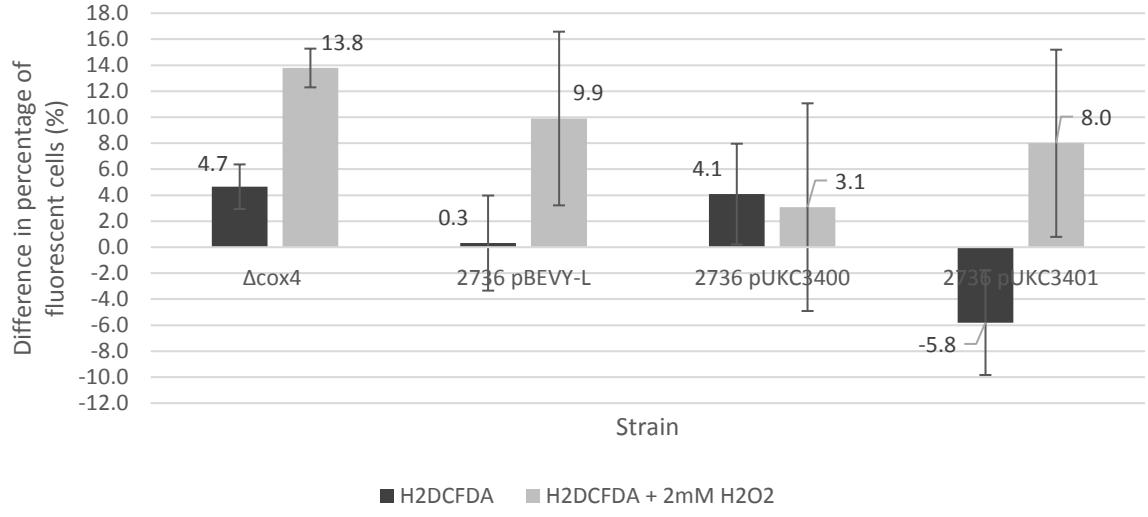

Fig 3.52. Percentage of fluorescent cells in populations of 2736 expressing native GPx7 and GPx8 in presence and absence of 2mM H_2O_2.
A population of 10,000 cells measured by flow cytometry with a baseline for each strain set at 50% fluorescent cells before the addition of H_2DCFDA ROS probe dye. The increase in percentage of fluorescent cells as a result of addition of just H_2DCFDA (black) and H_2DCFDA with 2mM H_2O_2 (grey) are shown for 2736 expressing native GPx7 and GPx8 with a pBEVY-L control and Δcox4 strain positive control. Experiment performed in biological triplicate with standard error bars are present for all samples

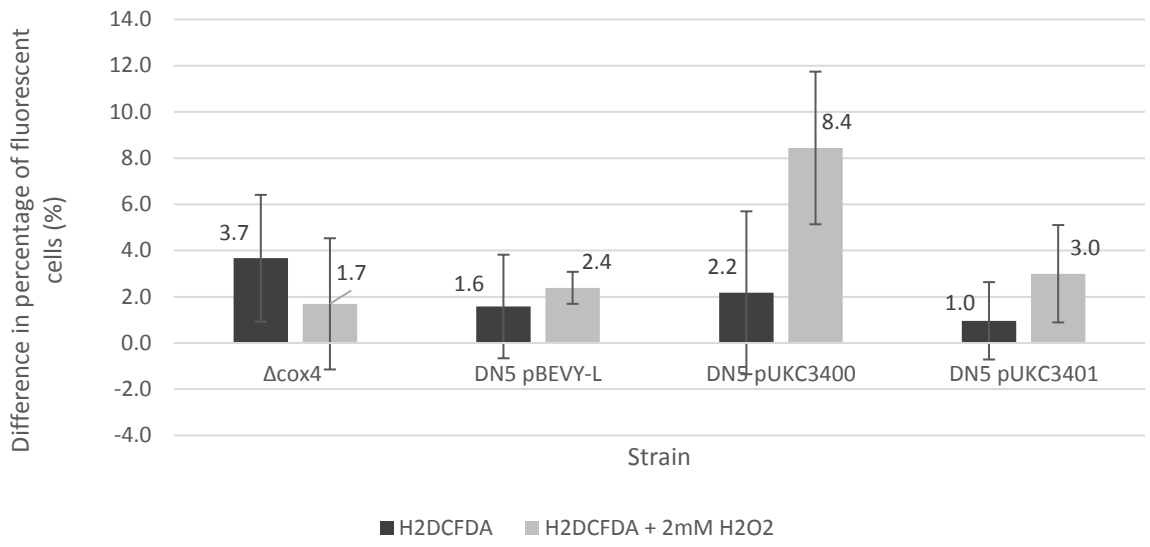

Fig 3.53. Percentage of fluorescent cells in populations of DN5 expressing native GPx7 and GPx8 in presence and absence of 2mM H_2O_2.
A population of 10,000 cells measured by flow cytometry with a baseline for each strain set at 50% fluorescent cells before the addition of H_2DCFDA ROS probe dye. The increase in percentage of fluorescent cells as a result of addition of just H_2DCFDA (black) and H_2DCFDA with 2mM H_2O_2 (grey) are shown for DN5 expressing native GPx7 and GPx8 with a pBEVY-L control and Δcox4 strain positive control. Experiment performed in biological triplicate with standard error bars are present for all samples

The data from these experiments did not match the correlation seen in the initial experiment, in all 3 of these experiments there was a large variability between experimental biological triplicates shown by the standard error bars (Fig 3.51. – Fig 3.53.). Due to the standard error of the data a reliable conclusion could not be drawn as for the averages of some strains there was a decrease in percentage of fluorescent cells after addition of the dye and strains that after addition of H_2O_2 had lower percentages of fluorescent cells than without H_2O_2 (Fig 3.51. – Fig 3.53.). The potency of the dye was therefore questioned.

A fresh H_2DCFDA dye stock was made rather than using pre-existing stocks as freeze-thaw cycles may have resulted in degradation of the dye. This was used to perform FACS analysis on freshly transformed BY4741, 2736 and DN5 strains with pUKC3400 and pUKC3401.

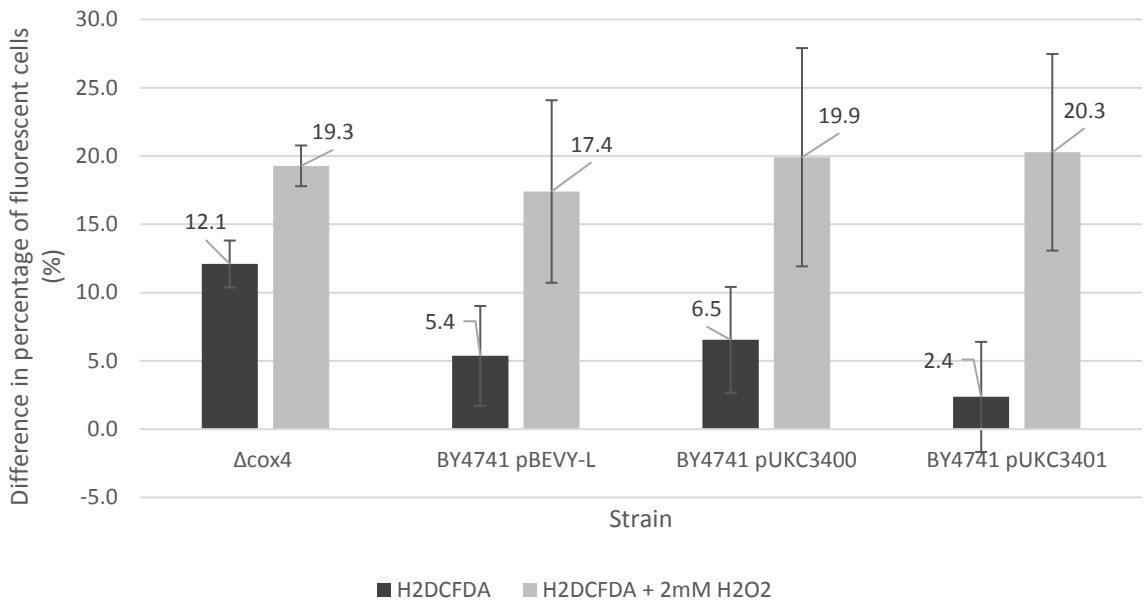

Fig 3.54. Percentage of fluorescent cells in populations of BY4741 expressing native GPx7 and GPx8 in presence and absence of 2mM H_2O_2.
A population of 10,000 cells measured by flow cytometry with a baseline for each strain set at 50% fluorescent cells before the addition of H_2DCFDA ROS probe dye. The increase in percentage of fluorescent cells as a result of addition of just H_2DCFDA (black) and H_2DCFDA with 2mM H_2O_2 (grey) are shown for BY4741 expressing native GPx7 and GPx8 with a pBEVY-L control and Δcox4 strain positive control. Experiment performed in biological triplicate with standard error bars are present for all samples

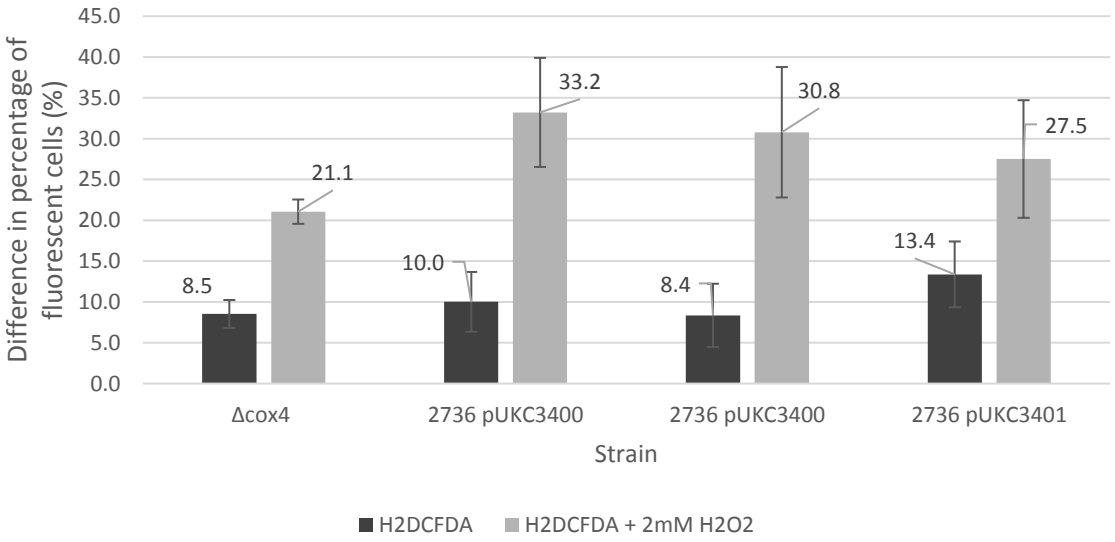

Fig 3.55. Percentage of fluorescent cells in populations of 2736 expressing native GPx7 and GPx8 in presence and absence of 2mM H_2O_2.
A population of 10,000 cells measured by flow cytometry with a baseline for each strain set at 50% fluorescent cells before the addition of H_2DCFDA ROS probe dye. The increase in percentage of fluorescent cells as a result of addition of just H_2DCFDA (black) and H_2DCFDA with 2mM H_2O_2 (grey) are shown for 2736 expressing native GPx7 and GPx8 with a pBEVY-L control and Δcox4 strain positive control. Experiment performed in biological triplicate with standard error bars are present for all samples

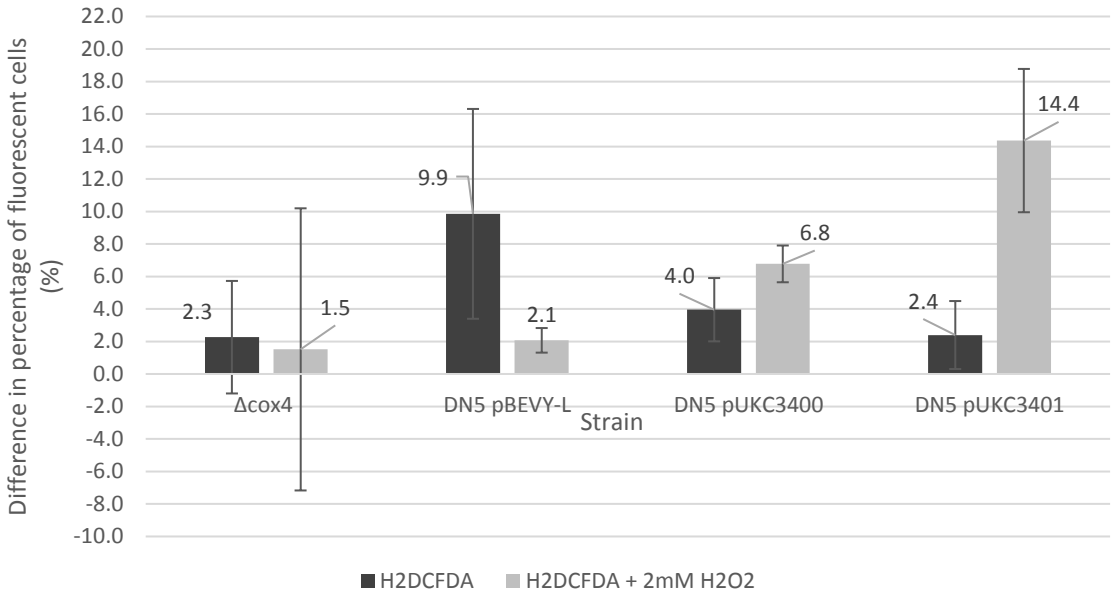

Fig 3.56. Percentage of fluorescent cells in populations of DN5 expressing native GPx7 and GPx8 in presence and absence of 2mM H_2O_2.
A population of 10,000 cells measured by flow cytometry with a baseline for each strain set at 50% fluorescent cells before the addition of H_2DCFDA ROS probe dye. The increase in percentage of fluorescent cells as a result of addition of just H_2DCFDA (black) and H_2DCFDA with 2mM H_2O_2 (grey) are shown for DN5 expressing native GPx7 and GPx8 with a pBEVY-L control and Δcox4 strain positive control. Experiment performed in biological triplicate with standard error bars are present for all samples

BY4741 and 2736 strains showed the expected trend of having an increase in numbers of fluorescent cells as a result of addition of the H_2DCFDA dye and then an even greater increase from addition of H_2O_2 (Fig 3.54., Fig 3.55.). Nevertheless, there was no statistically significant change in levels of intracellular H_2O_2 as a result of expression of GPx7 and GPx8, with no unpaired two-tailed t-test P value less than the significance interval of 0.05. There was also a large degree of standard error in all of these samples with a large amount of variability between replicates (Fig 3.54., Fig 3.55.).

The analysis of the DN5 FACS data showed peculiar results, with large amounts of error as well as for some strains having lower numbers of fluorescent cells after the addition of H_2O_2 (Fig 3.56.). This was the last experiment to be performed from the new dye stock and so the freeze thawing from the first 2 experiments may have resulted in dye expiration.

The Δcox4 strain, a strain in which the Cytochrome C subunit 4 has been knocked out and hence has decreased detoxification of H_2O_2, was used as a positive control,

however, consistently throughout the flow cytometry experiments a dramatic increase in fluorescence as a response to addition of H_2DCFDA in this strain was not witnessed (Fig 3.50. – Fig 3.58.).

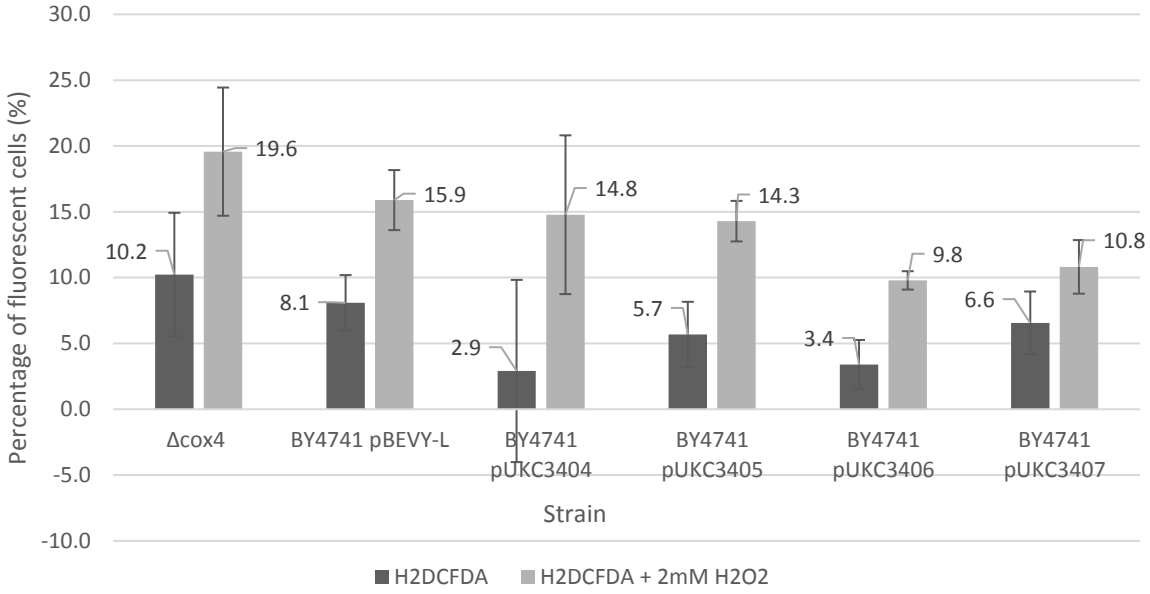

Fig 3.57. Percentage of fluorescent BY4741 cells expressing GPx7 and GPx8 with ER retention sequence from addition of H_2DCFDA and addition of 2mM H_2O_2. The intracellular levels of ROS are indicated by the percentage of fluorescent cells, the Δcox4 positive control strain was used as well as BY4741 transformed with pBEVY-L empty vector from which the changes in percentage of fluorescent cells for BY4741 expressing pUKC3404 and pUKC3405 was compared to. Experiment repeated in biological triplicate with standard error bars shown

3.2.4.2 Intracellular hydrogen peroxide in BY4741 expressing glutathione peroxidases 7 and 8 constructs

Following a negligible decrease in intracellular H_2O_2 as a result of expressing native GPx7 and GPx8 BY4741 was transformed with plasmids pUKC3404, pUKC3405, pUKC3406 and pUKC3407 and hence expressed GPx7 and GPx8 with ER retention sequences only and ER retention sequences as well as ER signal sequences. Therefore if residing in the ER was essential to GPx7 and GPx8 mediated H_2O_2 detoxification this would be indicated through FACS analysis.

Expressing GPx7 and GPx8 in BY4741 resulted in a decrease in the mean percentage of fluorescent cells compared with the pBEVY-L control in both the absence and presence of H_2O_2 (Fig 3.57.). Expression of either GPx7 ER localisation signal construct caused a greater decrease than that of GPx8 in the presence of just H_2DCFDA dye, while in the presence of H_2DCFDA as well as 2mM

H_2O_2 it appears that GPx7 and GPx8 with both ER retention sequence as well as ER signal sequence caused a greater decrease in percentage of fluorescent cells(Fig 3.57.). However, due to the wide variability between replicates none of the GPx7 or GPx8 constructs had an unpaired two-tailed t-test P value less than the significance interval of 0.05, and hence no statistically significant change in percentage of fluorescent cells, and by extension, intracellular H_2O_2.

3.2.4.3 Intracellular hydrogen peroxide in a Δ*pdi1* strain expressing glutathione peroxidases 7 and 8 constructs

For similar reasons to 3.2.3.1.3 a Δ*pdi1* strain was tested to check if GPx7 and GPx8 had any *in vivo* effect on detoxification of H_2O_2. Using FACS analysis for intracellular H_2O_2 gave a more direct measurement of this, whereas growth curve analysis are influenced by more factors.

Intracellular ROS concentrations are relatively unaffected in DN5 as a result of expressing ER localised GPx7 and GPx8 proteins. The two strains expressing GPx8 constructs had mean percentages of fluorescent cells roughly half that of the pBEVY-L control in absence of H_2O_2, while expression of the GPx8 constructs resulted in percentages of fluorescent cells approximately the same as the control in the absence of H_2O_2 (Fig 3.58.). Additionally, only in DN5 expressing GPx7 with ER retention sequence only was there a decrease in percentage of fluorescent cells that did not overlap standard error bars with the control (Fig 3.58.). Nevertheless, results for change in percentage of fluorescent cells in both presence and absence of H_2O_2 were not deemed statistically significant, as no unpaired two-tailed t-test P values were less than the significance interval of 0.05, and hence expression of GPx7 and GPx8 constructs does not result in increased *in vivo* H_2O_2 processing.

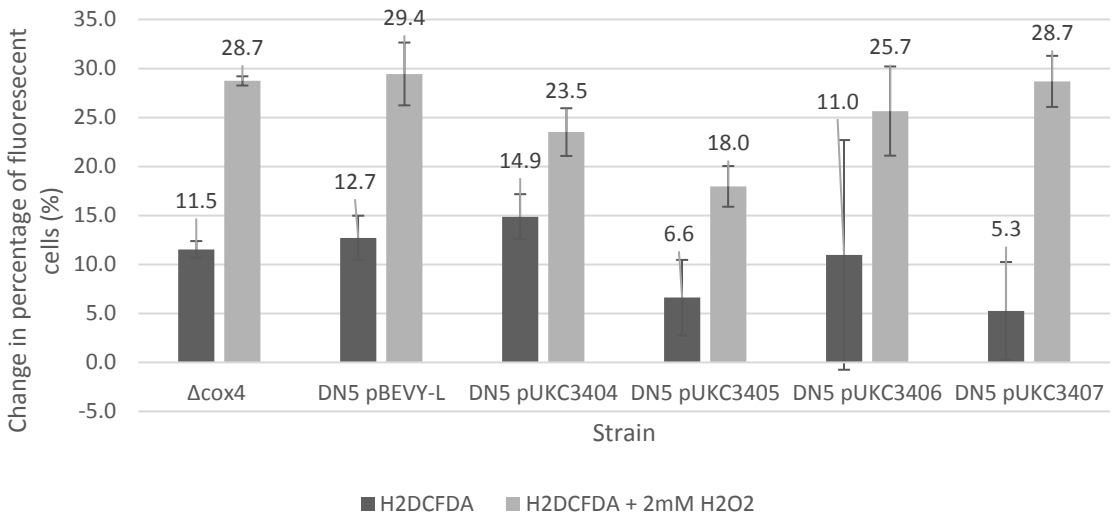

Fig 3.58. Percentage of fluorescent cells in populations of DN5 expressing GPx7 and GPx8 constructs in presence and absence of 2mM H_2O_2.
A population of 10,000 cells measured by flow cytometry with a baseline for each strain set at 50% fluorescent cells before the addition of H_2DCFDA ROS probe dye. The increase in percentage of fluorescent cells as a result of addition of just H_2DCFDA and H_2DCFDA with 2mM H_2O_2 are shown for DN5 expressing GPx7 and GPx8 constructs with a pBEVY-L control and Δcox4 strain positive control. Experiment was performed in biological triplicate and standard error bars shown

3.2.5 Effects of glutathione peroxidases 7 and 8 on the rate of oxidative folding *in vivo*

GPx7 and GPx8 couple H_2O_2 peroxide generated from disulphide bond formation to Pdi1p oxidation enabling it to further form disulphide bonds hence increasing the rate of OPF. GPx7 and GPx8 may therefore have a similar effect when transformed into yeast.

3.2.5.1 Sensitivity of BY4741 expressing glutathione peroxidases 7 and 8 constructs to 1,4 -Dithiothreitol

To investigate the ability of GPx7 and GPx8 to assist PDI increasing the rate of OPF 1,4-Dithiothreitol (DTT) was using. DTT is a powerful reducing agent that prevents $OPF^{(RH)}$. Through disulphide exchange reactions it non discriminately reduces folded protein causing them to unfold while itself entering the oxidised state forming a 6 membered ring[89]. This leads to triggering of the Unfolded Protein Response (UPR) as a result of the increased ER stress. DTT inhibits growth through its effects

and therefore a strain more efficient at OPF can better counteract the reductive activity of DTT and hence growth inhibition is decreased.

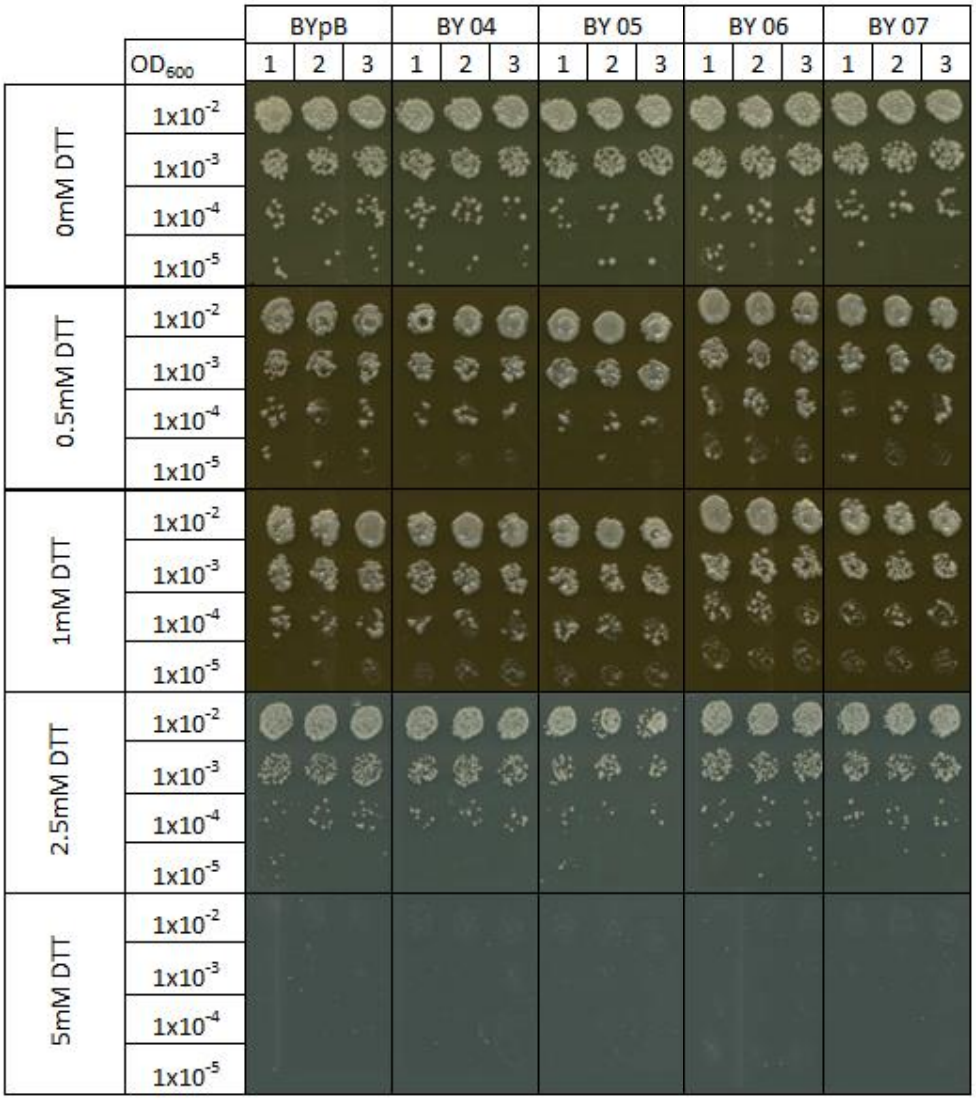

Fig 3.59. Growth of BY4741 expressing GPx7 and GPx8 constructs at varying cell densities on solid YNB-Ura medium in 0mM to 5mM DTT
BY4741 strain yeast transformed with pBEVY-L control, pUKC3404, pUKC3405, pUKC3406 and pUKC3407 plated onto YNB-Leu Agar by replica plating in 4 1/10 serial dilutions from OD_{600} 10^{-2} to OD_{600} 10^{-5} with DTT concentrations ranging from 0mM to 5mM. Performed in biological triplicate

Growth of BY4741 strains expressing GPx7 and GPx8 constructs on YNB-Ura medium with 0mM to 5mM DTT shows no changes in resistance to DTT when compared with a BY4741 control transformed with pBEVY-L (Fig 3.59.). The increment from 2.5mM to 5mM is larger than any of the prior increments and as a result only moderate impairment to growth was seen in 2.5mM DTT while there was

no growth at 5mM. Concentrations of DTT up to 10mM were used as growth on drop out medium containing 10mM DTT was seen in the work of L.Hjelmqvist[90], however, no growth seen at 10mM during this experiment and so data omitted.

3.2.5.2 Secretion of an over expressed extracellular disulphide bonded protein

To test for the efficiency of disulphide bond formation a PDI expressing strain and a Δ*pdi1* were transformed with plasmid pVT100U-K1 encoding for the secreted K1 toxin: a heterodimeric protein containing three disulphide bonds[91] which induces cell death of sensitive strains through formation of a membrane pore[92].

3.2.5.2.1 Levels of killer toxin secretion in BY4741 expressing native glutathione peroxidases 7 and 8

BY4741 was simultaneously transformed with pVT100U-K1 and pUKC3400, pUKC3401 or pBEVY-L control. Whether native GPx7 or GPx8 had any effect on killer toxin secretion, and by extension OPF, was assayed for by calculating the area of a zone of killer toxin mediated clearing of sensitive S6 strain around cells expressing killer toxin, which were added to an antimicrobial disk on an agar containing the S6 strain. The area of the zone of killing is therefore directly proportional to the levels of K1 toxin secretion.

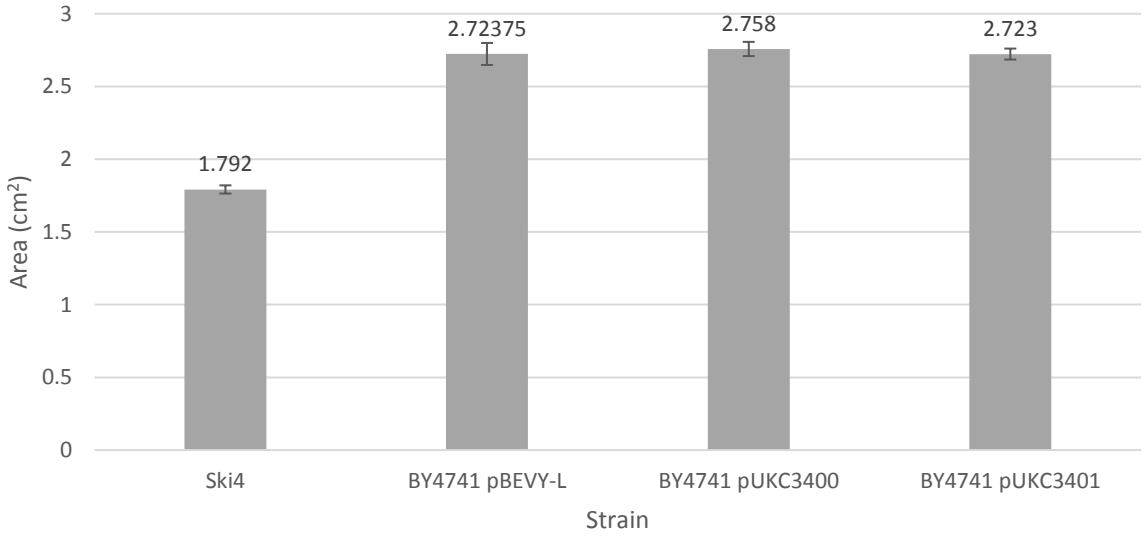

Fig 3.60. Area of the zone of killing resulting from expression of the disulphide bonded secretory protein: killer toxin in BY4741 expressing native GPx7 and GPx8. The secretion of killer toxin by strains transformed with pVT100U-K1 plasmid results in formation of a zone of killing surrounding the antimicrobial disk on which they were added. The area of the zone of killing was measured using ImageJ 1.x[93]. BY4741 expressing native GPx7 and GPx8 was compared to BY4741 pBEVY-L control, ski4 natural killer toxin secretor control also used. Experiment performed in biological and technical duplicate and standard error bars shown.

The area of the zone of killing for both BY4741 expressing native GPx7 and GPx8 does not statistically significantly differ from the area of the pBEVY-L control strain (Fig 3.60.), as the unpaired two-tailed t-test P values are 0.75 for GPx7 and 0.99 for GPx8. Neither of these P values are less than the significance interval of 0.05. Therefore GPx7 and GPx8 has no effect on levels of killer toxin secretion, and thus no effect on oxidative folding *in vivo*.

3.2.5.2.2 Levels of killer toxin secretion in BY4741 expressing glutathione peroxidases 7 and 8 constructs

-2For GPx7 or GPx8 to oxidise Pdi1p they must be localised to the ER, and therefore GPx7 and GPx8 constructs with ER localisation signal were used to check whether the lack of ability for native GPx7 and GPx8 to increase the rate of OPF was intrinsic to the interaction of GPx7 and GPx8 with yeast Pdi1p or whether it was a result of not being localised to the ER.

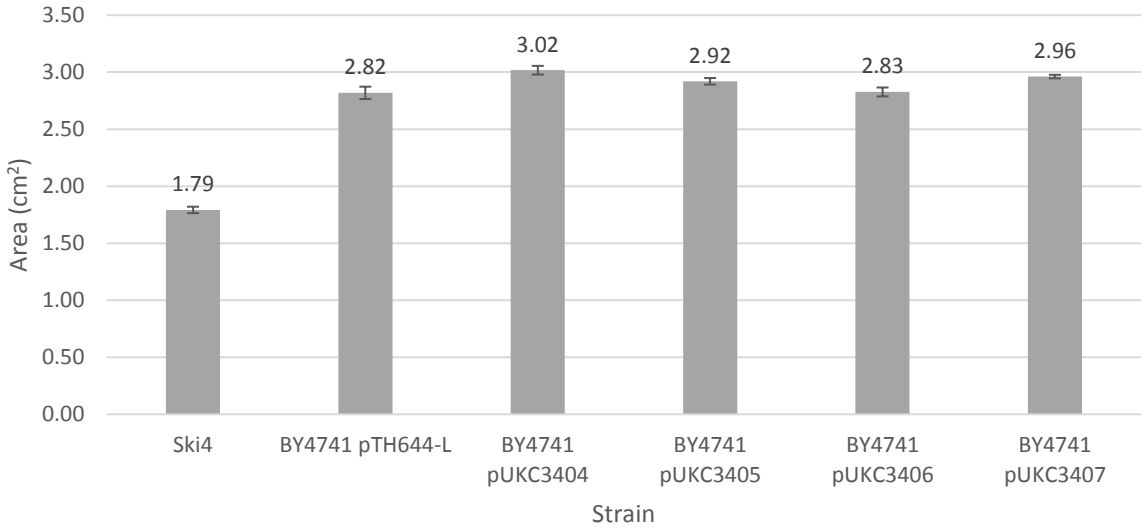

Fig 3.61. Area of the zone of killing resulting from expression of the disulphide bonded secretory protein: killer toxin in BY4741 expressing GPx7 and GPx8 constructs.
The secretion of killer toxin by strains transformed with pVT100U-K1 plasmid results in formation of a zone of killing surrounding the antimicrobial disk on which they were added. The area of the zone of killing was measured using ImageJ 1.x[93]. BY4741 expressing GPx7 and GPx8 constructs were compared to BY4741 pTH644 control, ski4 natural killer toxin secretor control also used. Experiment performed in biological and technical duplicate and standard error bars shown

The expression of GPx7 and GPx8 constructs in BY4741 did not result in a statistically significant increase in the area of the zone of killing, with no unpaired

two-tailed t-test P value less than the significance interval of 0.05, with the exception of BY4741 transformed with pUKC3404. GPx7 with an ER retention sequence only gave a very slight, but statistically significant, increase in the area by ~0.2cm^2, - approximately a 7% increase (Fig 3.61.). This unpaired two-tailed t-test P value was 0.041; less than the significance interval of 0.05. Overall, expression of GPx7 and GPx8 in BY4741 did not result in a dramatic increase in killer toxin secretion, and therefore OPF.

3.2.5.2.3 Levels of killer toxin secretion in a Δ*pdi1* strain expressing native, and chimeric construct versions of glutathione peroxidases 7 and 8

GPx7 and GPx8 require an interaction with Pdi1p to increase OPF, therefore expression of GPx7 and GPx8 in a Δ*pdi1* strain would not result in an increase in rate of OPF and thus it would not be expected that there would be an increase in killer toxin secretion.

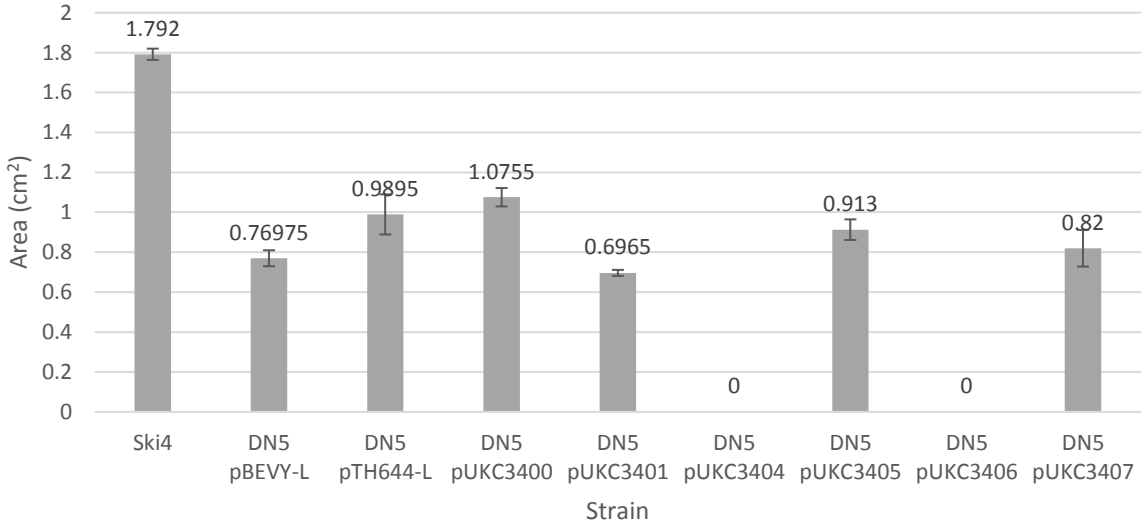

Fig 3.62. Area of the zone of killing resulting from expression of the disulphide bonded secretory protein: killer toxin in DN5 expressing native GPx7 and GPx8 as well as GPx7 and GPx8 constructs.
The secretion of killer toxin by strains transformed with pVT100U-K1 plasmid results in formation of a zone of killing surrounding the antimicrobial disk on which they were added. The area of the zone of killing was measured using ImageJ 1.x[93]. DN5 expressing GPx7 and GPx8 constructs was compared to DN5 pTH644-L control, ski4 natural killer toxin secretor control also used. Experiment performed in biological and technical duplicate and standard error bars shown

Secretion of the disulphide bonded killer toxin from DN5 strains is significantly lower than that of BY4741, there was also no statistically significant increase in killer toxin

secretion resulting from expressing GPx7 or GPx8, with no P value of an unpaired two-tailed t test less than the significance interval of 0.05, with the exception of the increase in killer toxin resulting from expression of native GPx7 in which there was an increase from 0.77cm^2 to 1.08cm^2 (Fig 3.62.), having an unpaired two-tailed t-test P value of 0.0049; less than the significance interval of 0.05. There was also a dramatic decrease to no detectable killer toxin secretion for DN5 transformed with GPx7 constructs that localise to the ER (Fig 3.62.).

3.2.5.3 Effect of glutathione peroxidases 7 and 8 on rate of expression of an intracellular disulphide bonded protein

To assay for the levels of expression of an intracellular disulphide bonded protein in BY4741 and DN5 expressing native GPx7 and GPx8 as well as GPx7 and GPx8 constructs gaussia luciferase was used, encoded for by the GLuc plasmid. This plasmid was transformed into strains of interest along with a PGK loading control and a western blot performed to ascertain levels of expression. Although bands corresponding to PGK were seen, bands at ~19kDa, that would indicate expression of gaussia luciferase, were not seen. An intracellular gaussia luciferase positive control was not available and so it cannot be assumed that absence of bands means the strains were not expressing gaussia luciferase over a potential problem with imaging of the western blot.

3.2.6 The effect of glutathione peroxidases 7 and 8 on oxidative folding with yeast Pdi1p *in vitro*

As assays performed for the efficiency of OPF *in vivo* suggested that GPx7 and GPx8 were unable to interact with yeast Pdi1p, this was also explored *in vitro.* The effect that GPx7 and GPx8 had on the OPF ability of yeast Pdi1p *in vitro* was tested to see whether there was a direct lack of interaction between GPx7 and GPx8, or whether the inhibition of interaction came about through some other means *in vivo*.

Consumption of ambient oxygen in a closed system can be used as an indicator for the rate of OPF, as for each disulphide bond formed an oxygen molecule is converted to H_2O_2. The oxygen consumption with time for 5µM Pdi1p with 1µM Ero1p and 40mM free thiol GSH substrate without, or with, GPx7 or GPx8 was measured in duplicate.

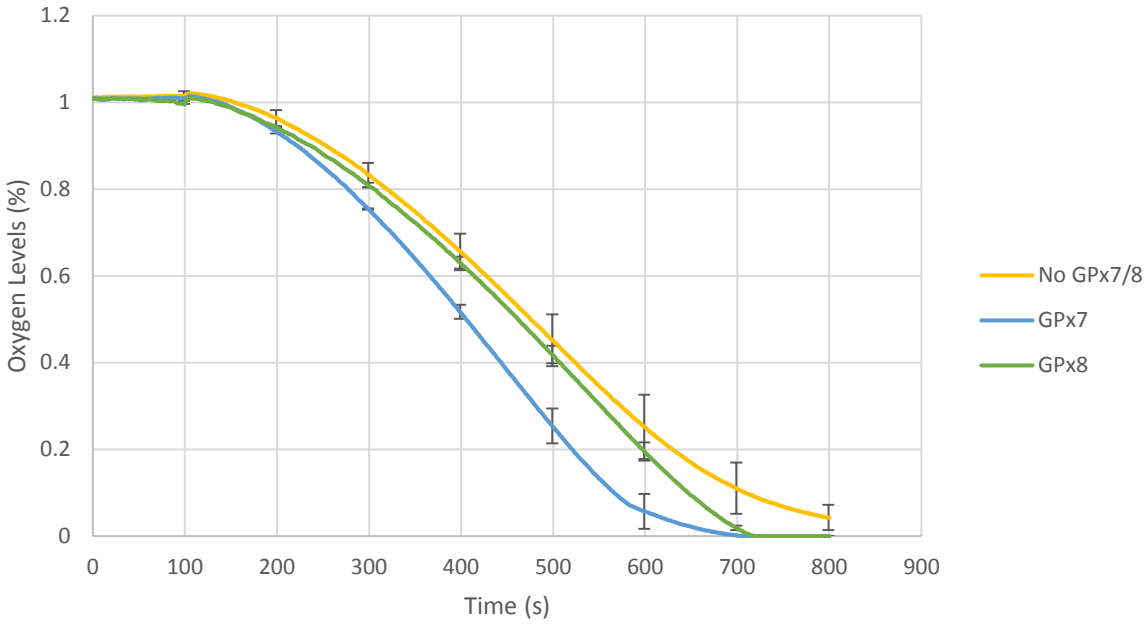

Fig 3.63. Levels of oxygen consumption with time to indicate rate of *in vitro* disulphide bond formation by Pd1p and the changes in this rate resulting from presence of native GPx7 and GPx8.
The consumption of ambient oxygen in a closed system from the activity of 5µM yPdi1p and 1µM Ero1p with 40µM free thiol GSH substrate indicated rates of disulphide bond formation *in vitro*, GPx7 and GPx8 were added to investigate as to whether these proteins were able to supplement oxidative folding. Experiment was performed in duplicate and standard error bars shown

Sample	**Mean Max Rate (d(O_2 levels)/d(time))**
No GPx7/8	2.05×10^{-3} +/- 1.5×10^{-4}
GPx7	2.5×10^{-3} +/- 3×10^{-4}
GPx8	2.15×10^{-3} +/- 5×10^{-5}

Fig 3.64. Mean max rate of oxygen consumption for PDI, Ero1p and GSH, in the absence and presence of GPx7 and GPx8.
The mean max rate calculated from the oxygen consumption assay (Fig 3.62.) in presence and absence of GPx7 and GPx8. The range of data is shown next to the mean max rate.

GPx8 had a very similar curve to that of the control, while the curve for GPx7 suggested an increased rate of oxygen consumption (Fig 3.63.). The mean max rate of oxygen consumption for each sample, however, indicated that there was no statistically significant difference between the rates as although GPx7 had a mean max rate $4.5x10^{-4}$ s^{-1} greater than that of the control (Fig 3.64.), this finding is not statistically significant as it has an unpaired two-tailed t-test P value of 0.318; greater than the significance interval of 0.05. Therefore, native GPx7 and GPx8 have no impact upon rate of oxygen consumption, and by extension, disulphide bond formation *in vitro*.

Chapter 4 – Discussion

Many pharmaceutical products are produced in biological systems, and hence are termed biopharmaceuticals. Many of these biopharmaceuticals require oxidative folding and hence this is a limiting factor in their production. There is much yet to be discovered regarding the yeast oxidative protein folding pathway, in particular the role that the PDI homologues play. Better characterisation of this pathway will allow for adaption of the yeast ER to increase *in vivo* oxidative folding.

As these disulphide bonded biopharmaceuticals need to be produced in large amounts they are overexpressed. In a eukaryotic system this leads to rapid production of H_2O_2 as a result of the oxidative folding pathway. As this generation of ROS is beyond what was evolutionarily required of the organism it is surely a limiting factor in biopharmaceutical production. Therefore through expression of recombinant proteins that alleviate this ROS stress the limiting factor can be removed and the rate of oxidative folding increased.

4.1 Can viable Δ*pdi1* mutants be generated?

In yeast *pdi1* is an essential gene, however, it is not clear as to exactly why this as overexpression of PDI homologues Mpd1p and Mpd2p are both able to rescue viability of a Δ*pdi1* strain. Therefore to investigate whether there is a mutation that would rescue viability following a *pdi1* knock out viable Δ*pdi1* mutants were screened for.

Over the course of the project five spontaneously arising, viable Δ*pdi1* mutants were isolated together with a further 15 following UV mutagenesis. All of these mutants were selected due to their resistance to 5-FOA using a strain carrying a Δ*pdi1* knockout covered by a plasmid-borne copy of the *PDI1* gene with a *URA3* selectable marker. Resistance to 5FOA would suggest these mutants had lost the *URA3-PDI1* plasmid, but Western blot analysis showed that all but 2 of the mutants (PDISR4 and PDISR5) were still expressing PDI (Fig 3.5., Fig 3.6.). Neither of these two viable Δ*pdi* strains could be revived from -80˚C glycerol stocks, likely due to cell wall instability. This may have occurred as disulphide bonds are required for the stability of the yeast cell wall. 1,3-beta-glucanosyltransferases are responsible for biogenesis of the yeast cell wall and require oxidative folding for their activity[95][96].

As these majority of the Δ*pdi1* strains that were 5-FOA resistant were still expressing PDI, this indicated that the mutations leading to growth on 5-FOA media were unlikely to be ones that restored viability in the absence of PDI. For these mutants to emerge the simultaneous absence of plasmid and a suppressor to Δ*pdi* lethality (*supX)* would be required. Instead a recombination event may be occurring, in which the *PDI1* gene from the plasmid inserts into the genome and the *URA3* gene is lost, hence resulting in 5-FOA resistance while maintaining expression of PDI. Another possible explanation is a mutation resulting in direct increased resistance to 5-FOA, either through inhibited 5-FOA uptake, or its conversion to 5-FU (Fig 3.1)

Inhibited uptake of 5-FOA may be mediated by mutations that result in decreased activity in components of uracil salvage pathway, such as uracil permease which regulates the uptake of uracil[97]. Alternatively, there is an *S. cerevisiae* protein with functional homology to that of the human organic anion transporter (OAT2), which in humans has been shown to transport orotic acid, the unmodified analogue to of 5-FOA[98].

The inhibited conversion of 5-FOA to 5-FU may also have occurred through a mutation resulting in downregulation of expression of the *URA3* or *URA5* genes such as in *cis*- and *trans*-Acting regulatory elements[99] or through a mutation that decreases the activity of the products of *URA3* and *URA5*: OCDase and OPRTase[100] respectively, through a point mutation that results in a missense or nonsense mutation.

All of the 5FOA resistant strains, with the exception of one of the Δ*pdi1* mutant PDISR1-5, showed growth on YNB-Ura medium, albeit papillae growth (Fig 3.3., Fig 3.4.). This suggests that either the *URA3* gene is being retained and resistance to 5-FOA is mediated through mutation affecting uptake or its conversion to 5-FU. A *URA3* point mutation that may have resulted in decreased expression, or activity, of the ODCase protein, hence providing 5FOA resistance may be reverting in some of cells of the population plated onto YNB-Ura selective media, explaining the papillae growth.

Another explanation is that due to a reversion event of the missense point mutation in the genomic *ura3-1* allele the wild type *URA3* gene is restored. In the PDIS/MRx mutants, however, this reversion event appeared to occur at a much higher frequency than the homozygous *ura3/ura3* diploid heterozygous *ura3-1/ura3-52*

DN5 control strain (Fig 3.4.). This result is unsurprising as the most likely 5-FOA resistant strains, either through loss of the plasmid and a *supX* mutation, or through a mutation that directly inhibits the cytotoxic mechanism of 5-FOA, would most likely occur in a strain with impaired proofreading ability, such as through point mutations within the conserved FDIET region that results in lowered 3'-5' exonuclease activity of DNA polymerases[101][102]. As a result of the lowered mismatch repair mechanisms the reversion of *ura3-1* in the PDIS/MRx mutants would occur at a higher frequency.

The growth of the PDIS/MR1x strains in YEPD showed consistently that all of the mutants had a lag phase of increased duration when compared to the 2736 control strain (Fig 3.8., Fig 3.9.). This supports the hypothesis of direct resistance to the cytotoxic effects of 5-FOA as the transition of a stationary phase culture to entry of log phase quickly requires rapid protein synthesis to adapt to the new conditions. A strain with decreased uracil uptake or impaired OCDase or OPRTase activity would produce uridine monophosphate at a slower rate, slowing formation of nascent mRNA and with it a reduction in protein synthesis.

As the likelihood of the emergence of a strain that had lost the *PDI1-URA3* plasmid and had a *supX* mutation appeared to be low compared to generating strains that retained the *pdi1* gene but gained 5-FOA resistance, alternate approaches should be considered. One possible approach is to use 2736 strain yeast with increasing concentrations of DTT to select for a mutant that is more resistant to increased unfolded protein, as would be expected to occur in a *pdi1*-defective strain. The reducing agent DTT causes an increase in unfolded protein and ER oxidative stress by indiscriminately reducing disulphide bonded proteins[90]. The mutants with increased resistance to unfolded protein would then be transferred to plates containing 5-FOA to select for loss of the *PDI1-URA3* plasmid and hopefully to successfully generate Δ*pdi1* strains with viability restored by a secondary mutation i.e. *supX*. This was attempted in a preliminary experiment where 5 colonies of 2736 strain were grown on 20mM DTT, then transferred to 30mM DTT. However, at higher concentrations of DTT cells grew considerably slower and so emergence of colonies on higher concentrations of DTT could not be attributed to increased DTT resistance rather than degradation of DTT, as it is a temperature sensitive compound.

An alternate strategy to generate viable Δ*pdi1 supX* mutants without inducing direct resistance to 5-FOA would be to place the expression of the *PDI1* gene under the control of a tetracycline-regulated promoter system[103]. Through gradual decrease in the concentration of tetracycline or doxycycline[104] in the solid medium one could select for cells that emerge on lower concentrations of tetracycline or doxycycline. This will gradually select for Δ*pdi1 supX* mutants that retain viability on solid medium with no tetracycline or doxycycline and hence no expression of *PDI1;* such mutants should have *supX*. Rather than a plasmid based expression system ideally the *PDI1* gene should be integrated into the genome under the control of the tetracycline expression system. This would prevent a recombination event resulting in removal of the tetracycline promoter.

It is therefore apparent that *pdi1* is an essential gene as although PDISR4 and PDISR5 are Δ*pdi1* strains, it is clear that there is a low frequency mutation that results in this maintained viability. Therefore there is not a native mechanism for the upregulation of any of the PDI homologues, or at least not to a level at which viability is maintained.

4.2 What are the impacts of expression of native human glutathione peroxidases 7 and 8 in yeast?

4.2.1. Engineering expression of glutathione peroxidases 7 and 8 in yeast

It was hypothesised that the expression of GPx7 and GPx8 in yeast would have increased the rate of oxidative folding as they utilise intracellular H_2O_2 produced by Ero1p to oxidise PDI. Therefore there would also be a decrease in levels of intracellular H_2O_2.This would alleviate ROS stress under constitutive expression of a disulphide bond containing protein and increase the rate of oxidative folding of this protein.

To investigate whether native GPx7 or GPx8 was able to detoxify H_2O_2 *in vivo* cDNAs encoding one or the other were expressed in yeast. Sensitivity to H_2O_2 was then investigated through growth curves (Fig 3.25 – Fig 3.33) and a sensitivity assay for growth on solid media in concentrations of 0mM to 4mM H_2O_2 (Fig 3.48), both of these showed no increase in resistance to H_2O_2 as a result of expressing native human GPx7 or GPx8. A more direct measure on levels of intracellular H_2O_2 was also performed using an intracellular ROS detector dye: H_2DCFDA in conjunction

with FACS analysis. Although an initial experiment showed statistically significant changes in levels of intracellular ROS as a result of expressing GPx7 (Fig 3.50) this was not seen in any repeats of this experiment (Fig 3.54, Fig 3.55). These results therefore failed to support the hypothesis that expression of native GPx7 or GPx8 would have a significant impact on H_2O_2 detoxification.

To investigate the effects of native GPx7 and GPx8 on the rate of intracellular oxidative folding the levels of secretion of the disulphide bonded protein killer toxin was also measured (Fig 3.60.). This showed that neither GPx7 nor GPx8 had any statistically significant effect on the rate of oxidative folding *in vivo.* It was therefore considered that absence of yeast ER signal sequences or retention sequences was resulting in either cytoplasmic localisation of these ER proteins or that there was secretion of the protein and this was further investigated.

4.2.2 Identifying Native GPx7 and GPx8 localisation

To conclude as to whether native GPx7 and GPx8 were localised to the ER or cytoplasm, an attempt was made to create GFP fusions of these proteins using plasmid p6431 (Fig 2.1.). PCR was used to amplify GPx7 and GPx8 for insertion into the p6431 vector, but following ligation and purification the DNA, the yield was very low and similarly a low number of *E.coli* transformants were present. A sequence of the plasmid was provided by Tuite, M.F. (School of Biosciences, University of Kent) and a second *Xba*I restriction site was located 219 bp upstream of the gene insert site in the *CUP1* promoter in plasmid p6431. The presence of this second *Xba*I site would have led to ligation failure as not only could the complete vector with insert have formed, but additional DNA fragments of would be generated. A double restriction digest of the plasmid with BamHI and XbaI did not show the ~220bp fragment by agarose gel (Fig 3.16), however, it is likely due to its small size to have migrated off the gel.

Additional DNA fragments were seen on the agarose gel used for gel extraction and purification following the restriction digest in preparation of native human GPx7 and GPx8 for ligation into p6431. These were approximately 4kb for GPx7 and 3kb for GPx8. The sizes of pKEHS780 plasmid and Human GPx8 cDNA clone plasmid were 4.2kb and 3.4kb respectively (table 2.1.6). The additional bands for contaminant DNA for GPx7 and GPx8 were approximately the size of their respective *E.coli* vectors and so may have been this vector in its linearised form. An additional DNA

band was also seen in the GPx8 control, albeit faint, that migrated to a similar position to that of the linearised human GPx8 cDNA vector. It is therefore likely that the linearised plasmid containing the cDNA of interest for PCR amplification was seen as a contaminant in the sample despite PCR purification. None of these DNA fragments were seen prior to double restriction digest and therefore the diffuse band that results from the multiple conformations of circularised DNA may have caused the residual plasmid not being detected.

To identify intracellular localisation of GPx7 and GPx8 either an alternate plasmid for generating GFP fusions could be used or creation of new primers for the inclusion of any compatible pair of restriction enzymes between the CUP1 promoter and sGFP ORF in the p6431 vector (Fig 2.1.). This would avoid multiple cut sites as occurring from use of XbaI.

4.3 Does addition of a yeast ER signal sequence and ER retention sequence to glutathione peroxidases 7 and 8 result in any favourable phenotypic characteristics?

The retention of the expressed GPx7 and GPx8 in the cell was indicated by absence of these proteins in the medium as shown by western blot (Fig 3.23.) and so intracellular effects of these proteins would be expected if they were active in yeast. Due to the lack of success in generating GFP fusions the ER localisation of these protein constructs could not be directly confirmed.

As a result of expressing GPx7 and GPx8 with yeast ER localisation signals the mean intracellular levels of H_2O_2 were observed to decrease compared to the control (Fig 3.57). However, the results were not statistically significant suggesting that neither GPx7 nor GPx8 were detoxifying H_2O_2 to a significant extent *in vivo*. Both GPx7 and GPx8 have been shown *in* vitro to be able to couple the detoxification of H_2O_2 with the oxidation of GSH[47], albeit at a much lower efficiency than that of PDI. However, this indicates that the utilisation of GSH by GPx7 and GPx8 to detoxify H_2O_2 either does not occur *in vivo* or at a rate undetectable by this assay.

The growth of strains expressing ER localised GPx7 and GPx8 in presence of H_2O_2 showed only a slight decrease in duration of lag phase at higher concentrations (2mM-4mM) of H_2O_2 compared with the control strain (Fig 3.40). The control strain

used, however, was BY4741 transformed with pBEVY-L plasmid, rather than a more appropriate control of BY4741 transformed with pTH644-L vector, as this is the plasmid backbone for plasmids pUKC3404-7. This transformation was attempted, but was unsuccessful and due to time constrains the pBEVY-L control was used. The pTH644-L vector is a derivative of pBEVY-L, however, there are important differences, namely that pTH644-L is a CEN/ARS low copy plasmid containing the *CEN6* centromere and thus generating only 2-5 copies per cell while pBEVY-L is a 2µ high copy plasmid containing 14-34 copies per cell[105], although copy number is dependent upon other gene(s) added to the plasmid. The growth rates of strains containing 2µ plasmids are typically lower than CEN/ARS strains[105], and hence may have resulted in pUKC3404 - 7 transformed strains having slightly higher growth rates than the pBEVY-L control. Coupled with the results from the flow cytometry analysis of the intracellular H_2O_2 it was therefore concluded that expression of GPx7 or GPx8 with ER localisation signal does not incur resistance to H_2O_2 and doesn't lead to faster growth rates in the absence of H_2O_2 when compared to a suitable control strain i.e. BY4741 + pTH644-L. Further support was provided by the observation that expression of GPx7 or GPx8 in yeast caused no change in levels of growth when cells were plated onto minimal medium containing 0-4mM H_2O_2 (Fig 3.49).

Despite the absence of an increase in H_2O_2 resistance, the expression of GPx7 and GPx8 could be contributing to a faster rate of oxidative folding in the yeast ER. This was measured through several ways, the first was to test for sensitivity to DTT, as proteins with more efficient oxidative folding efficiency would be more able to overcome the stresses incurred from an accumulation of unfolded protein within the ER caused by DTT. There was no increased resistance observed as a result of expressing GPx7 or GPx8, however, the concentrations of DTT were too widely spread to ascertain if there are subtle changes in resistance to DTT (Fig 3.59). Therefore in future experiments additional intermediate concentrations should be used as well as performing growth analyses in the presence of DTT to better characterise the effects GPx7 and GPx8 on oxidative stress in the yeast ER.

Another method by which levels of oxidative folding were measured was by determining the levels of secretion of a disulphide bonded protein; killer toxin (Fig 3.60, Fig 3.61). The only statistically significant increase in killer toxin secretion

observed was in cells carrying plasmid pUKC3404 encoding GPx7 with HDEL ER retention sequence. The strain transformed with pUKC3406, a GPx7 construct with both ER retention sequence and signal sequence, however, did not show this same trend. The area of the zone of killing for BY4741 expressing GPx7 with ER retention sequence and K1 toxin was only ~7% greater than the control, and GPx7 with both a yeast ER retention sequence and ER signal sequence gave no statistically significant effect on the rate of oxidative folding as judged by this assay. Therefore as GPx7 did not have a dramatic effect on the rate of oxidative folding it would be expected that it is not interacting, or is interacting with poor specificity, with the endogenous yeast PDI. Likewise the various GPx8 constructs, having no statistically significant change in oxidative folding as a result of their expression, would also not be expected to interacting with PDI.

The secretion of another disulphide-bonded protein, Gaussia luciferase, was also attempted and levels of secretion were to be determined by Western Blot analysis. However, no bands were seen for Gaussia luciferase at 19kDa. As a PGK primary antibody was used along with the Gaussia Luciferase antibody as a control so that imageJ software could have been used to determine relative intensity of bands of Gaussia Luciferase to PGK. The presence of PGK may have interfered with the association of the GLuc Ig to the membrane as both PGK and GLuc antibodies were raised in rabbit hosts, this may result in cross-reactivity between the two primary antibodies. A repeat of this should be performed in absence of PGK to test exclusively for Gaussia Luciferase. Should the PGK1 primary antibody be the cause, an alternative loading control such as an antibody to actin could be used. Furthermore, a luciferase assay could be performed to produce quantitative results for intracellular levels of active, secreted Gaussia luciferase.

An *in vitro* study of the interactions between yPDI with GPx7 and GPx8 showed that these proteins have no effect on the rate of oxygen consumption in a system of yPDI and yEro1p with GSH substrate. The recycling of H_2O_2 by GPx7 or GPx8 formed from the reduction of molecular oxygen as the final electron acceptor resulting in re-oxidation of PDI would be expected caused a faster rate of oxygen consumption. This is due to more PDI kept in the oxidised form and hence a greater number of oxidative folding reactions can occur per second in the system. This indicates that *in vitro* GPx7 and GPx8 are unable to utilise H_2O_2 to re-oxidise yPDI (Fig 3.63, Fig

3.64). Further investigations are required to characterise the mechanism of this inhibited interaction. GPx7 and GPx8 may still be able to detoxify H_2O_2 in the system by utilising GSH as an electron donor[47], or by forming an intramolecular disulphide bond to remove the sulfenic acid group formed as the first step of H_2O_2 detoxification.

This *in vitro* assay could be improved through use of an alternate substrate that requires oxidative folding by PDI such as reduced ribonuclease A[102], as GSH has been shown to be a substrate for both GPx7 and GPx8[47][50]. This would ensure that GPx7 and GPx8 have no alternate substrate to yPDI, as due to the stoichiometric excess of GSH substrate there may be competition between GSH and yPDI as a substrate for GPx7 and GPx8[52].

Overall there appears to be no interaction of GPx7 and GPx8 with yPDI both *in vitro* and *in vivo*, therefore to increase the rate of oxidative folding in yeast cells human PDI, human Ero1p, instead of their endogenous homologues and GPx7 or GPx8 should be expressed in yeast simultaneously. Both GPx7 and GPx8 have been shown to interact with hPDI[47] while hEro1p would be required for proper reoxidation of hPDI.

4.4 Does expression of glutathione peroxidases 7 and 8 result in any changes to the phenotype of a Δ*pdi1* strain?

As GPx7 and GPx8 have been shown to be able to oxidise hPDI, these proteins were also expressed in DN5, a viable Δ*pdi* strain. This was to compare whether the phenotypic changes that occur as a result of GPx7 and GPx8 expression differ from that of transformed BY4741. For all experiments with DN5 transformed with GPx7 and GPx8, with the exception of an assay for the secretion of a disulphide bonded protein, pBEVY-L empty vector control was used, as again transformation with the more suitable control plasmid of pTH644-L empty vector was unsuccessful.

The control strain showed growth characteristics distinct from those shown by the GPx7 and GPx8 expressing strains as the growth of the control had extensive spiking as well as reaching stationary phase at OD_{600} ~1.9, while the strains expressing GPx7 and GPx8 reached stationary phase at OD_{600} ~2.1 (Fig 3.41-3.45). Spiking of the control strain was only seen at 0mM and 2mM H_2O_2 concentrations (Fig 3.41, Fig 3.43), therefore spiking is likely to have resulted from contamination.

As many bacterial species commonly aggregate in liquid media[106] this would result in spiking of the growth curve cell aggregates come between the lamp and detector, an absorbance reading that is artificially high for the sample will be produced.

For all DN5 strains transformed with GPx7 and GPx8 constructs stationary phase was reached with a higher OD_{600} and therefore with a higher biomass than the DN5 pBEVY-L control (Fig 3.41-3.45). This suggests less inhibition of growth at low nutrient availability. This may have been the result of differences between the pBEVY-L vector used as the control and the pTH644 plasmid as they are multicopy 2µ and single copy CEN plasmids respectively. In any case this difference in biomass at which stationary phase is reached is not an indication of H_2O_2 resistance resulting from expression of GPx7 and GPx8.

It was originally proposed that in the absence of PDI, GPx7 and GPx8 would be unable to link H_2O_2 detoxification with PDI oxidation. Hence they would either have to utilise an alternate substrate such as GSH which would not actively cycle between the reduced and oxidised form, or would auto-oxidise to remove the sulfenic acid group formed as a result of H_2O_2 detoxification. This would therefore result in a non-perpetual system of H_2O_2 detoxification and hence there would be less of an effect on intracellular levels of ROS. Antagonistically, however, the absence of PDI, and hence its oxidative effects, would cause a more reducing ER in which the reduced states of GPx7 and GPx8 would be favoured and hence enabling them to detoxify H_2O_2.

The intracellular levels of H_2O_2 in DN5 were unaffected by the presence of GPx7 or GPx8 (Fig 3.58). Although DN5 expressing GPx8 with ER retention sequence only and expressing GPx8 with both ER signal sequence and ER retention sequence appeared to have reproducibly lower levels of intracellular ROS in the absence of H_2O_2 stress, neither of these results were statistically significant.

The absence of a statistically significant change in intracellular H_2O_2 levels support the original hypothesis that there would be no effect on intracellular H_2O_2 levels as a result of expressing GPx7 and GPx8 in a Δ*pdi1* strain as GPx7 and GPx8 would be lacking PDI as a substrate. However, it was discovered that GPx7 and GPx8 had no effect on intracellular H_2O_2 in a strain expressing yPDI. Therefore there is no a definitive correlation that an absence of expression of yPDI leads to the inability of GPx7 and GPx8 to detoxify H_2O_2 utilising yPDI *in vivo*. The finding that there is no

statistically significant change in levels of intracellular H_2O_2 in both a strain expressing PDI and a Δ*pdi1* strain provides further evidence of the inability of GPx7 and GPx8 to utilise GSH to detoxify H_2O_2.

Throughout the project FACS analysis had low repeatability as well as a relatively low increase in the percentage of fluorescent cells as a result of addition of the H_2DCFDA dye. This was also been evident in the Δ*cox4* stain, reportedly a producer of high levels of intracellular H_2O_2[107] and which was used as a control strain. This was likely the result of the duration of incubation of cultures with H_2DCFDA being too short for intracellular uptake of the dye to generate a sizable difference in the percentage of fluorescent cells as a result of the dye. The duration of this incubation phase could not be increased as the uptake of the dye was significantly impaired in minimal medium. As the *gpx7 and gpx8* genes are carried on plasmids, YNB-Leu media was required to prevent loss of the plasmid and therefore the incubation step in YNB-Leu media and dye had to be limited to 2hrs. Genomic integration of the *gpx7* and *gpx8* would allow overnight growth in YPD with H_2DCFDA.

It was expected that levels of secretion of a recombinant disulphide-bonded protein would be reduced in the DN5 strain when compared to BY4741 strain as a result of impaired oxidative folding resulting from the absence of *pdi1*. Despite the absence of PDI there would have to be oxidative folding in order for the strain to remain viable. Furthermore, expression of GPx7 and GPx8 in DN5 would not result in an increase in oxidative folding as there is no PDI to keep in the oxidised form.

There were no statistically significant changes in the levels of killer toxin (Fig 3.62), an homologous secreted disulphide-bonded protein, with the exception of DN5 expressing ER localised GPx7 constructs. Expression of these constructs resulted in complete inhibition of killer toxin secretion. This was a trend that was not exhibited by strains expressing non-ER localised GPx7 or by expression of the GPx7 constructs with ER localisation signals in BY4741 parent strain. The fact that only expression of GPx7 with ER localisation signals resulted in the prevention of killer toxin secretion may mean that disulphide bond formation was inhibited. However, if this was the case, a corresponding decrease in growth rate as a result would have been expected. Or perhaps only in the case of over expression of a disulphide-bonded protein, as is the case for killer toxin, does GPx7 result in hindrance of disulphide bond formation rather than assistance. The reason why expression of

GPx7 resulted in this dramatic decrease in killer toxin secretion while GPx8 does not is not yet clear. As the viability following the *pdi1* knock out in DN5 is most likely restored by a 116 amino acid long truncated form of *PDI1*$^{(108)}$ it is possible that the mechanism by which GPx7 and GPx8 bind substrate are different. This would result in GPx7 interacting with the truncated PDI and sequestering it, preventing its activity in disulphide bond formation, while GPx8 is unable to bind the same peptide fragment. Nevertheless, additional experiments are required to accurately characterise the mechanism, such as confirming the truncated PDI that restores viability to DN5 and performing *in vitro* analysis for test for interactions with both GPx7 and GPx8.

References

1) Sone, M., Akiyama, Y., Ito, K. (1997) Differential *in vivo* roles played by DsbA and DsbC in the formation of protein disulfide bonds. *The Journal of Biological Chemistry* **272**: 10349-10352

2) Parakh, S., Atkin, J. D. (2015) Novel roles for protein disulphide isomerase in disease states: a double edged sword? *Frontiers in Cell and Developmental Biology* **3**: 30

3) Galligan, J. J., Peterson, D. R. (2012) The human protein disulfide isomerase gene family. *Human Genomics* **6**: 6

4) Nørgaard. P., Westphal. V., Tachibana. C., Alsøe. L., Holst, B., Winther, J. R. (2001) Functional differences in yeast protein disulfide isomerases. *Journal of Cell Biology* **152**: 553-562

5) Kulak, N. A., Pichler, G., Paron, I., Nagaraj, N., Mann, M. (2014) Minimal, encapsulated proteomic-sample processing applied to copy-number estimation in eukaryotic cells. *Nature Methods* **11**: 319-324

6) Laboissière, M. C. A., Stephen L. Sturley, S. L., Raines, R. T. (1995) The essential function of protein-disulfide isomerase is to unscramble non-native disulfide bonds. *The Journal of Biological Chemistry* **270**: 28006-28009

7) Tian, G., Xiang, S., Noiva, R., Lennarz, W. J., Schindelin, H. (2006) The crystal structure of yeast protein disulfide isomerase suggests cooperativity between its active sites. *Cell* **124**: 61-73

8) Ren, G., Stephan, D., Xu, Z., Zheng, Y., Tang, D., Harrison, R. S., et al. (2009) Properties of the thioredoxin fold superfamily are modulated by a single amino acid residue. *Journal of Biological Chemistry* **284**: 10150-10159

9) Westphal, V., Darby, N. J., Winther, J. R. (1999) Functional properties of the two redox-active sites in yeast protein disulphide isomerase *in vitro* and *in vivo*. *Journal of Molecular Biology* **286**: 1229-1239

10) Kimura, T., Nishida, A., Ohara, N., Yamagishi, D., Horibe, T., Kikuchi, M. (2004) Functional analysis of the CXXC motif using phage antibodies that cross-react with protein disulphide-isomerase family proteins. *Biochemistry Journal* **382**:169-172

11) Römer, R. A., Wells, S. A., Jimenez-Roldan, J. E., Bhattacharyya, M., Vishweshwara, S., Freedman, R. B. (2016) The flexibility and dynamics of protein disulfide isomerase. *Proteins* **84**: 1776-1785

12) T) Vitu, E., Kim, S., Sevier, C. S., Lutzky, O., Heldman, N., Bentzur, M., et al. (2010) Oxidative activity of yeast ero1p on protein disulfide isomerase and related oxidoreductases of the endoplasmic reticulum. *Journal of Cell Biology* **285**: 18155-18165

13) F) Xiao, R., Wilkinson, B., Solovyov, A., Winther, J. R., Holmgren, A., Lundström-Ljung, J., Gilbert, H. F. (2004) The contributions of protein disulfide isomerase and its homologues to oxidative protein folding in the yeast endoplasmic reticulum. *Journal of Biological Chemistry* **279**: 49780-49786

14) G) Solovyov, A., Xiao, R., Gilbert, H. F. (2004) Sulfhydryl oxidation, not disulfide isomerization, is the principal function of protein disulfide isomerase in yeast saccharomyces cerevisiae. *Journal of Biological Chemistry* **279**: 34095-34100

15) Tian, R., Li, S. Wang, D., Zhao, Z., Liu, Y., He, R. (2004) The acidic c-terminal domain stabilizes the chaperone function of protein disulfide isomerase. *Journal of Biological Chemistry* **279**: 48830-48835

16) Darby, N. J., Creighton, T. E. (1995) Functional properties of the individual thioredoxin-like domains of protein disulfide isomerase. *Biochemistry* **34**: 11725 – 11735.

17) Kemmink, J., Darby, N. J., Dijkstra, K., Nilges, M., Creighton, T. E. (1996) Structure determination of the n-terminal thioredoxin-like domain of protein disulfide isomerase using multidimensional heteronuclear 13C/15N NMR spectroscopy. *Biochemistry* **35**: 7684-7691

18) Klappa, P., Ruddock, L. W., Darby, N. J., Freedman, R. B. (1998) The b' domain provides the principal peptide-binding site of protein disulfide isomerase but all domains contribute to binding of misfolded proteins. *The EMBO Journal* **17**: 927-935

19) Frand, A. R., Kaiser, C. A. (1998) The ERO1 gene of yeast is required for oxidation of protein dithiols in the endoplasmic reticulum. *Molecular Cell* **1**: 161-170

20) Tu, B. P., Ho-Schleyer, S. C., Travers, K. J., Weissman, J. S. (2000) Biochemical basis of oxidative protein folding in the endoplasmic reticulum. *Science* **290**: 1571-1574

21) Frand, A. R., Kaiser, C. A. (2000) Two pairs of conserved cysteines are required for the oxidative activity of ero1p in protein disulfide bond formation in the endoplasmic reticulum. *Molecular Biology of the Cell.* **11**:2833-2843

22) Gross, E., Kastner, D. B., Kaiser, C. A., Fass, D. (2004) Structure of Ero1p, source of disulfide bonds for oxidative protein folding in the cell. *Cell* **117**: 601-610

23) Sevier, C., Kaiser, C. A. (2006) Disulfide transfer between two conserved cysteine pairs imparts selectivity to protein oxidation by Ero1. *Molecular Biology of the Cell* **17**: 2256-2266

24) Sevier, C., Qu, H., Heldman, N., Gross, E., Fass, D., Kaiser, C. A. (2007) Modulation of cellular disulfide-bond formation and the ER redox environment by feedback regulation of Ero1. *Cell* **129**: 333-344

25) Irvine, A. G., Wallis, A. K., Sanghera, N., Rowe, M. L., Ruddock, L. W., Howard, M. J., et al. (2014) Protein disulfide-isomerase interacts with a substrate protein at all stages along its folding pathway. *PLoS One* **9**: e82511

26) Bjørn Holst, B., Tachibana, C., Winther, J. R. Active site mutations in yeast protein disulfide isomerase cause dithiothreitol sensitivity and a reduced rate of protein folding in the endoplasmic reticulum. *Journal of Cell Biology* **138**: 1229-1238

27) Araki, K., Iemura, S., Kamiya, Y., Ron, D., Kato, K., Natsume, T., Nagata, K. (2013) Ero1-α and PDIs constitute a hierarchical electron transfer network of endoplasmic reticulum oxidoreductases. *Journal of Cell Biology* **202**: 861-874

28) Masui, S., Vavassori, S., Fagioli, C., Sitia, R., Inaba, K. (2011) Molecular bases of cyclic and specific disufide interchange between human ERO1α protein and protein-disulfide isomerase (PDI). *Journal of Biological Chemistry* **286**: 16261-16271

29) Gross, E., Sevier, C. S., Heldman, N., Vitu, E., Bentzur, M., Kaiser, C. A., et al. (2006) Generating disulfides enzymatically: Reaction products and electron acceptors of the endoplasmic reticulum thiol oxidase Ero1p. *Proceedings of the National Academy of Sciences* **103**: 299-304

30) Lyles, M. M., Gilbert, H. F. (1991) Catalysis of the OPF of ribonuclease A by protein disulfide isomerase: dependence of the rate on the composition of the redox buffer. *Biochemistry* **30**: 613-619

31) Tsai, B., Rodighiero, C., Lencer, W. I., Rapoport, T. A. (2001) Protein disulfide isomerase acts as a redox-dependent chaperone to unfold cholera toxin. *Cell* **104**: 937-948

32) Kim, S., Sideris, D. P., Servier, C. S., Kaiser, C. A. (2012) Balanced Ero1 activation and inactivation establishes ER redox homeostasis. *Journal of Cell Biology* **196**: 713-725

33) Heldman, N., Vonshak, O., Sevier, C. S., Vitu, E., Mehlman, T., Fass, D. (2010) Steps in reductive activation of the disulfide-generating enzyme Ero1p. *Protein Science* **19**: 1863-1876

34) Bienert, G. P., Schjoerring, J. K., Jahn, T. P. (2006) Membrane transport of hydrogen peroxide. *Biochimica et Biophysica Acta – Biomembranes* **8**: 994-1003

35) Kimura, T., Hosoda, Y., Sato, Y., Kitamura, Y., Ikeda, T., Horibe, T. and Kikuchi, M. (2005) Interactions among yeast protein-disulfide isomerase proteins and endoplasmic reticulum chaperone proteins influence their activities. *Journal of Biological Chemistry* **280**: 31438-31441

36) Biran, S., Gat, Y. and Fass, D. (2014) The Eps1p protein disulphide isomerase conserves classic thioredoxin superfamily amino acid motifs but not their functional geometrics. *PLoS One* **9**: e113431

37) Vitu, E., Grosse, E., Greenblatt, H. M., Sevier, C. S., Kaiser, C. A. and Fass, D. (2008) Yeast Mpd1 reveals the structural diversity of the protein disulphide isomerase family. *Journal of Molecular Biology* **384**: 631-640

38) Kim, J. H., Zhao, Y., Pan, X. He, X. and Gilbert, F. H. (2009) The unfolded protein response is necessary but not sufficient to compensate for defects in disulphide isomerisation. *Journal of Biological Chemistry* **284:** 10400-10408

39) Wang, L., Zhang, L., Niu, Y., Sitia, R. and Wang, C. (2014) Glutathione peroxidase 7 utilizes hydrogen peroxide generated by ero1α to promote oxidative protein folding. *Antioxidants and Redox Signalling* **20**: 545-556

40) Tavender, T. J., Bulleid, N. J. (2010) Peroxiredoxin IV protects cells from oxidative stress by removing H2O2 produced during disulphide formation. *Journal of Cell Science* **123**: 2672-2679

41) Altschul, S.F., Gish, W., Miller, W., Myers, E.W. & Lipman, D.J. (1990) Basic local alignment search tool. *Journal of Molecular Biology*. **215**: 403-410

42) Munhoz, D. C. and Netto, L. E. S. (2004) Cytosolic thioredoxin peroxidase I and II are important defenses of yeast against organic hydroperoxide insult: catalases and peroxiredoxins cooperate in the decomposition of H2O2 by yeast. *Journal of Biological Chemistry* **279**: 35219-35227

43) Avery, A. M. and Avery, S. V. *Saccharomyces cerevisiae* expresses three phospholipid hydroperoxide glutathione peroxidases. *Journal of Biological Chemistry* **276**: 33730-33735

44) Huh, W. K., Falvo, J. V., Gerke, L. C., Carroll, A. S., Howson, R. W., Weissman, J. S. and O'Shea, E. K. Global analysis of protein localization in budding yeast. *Nature* **425**: 686-691

45) Lee, S. Y., Song, J. Y., Kwon E.S. and Roe, J. H. Gpx1 is a stationary phase-specific thioredoxin peroxidase in fission yeast. *Biochemical and Biophysical Research Communications* **367**: 67-71

46) Sharma, P., Jha, A. B., Dubey, R. S. and Pessarakli, M. Reactive oxygen species, oxidative damage, and antioxidative defense mechanism in plants under stressful conditions. *Journal of Botany* article ID 217037, 2012, 26 pages, doi:10.1155/2012/217037

47) Nguyen, V. D., Saaranen, M. J., Karala, A. R., Lappi, A. K., Wang, L., et al. (2011) Two endoplasmic reticulum PDI peroxidases increase the efficiency of the use of peroxide during disulfide bond formation. *Journal of Molecular Biology* **406**: 503-515

48) Utomo, A., Jiang, X., Furuta, S., Yun, J., Levin, D. S., Yi-Chun J. Wang, Y. J., et al. (2004) Identification of a novel putative non-selenocysteine containing phospholipid hydroperoxide glutathione peroxidase (npgpx) essential for alleviating oxidative stress generated from polyunsaturated fatty acids in breast cancer cells. *Journal of Biological Chemistry* **279**: 43522-45329

49) Perry, A. C. F., Jones R., Niang, L. S. P., Jackson, R. M, Hall, L. (1992) Genetic evidence for an androgen-regulated epididymal secretory glutathione peroxidase whose transcript does not contain a selenocysteine codon. *Biochemical Journal* **285**: 863-870

50) Bosello-Travain, V., Conrad, M., Cozzac, G., Negroc, A., Quartesana, S., Rossettoa, M., et al. (2013) Protein disulfide isomerase and glutathione are alternative substrates in the one Cys catalytic cycle of glutathione peroxidase 7. *Biochimica et Biophysica Acta – General Subjects* **1830**: 3846-3857

51) Bae, Y. A., Cai, G. B., Kim, S. H., Zo, Y. G., Kong, Y. (2008) Modular evolution of glutathione peroxidase genes in association with different biochemical properties of their encoded proteins in invertebrate animals. *BMC Evolutionary Biology* **9**: 72

52) Maiorino, M., Bosello-Travain, V., Cozza, G., Miotto, G., Roveri, A., Toppo, S., et al. (2015) Understanding mammalian glutathione peroxidase 7 in the light of its homologs. *Free Radical Biology and Medicine* **83**: 352-360

53) Toppo, S., Flohéb, L., Ursinia, F., Vaninc, S., Maiorino, M. (2009) Catalytic mechanisms and specificities of glutathione peroxidases: variations of a basic scheme. *Biochimica et Biophysica Acta – General Subjects* **1790**: 1486-1500

54) Wei, P-C., Hsieh, Y-H., Su, M-I., Jiang, X-J., Hsu, P, H., Lo, W-T., et al. (2012) Loss of the oxidative stress sensor NPGPx compromises GRP78 chaperone activity and induces systemic disease. *Molecular Cell* **48**: 747-759

55) Wang, M., Wey, S., Zhang, Y., Ye, R., Lee, A. S. (2009) Role of the unfolded protein response regulator GRP78/BiP in development, cancer, and neurological disorders. *Antioxidants and Redox Signaling* **11**: 2307-2316

56) Nguyen, V. D., Saaranen, M. J., Karala, A. R., Lappi, A. K., Wang, L., Raykhel, I. B., et al. (2011) Two endoplasmic reticulum pdi peroxidases increase the efficiency of the use of peroxide during disulfide bond formation. *Journal of Molecular Biology* **406**: 503-515

57) Ramming, T., Hansen, H. G., Nagata, K., Ellgaard, L., Appenzeller-Herzog. (2014) GPx8 peroxidase prevents leakage of H2O2 from the endoplasmic reticulum. *Free Radical Biology and Medicine* **70**: 106-116

58) Morikawa, K., Gouttenoire, J., Hernandez, C., Thi, V. L. D., Tran, H. T. L., Lange, C. M., et al. (2013) Quantitative proteomics identifies the membrane-associated peroxidase GPx8 as a cellular substrate of the hepatitis C virus NS3-4A protease. *Hepatology* **59**: 423-433

59) Wei, P-C., Hsieh, Y-H., Su, M-I., Jiang, X-J., Hsu, P, H., Lo, W-T., et al. (2012) Loss of the oxidative stress sensor NPGPx compromises GRP78 chaperone activity and induces systemic disease. *Molecular Cell* **48**: 747-759

60) Ramming, T., Kanemura, S., Okamura, M., Inaba, K, Appenzeller-Herzog. (2016) Cysteines 208 and 241 in Ero1α are required for maximal catalytic turnover. *Redox Biology* **7**: 14-20

61) Ramming, T., Okumura, M., Kanemura, S., Baday, S., Birk, J., Moes, S., et al. (2015) A PDI-catalyzed thiol–disulfide switch regulates the production of hydrogen peroxide by human Ero1. *Free Radical Biology and Medicine* **83**: 361-372

62) Nyathi, Y., Wilkinson, B. M., Pool, M. R. (2013) Co-translational targeting and translocation of proteins to the endoplasmic reticulum. *Biochimica et Biophysica Acta – Molecular Cell Research* **1833**: 2392-2402

63) Fitzgerald, I., Glick, B. S. (2014) Secretion of a foreign protein from budding yeasts is enhanced by cotranslational translocation and by suppression of vacuolar targeting. *Microbial Cell Factories* **13**: 125

64) Belden, W. J., Barlowe, C. (2001) Role of Erv29p in collecting soluble secretory proteins into er-derived transport vesicles. *Science* **294**: 1528-1531

65) Pelham, H. R. B., Hardwick, K. G., Lewis, M. J. (1988) Sorting of soluble ER proteins in yeast. *The EMBO Journal* **7**: 1757-1762

66) Scheel, A. A., Pelham, H. R. B. (1998) Identification of amino acids in the binding pocket of the human KDEL receptor. *Journal of Biological Chemistry* **273**: 2467-2472

67) Townsley, F. M., Wilson, D. W., Pelham, H. R. B. (1993) Mutational analysis of the human KDEL receptor: distinct structural requirements for Golgi retention, ligand binding and retrograde transport. *The EMBO Journal* **12**: 2821-2829

68) Hardwick, K. G., Lewis, M. J., Semenza, J., Dean, N., Pelham, H. R. B. (1990) ERD 1, a yeast gene required for the retention of luminal endoplasmic reticulum proteins, affects glycoprotein processing in the Golgi apparatus. *The EMBO Journal* **9**: 623-630

69) Lewis, M. J., Pelham, H. R. B. (1996) SNARE-Mediated retrograde traffic from the golgi complex to the endoplasmic reticulum. *Cell* **85**: 205-215

70) Vito, E., Melo, E. P., Yang, Y., Wahlander, A., Neubert, T. A., Ron, D. (2010) Oxidative protein folding by an endoplasmic reticulum localized peroxiredoxin. *Molecular Cell* **40**: 787-797

71) Miller, C. A., Martinant, M. A., Hyman, L. E. (1998) Assessment of aryl hydrocarbon receptor complex interactions using pBEVY plasmids: expression vectors with bi-directional promoters for use in *Saccharomyces cerevisiae*. *Nucleic Acids Research* **26**: 3577-3583

72) Chu, D., Barnes, D. J., von der Haar, T. (2011) The role of tRNA and ribosome competition in coupling the expression of different mRNAs in Saccharomyces cerevisiae. *Nucelic Acids Research* **39**: 6705-6714

73) Colpan, M., Schorr, J., Herrmann, R., Feuser, P. (2002) US patent No. 6,383,393 B1, Chromatographic purification and separation process for mixtures of nucleic acids. United States Patent

74) Kibbe, W. A. (2007) OligoCalc: An online oligonucleotide properties calculator. *Nucleic Acids Res*earch. **35**: W43-W46

75) Riener, C. K., Kada, G., Gruber, H. J. (2002) Quick measurement of protein sulfhydryls with Ellman's reagent and with 4,4′-dithiodipyridine. *Analytical and Bioanalytical Chemistry* **373**: 266-276

76) Sancar, G. B., Smith, F. W. (1989) Interactions between yeast photolyase and nucleotide excision repair proteins in *Saccharomyces cerevisiae* and *Escherichia coli*. *Molecular Cell Biology* **9**: 4767-4776.

77) Tachibana, C., Stevens, T. H. (1992) The yeast EUG1 gene encodes an endoplasmic reticulum protein that is functionally related to protein disulfide isomerase. *Molecular Biology of the Cell* **12**: 4601-4611

78) Ko, N., Nishihama, R., Pringle, J. R. (2008) Control of 5-FOA and 5-FU resistance by saccharomyces cerevisiae YJL055W. *Yeast* **25**: 155-160

79) Hu, H., Boone, A., Yang, W. (2013) Mechanism of OMP decarboxylation in orotidine 5′-monophosphate decarboxylase. *Journal of American Chemical Society* **130**: 14493-14503

80) Chung, C. H., Kim, J. H., Chung, B. H. (2014) Detection of UV-induced mutagenic thymine dimer using graphene oxide. *Analytical Chemistry* **86**: 11586-11591

81) Rumora, A. E., Kolodziejczak, K. M., Wagner, A. M., Núñez, M. E. (2008) Thymine dimer-induced structural changes to the dna duplex examined with reactive probes. *Biochemistry* **47**: 13026-13035

82) Winston, F. (2008) EMS and UV mutagenesis in yeast. *Curr Protoc Mol Biol* **82**:13.3B.1–13.3B.5

83) Brachmann, C. B., Davies, A., Cost, G. J., Caputo, E., Li, J., Hieter, P., Boeke, J. D. (1998) Designer deletion strains derived from *saccharomyces cerevisiae* s288c: a useful set of strains and plasmids for pcr-mediated gene disruption and other applications. *Yeast* **14**: 115-132

84) Rose, M., Winston, F. (1984) Identification of a Ty insertion within the coding sequence of the *S. cerevisiae URA*$_3$ gene. *Molecular Genetics and Genomes.* **193**: 557-560

85) Shimomura, O., Johnson, H. F., Saiga, Y. (1962) Extraction, purification and properties of aequorin, a bioluminescent protein from the luminous hydromedusan, *Aequorea*. *Journal of Cellular Comparative Physiology.* **59**: 223-239

86) Peng, D., Belkhiri, A., Hu, T., Chaturvedi, R., Asim, M., Wilson, K. T., et al. (2013) Glutathione peroxidase 7 protects against oxidative dna damage in oesophageal cells. *Gut* **61**: 1250-1260

87) Bienert, G. P., Schjoerring, J. K., Jahn, T. P. (2006) Membrane transport of hydrogen peroxide. *Biochimica et Biophysica Acta Biomembranes* **1758**: 994-1003

88) Ameziane-El-Hassani, R., Dupuy, C. (2013) Detection of intracellular reactive oxygen species (CM-H2DCFDA). *Bio-protocol* **3**: e313

89) Bei, Y., Liu, Q. (2014) Reaction mechanisms for dithiothreitol as a measure of particulate matter induced oxidative potential activity by density functional theory. *Korean Journal of Chemical Engineering.* **31**: 1115-1119

90) Hjelmqvist, L., Tuson, M., Marfany, G., Herrero, E., Balcells, S., González-Duarte, R. (2014) ORMDL proteins are a conserved new family of endoplasmic reticulum membrane proteins. *Genome Biology* **6**: 1-16

91) Schmitt, M. J., Breinig, F. (2002) The viral killer system in yeast: from molecular biology to application. *FEMS Microbiology Reviews* **26**: 257-276

92) Martinac, B., Zhu, H., Kubalski, A., Zhou, X., Culbertson, M., Bussey, H., Kung, C. (1990) Yeast Ki killer toxin forms ion channels in sensitive yeast spheroplasts and in artificial liposomes. *Proceedings of the National Academy of Sciences* **87**: 6228-6232

93) Schneider, C. A., Rasband, W. S., Eliceiri, K. W. (2012) NIH Image to ImageJ: 25 years of image analysis. *Nature methods* **9**: 671-675

94) Popolo, L. Ragni, E., Carotti, C., Palomares, O., Aardema, R., Back, J. W., et al. (2008) Disulfide bond structure and domain organization of yeast β(1,3) glucanosyltransferases involved in cell wall biogenesis. *The Journal of Biological Chemistry* **283**: 18553-18565

95) Wu, R., Ma, Z., Liu, Z., Terada, L.S. (2010) Nox4-Derived H2O2 mediates endoplasmic reticulum signaling through local ras activation. *Molecular Cell Biology* **30**: 3553-3568

96) Pinson, B., Chevallier, J., Urban-Grimal, D. (1999) Only one of the charged amino acids located in membrane-spanning regions is important for the function of the Saccharomyces cerevisiae uracil permease. *Biochemistry Journal* **339**: 37-42

97) Fork, C., Bauer, T., Golz, S., Geerts, A., Weiland, J., Del Turco, D., et al. (2011) OAT2 catalyses efflux of glutamate and uptake of orotic acid. *Biochemistry Journal* **436**: 305-312

98) Belousov., V. V., Fradkov, A. F., Lukyanov, K. A., Staroverov, D. B., Shakhbazov, K. S., Terskikh, A. V., Lukyanov, S. (2006) Genetically encoded fluorescent indicator for intracellular hydrogen peroxide. *Nature Methods* **3**: 281-286

99) Gabriel, F., Sabra, A., El-Kirat-Chatel, S., Pujol, S., Fitton-Ouhabi, V., Bréthes, D., et al. (2014) Deletion of the uracil permease gene confers cross-resistance to 5-fluorouracil and azoles in *Candida lusitaniae* and highlights antagonistic interaction between fluorinated nucleotides and fluconazole. *Antimicrobial Agents Chemotherapy* **58**:4476-4485

100) Huang, B. K., Stein, K. T., Sikes, H. D. (2016) Modulating and measuring intracellular H2O2 using genetically encoded tools to study its toxicity to human cells. *American Chemical Society: Synthetic Biology* **5**: 1389-1395

101) Laboissière, M. C. A., Stephen L. Sturley, S. L., Raines, R. T. (1995) The essential function of protein-disulfide isomerase is to unscramble non-native disulfide bonds. *The Journal of Biological Chemistry* **270**: 28006-28009

102) Gossen, M., Bujard, H. (1992) Tight control of gene expression in mammalian cells by tetracycline-responsive promoters. *Proceedings of the National Academy of Sciences* **89**: 5547-5551

103) Campbell, L. J., Willoughby, J. J., Jenson, A. M. (2012) Two types of tet-on transgenic lines for doxycycline-inducible gene expression in zebrafish rod photoreceptors and a gateway-based tet-on toolkit. *PLoS One* **7**: e51270

104) Karim, A. S., Curran, K. A., Alper, H. S. (2012) Characterization of plasmid burden and copy number in saccharomyces cerevisiae for optimization of metabolic engineering applications. *FEMS Yeast Research.* **13**: 107-116

105) Kjærgaard, K., Schembri, M. A., Hasman, H., Klemm, P. (2000) Antigen 43 from *Escherichia coli* induces inter- and intraspecies cell aggregation and changes in colony morphology of *pseudomonas fluorescens*. *Journal of Bacteriology* **182**: 4789-4796

106) Leadsham, J. E., Sanders, G., Giannaki, S., Bastow, E.L., Hutton, R., Naeimi, W. R., et al. (2013) Loss of cytochrome c oxidase promotes RAS-dependent ROS production from the ER resident NADPH oxidase, Yno1p, in yeast. *Cell Metabolism* **18**: 279-286

107) Natalia, D. (1994) Studies on yeast protein disulphide isomerase. PhD thesis.